SMART SURGICAL NEEDLE ACTUATED BY SHAPE MEMORY ALLOYS FOR PERCUTENEOUS PROCEDURES

A Dissertation

Submitted to

the Temple University Graduate Board

In Partial Fulfillment

of the Requirements for the Degree

DOCTOR OF PHILOSOPHY

---

by

Bardia Konh

May 2016

Examining Committee Members:

Parsaoran Hutapea, Mechanical Engineering Department, Temple University

Jie Yin, Mechanical Engineering Department, Temple University

Keya Sadeghipour, Mechanical Engineering Department, Temple University

Mohammad Elahinia, Department of Mechanical, Industrial and Manufacturing Engineering, University of Toledo

Ruth Ochia, Bioengineering Department, Temple University

ABSTRACT

Background: Majority of cancer interventions today are performed percutaneously using needle-based procedures, i.e. through the skin and soft tissue. Needle insertion is known as one of the recent needle-based techniques that is used in several diagnostic and therapeutic medical procedures such as brachytherapy, thermal ablations and breast biopsy. The difficulty in most of these procedures is to attain a precise navigation through tissue reaching target locations. Insufficient accuracy using conventional surgical needles motivated researchers to provide actuation forces to the needle's body for compensating the possible errors of surgeons/physicians. Therefore, active needles were proposed recently where actuation forces provided by shape memory alloys (SMAs) are utilized to assist the maneuverability and accuracy of surgical needles. This work also aims to introduce a novel needle insertion simulation to predict the deflection of a bevel tip needle inside the tissue. Development of a model to predict the behavior of the needle steering in the soft tissue has been always a point of interest as it could improve the performance of many percutaneous needle-based procedures.

Methods: In this work first, the actuation capability of a single SMA wire was studied. The complex response of SMAs was investigated via a MATLAB implementation of the Brinson model and verified via experimental tests. The material characteristics of SMAs

were simulated by defining multilinear elastic isothermal stress-strain curves. Rigorous experiments with SMA wires were performed to determine the material properties as well as to show the capability of the code to predict a stabilized SMA transformation behavior with sufficient accuracy. The isothermal stress-strain curves of SMAs were simulated and defined as a material model for the Finite Element Analysis of the active needle.

In the second part of this work, a three-dimensional finite element (FE) model of the active steerable needle was developed to demonstrate the feasibility of using SMA wires as actuators to bend the surgical needle. In the FE model, birth and death method of defining boundary conditions, available in ANSYS, was used to achieve the pre-strain condition on SMA wire prior to actuation. This numerical model was validated with needle deflection experiments with developed prototypes of the active needle.

The third part of this work describes the design optimization of the active using genetic algorithm aiming for its maximum flexibility. Design parameters influencing the steerability include the needle's diameter, wire diameter, pre-strain, and its offset from the needle. A simplified model was developed to decrease the computation time in iterative analyses of the optimization algorithm.

In the fourth part of this work a design of an active needling system was proposed where actuation forces of SMAs as well as shape memory polymers (SMPs) were incorporated. SMP elements provide two major additional advantages to the design: (i) recovery of the SMP's plastic deformation by heating the element above its glass transition temperature, and (ii) achieving a higher needle deflection by having a softer stage of SMP at higher temperatures with less amount of actuation force.

Finally, in the fifth and last part of this study, an Arbitrary-Lagrangian-Eulerian formulation in LS-DYNA software was used to model the solid-fluid interactions between the needle and tissue. A 150mm long needle was considered to bend within the tissue due to the interacting forces on its asymmetric bevel tip. Some additional assumptions were made to maintain a reasonable computational time, with no need of parallel processing, while having practical accuracies. Three experimental tests of needle steering in a soft phantom were performed to validate the simulation.

Results: The finite element model of the active needle was first validated experimentally with developed prototypes. Several design parameters affecting the needle's deflection such as the needle's Young's modulus, the SMA's pre-strain and its offset from the neutral axis of the cannula were studied using the FE model. Then by the integration of the SMA characteristics with the automated optimization schemes an improved design of the active needle was obtained. Real-time experiments with different prototypes showed that the quickest response and the maximum deflection were achieved by the needle with two sections of actuation compared to a single section of actuation. Also the feasibility of providing actuation forces using both SMAs and SMPs for the surgical needle was demonstrated in this study.

The needle insertion simulation was validated while observing less than 10% deviation between the estimated amount of needle deflection by the simulation and by the experiments. Using this model the effect of needle diameter and its bevel tip angle on the final shape of the needle was investigated.

Conclusion: The numerical and experimental studies of this work showed that a highly maneuverable active needle can be made using the actuation of multiple SMA wires in series. To maneuver around the anatomical obstacles of the human body and reach the target location, thin sharp needles are recommended as they would create a smaller radius of curvature. The insertion model presented in this work is intended to be used as a base structure for path planning and training purposes for future studies.

To my parents, who raised me,

and my sister Mahsa, who motivated me

ACKNOWLEDGMENTS

I feel that I have to thank many people here, to whome I owe my success. In fact this work was not possible without mentorship, help, and support of so many. First and formost, I would like to express my deepest gratitude to my advisor, Dr. Parsaoran Hutapea, who gave me the opportunity to work in his active research team and supported me all of these years throughout my PhD studies. I am specially grateful for his trust on me, and the freedome he gave me to look into diverse areas. His continuous motivations kept me going despite of eventual failures. I would like to thank my Thesis Committee Members, Dr. Keya Sadeghipour, Dr. Jie Yin, Dr. Mohammad Elahinia, and Dr. Ruth Ochia for their valuable inputs. I also would like to thank Dr. Kurosh Darvish, and Dr. Howon Lee for their contributions in this work and Dr. Fei Ren for letting us use his instruments. I should also thank Dr. Mohammad Kiani and every single faculty in Mechanical Department of Temple University for their eventual support. I would also like to thank the Composites Laboratory team members with whom not only we did great but also formed the unforgettable memories of the past few years.

I would also like to thank Temple University Graduate School and the College of Engineering for their financial support and the opportunity to perform my research. This work was also financialy supported by the Department of Defense CDMRP Prostate Cancer Research Program (GRANT #W81XWH-11-1-0398), that I am grateful for.

Last but definitely not least, I would like to thank my family; my parents, Ebrahim and Behnoosh and my beautiful sister Mahsa for their unconditional support, love and encouragements.

TABLE OF CONTENTS

LIST OF TABLES

LIST OF FIGURES

CHAPTER 1

INTRODUCTION

1.1. Shape memory alloy as a suitable component for active systems

To date, many biomedical devices have utilized the pseudoelastic properties of advanced, active and adaptive materials such as coronary stents, eyeglasses and orthodontic wires (Auricchio, Taylor, & Lubliner, 1997). The actuation properties of the active materials have also attracted a lot of attention, especially in medical devices such as active cardiac catheters (Haga, Tanahashi, & Esashi, 1998), artificial muscles (Pfeiffer, DeLaurentis, & Mavroidis, 1999) and cochlea implants (Hagmann et al., 2015). Shape memory alloys (SMAs), well known smart materials, have become increasingly popular in various applications due to their ability to remember their initial shape. Their unique thermomechanical characteristics of pseudoelasticity, shape memory effect and biocompatibility have made them a suitable option to revolutionize many diagnostic and therapeutic biomedical tools (Morgan, 2004).

1.2. Material modeling and characterization of shape memory alloys

Knowledge of SMA material behavior is critical for the design and development of devices in which actuation capabilities of SMAs are utilized. Material characteristics of SMAs are complicated due to the history dependent hysteresis relationships between the materials' stress, strain and temperature. A comparatively large recoverable strain of SMAs is due to the transformation between two major internal phases known as martensite and austenite. Some constitutive models have been provided based on quasistatic assumptions in which the system's equilibrium at each step is required (Tanaka, Kobayashi, & Sato, 1986). Since the characteristic parameters such as transformation temperatures and Clausius-Clapeyron coefficients in these models are sensitive to manufacturing processes and heat treatments, they have to be found experimentally. The transformation temperatures are known as M_s, M_f, A_s, A_f, where M represent martensite, A austenite, while subscripts s and f shows the starting and finishing point of the transformation process, respectively. One-dimensional (1D) thermomechanical and actuation properties of SMA wires were discussed in previous studies especially for actuation utilization (Honarvar, Konh, Datla, Devlin, & Hutapea, 2013; Konh, Honarvar, & Hutapea, 2013; Konh & Hutapea, 2013). Several research groups (Eaton-Evans, Dulieu-Barton, Little, & Brown, 2007; Liang & Rogers, 1990; Tanaka et al., 1986) have develop mathematical models to predict the SMA's response. Brinson (Brinson, 1993) developed a model that includes the transformation between twinned and detwinned martensite (different crystallographic shapes of martensite). This model was able to predict the SMAs' Pseudoelasticity and shape memory effects, simultaneously. Also privileging from non-constant coefficients this model provided an enhanced accuracy with respect to the previously developed models (Liang & Rogers, 1990; Tanaka et al., 1986). Brinson model was used in this study for its accuracy and consistency with our SMA wires. Prior to implementation of the model, the characteristic parameters were determined experimentally using three experimental setups: constant-stress, constant-strain and isothermal tests. The phase transformation diagram was then formed to predict the martensitic fraction at each step of actuation.

1.3. Advancements in medical devices using shape memory alloy components

The primary concept of active surgical needle (Figure 1-1) was suggested by (Konh, Datla, & Hutapea, 2014) where the feasibility of using SMA wires to actuate the surgical needles was shown. The SMA wires, i.e., Nitinol wires in our design, supply bending forces to the needle body to guide the needle through desired trajectories inside the tissue. The active needle provides several advantages such as improvements in accuracy to reach the target locations, avoiding critical organs during insertion and minimizing trauma to patients. However, before the active needle becomes a reality, there are several aspects that must be investigated. Many practical issues have been considered in this study which will lead to an appropriate design closer to the clinical use.

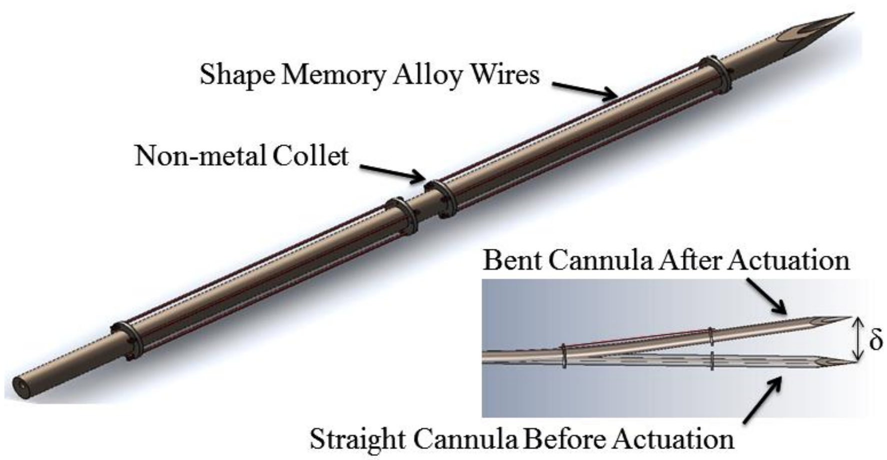

Figure. 1-1: Schematic of the proposed active needle design.

The success of many needle-based interventions such as brachytherapy, thermal ablation and biopsy highly depends on the accuracy of the needle placements at target locations. Therefore, improvement of the accuracy of needle placement has always been a point of interest; many groups have tried variety of options to activate the surgical needle for an improved precision. For example, Tang et al. (Tang, Chen, & He, 2007) used magnetic forces in order to help the navigation of the needle inside the body. Another method was used by Ayvali et al. (Ayvali, Liang, Ho, Chen, & Desai, 2012a) utilizing pre-curved SMA wires on the needle body to provide external actuations. The wires, which were initially straight, transform to a pre-curved shape when heated. Similarly, Ryu et al. (Ryu et al., 2012) used internal laser heating of SMA wires to bend the needle. The nonlinear beam deflection via actuation of a SMA wire was studied by Shu et al. (Shu, Lagoudas, Hughes, & Wen, 1997). The electrical resistance and the fatigue behavior of SMA wires used as actuators have been studied by Meier et al. (Meier, Czechowicz, & Haberland, 2009). They developed a control loop based on the electrical resistance feedback. Mechanics of an active needle inside tissue was studied by Datla et al. (Datla et al., 2013) using an analytical approach. Also behavior of a surgical needle within the tissue and the consequent probable thermal damage due to the existence of heating elements were studied by Datla et al. (Datla, Konh, Koo, et al., 2014).

1.4. History and background of design optimizations

In previous optimization studies with SMAs (Kohl, Skrobanek, & Miyazaki, 1999; Kota, Hetrick, Li, & Saggere, 1999; Masuda & Noori, 2002; Troisfontaine, Bidaud, & Larnicol, 1999), the desired dynamic properties were found by optimizing the placement of a single wire component to eliminate the high stress regions. The active material optimization was done by (Main, Garcia, & Howard, 1994; Seeley & Chattopadhyay, 1993) using analytical and gradient based studies. In other works, design optimization of a system with a SMA spring was investigated by Dumont and Kuhl (Dumont & Kühl, 2005) using genetic algorithm. To dampen the structural vibration, Ozbulut et al. (Ozbulut, Roschke, Lin, & Loh, 2010) optimized the installation of a SMA wire based on a genetic algorithm. A design optimization for an actuated robotic catheter was done by Crews and Buckner (Crews & Buckner, 2012). They implemented a free energy model (Heintze, Seelecke, & Bueskens, 2003) into finite element analysis (FEA) package, COMSOL for their optimization strategies. Although their work covers many aspects of structural analysis, there are some limitations need to be addressed such as SMA's constitutive model and the computationally expensive run time that require improvements. To overcome these limitations, we present an automated optimization approach based on a simplified model that benefits from extensive experimental and numerical studies on SMA actuators. Moreover, the implementation of the isothermal stress-strain curves as material properties for the active components and showing a reasonable accuracy of the model are among the challenging tasks in this study.

1.5. Aims and scopes of this dissertation

In this study, the optimized design of the active needle has also been presented. The past design and developments of systems consisting SMAs had been based on graphical design trial and error (the related discussion can be found in (Hartl, Lagoudas, & Calkins, 2011)). The inelastic transformation strain of SMAs as an independent quantity has not been implemented in such methods; therefore, a new empirical curve at each modified design configuration was required. The automated tools of the commercial software (ANSYS) have been used here to develop a predictive algorithm to assess the active needle response. The best design configuration was found using well-established methods and implementing appropriate tools. The novelty of our design optimization study lies on the incorporation of smart materials in our system. Prior to constructing an optimization algorithm, implementation of a constitutive model capable of predicting the inelastic strain response of SMAs is necessary. As the material properties of SMA wires can be different due to a different manufacturing process, the details of the constitutive model have been described so that other researchers can use it as a tool to model their particular active components. The inelastic response of SMA wires with different diameters was first studied via both experimental and numerical approaches. This model was then used in optimization algorithm to perform a predictive analysis seeking the best configuration. The main aim of this study was not only to characterize the smart materials but also to provide a general methodology with all the tools required to study an active complex structure and suggest optimized solutions.

1.6. This dissertation is organized as described below

This work is organized as follows: An overall view of all the methods used in this dissertation is introduced in chapter 2.1, followed by a discussion about the SMAs' constitutive model in chapter 2.2. Chapter 3 describes the whole materials and methods used for the diverse directions of this study. It starts with the experimental tests developed to characterize the actuators (chapters 3.1.1 to 3.1.4); then based on the parameters found in this step a MATLAB code was generated to predict the SMAs' response and their temperature profile, chapter 3.2 and 3.3, respectively. To show the feasibility of the active needle, a finite element model was developed in chapter 3.4; this model is validated by the prototype of chapter 3.5. As it was desired to optimize the design of the active needle, two parallel studies were performed simultaneously: (i) an experimental approach with the active needle prototype to study the design parameters (explained in chapter 3.6), and (ii) a numerical approach to iteratively optimize the design in an automated fashion by using computer tools (explained in chapter 3.7). After optimizing the design an advanced prototype was developed in chapter 3.8. This prototype privileges from the additional actuations of shape memory polymer (SMP) components, along with the SMA wires. To investigate how this device would interact within the tissue, an insertion test and a simulation of chapter 3.9 and 3.10 were developed, respectively. The results obtained from each sections of chapter 3 are explained in chapter 4 along with discussions, validations and considerations of possible sources of errors. Finally, chapter 5 links all areas together, brings up the conclusions, and suggests the possible future works.

CHAPTER 2

GENERAL METHODOLOGY

2.1. Analysis tools to optimize the active needle design

In this section engineering analysis tools used to accomplish the ultimate goal of parametric study and optimization of the active needle is discussed. Figure 2-1 shows schematically the methodology used for the first part of this study with the main objective of showing the feasibility of using SMA wires as actuators for the active needle. As illustrated in the figure the automated simulation process makes it possible to have an efficient assessment of the structural response of our design. The thermomechanical behavior of SMAs needs to be included in the analysis as they are the most important components of the structure. Three experimental setups developed to study the complex behavior of SMAs are discussed in detail in chapter 3.1.1, 3.1.2, and 3.1.3. Since different diameters of the wires show different characteristic parameters, these experiments were performed on every diameters of wires separately. Numerical and experimental studies on SMA wires prior to the finite element analysis ensured a coherent material model to be used in the FE model of the next step. The isothermal stress-strain curves obtained from a MATLAB implementation of Brinson model and provided as the material model for the

FE analysis. The detail of this constitutive model is explained in chapter 3.2. Birth and death method was used as a part of a three-step solution process in ANSYS.

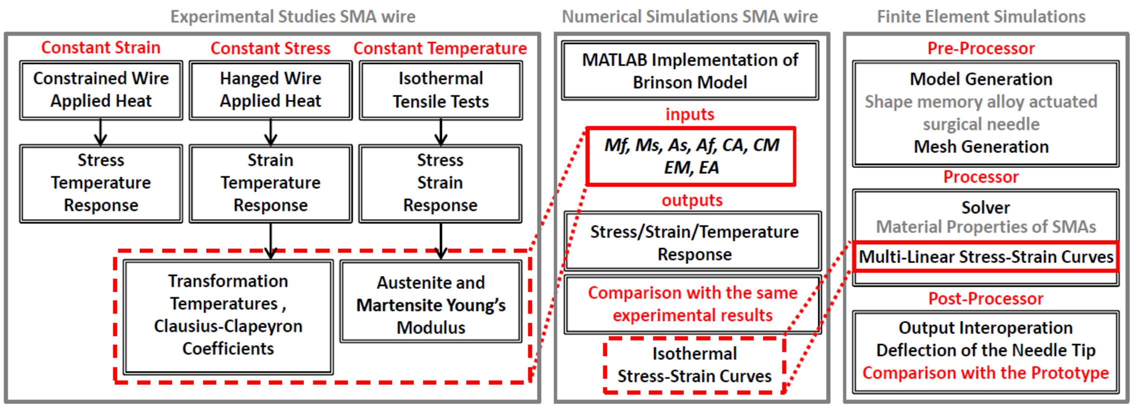

Figure 2-1: Engineering tools used to show the actuation capability of SMA wires in the active needle design.

The process of design optimization is shown schematically in Figure 2-2. This automated method of analytical structural assessment made the optimization of systems including active components more efficient. Our design objective targets the highest deflection of the active needle considering some limitations such as maximum stress, strain and elastic deformation of different components. Using this approach different design configurations were evaluated to come up with the best design. The iterative structural analysis was performed over the defined domain of design parameters considering constrains and limitations achieving the design objective. The ANSYS design optimization module was used for this objective that is capable of being linked to the ANSYS Parametric Design Language (APDL) module of the software where the FE model was generated and run the analysis automatically. Design of Experiment (DOE) was also studied to obtain an overview of possible configurations over the design space. The optimization process consists of an APDL input file with all design parameters and the necessary output parameters defined which was iteratively solved though the whole domain. The APDL input file is being written by the optimization module, solved by ANSYS and then the output is being interpreted considering constrains and limitations which leads to the best possible design. The APDL input file should be constructed so that every design parameter has an assigned variable name, consisting run commands and capable of storing desired results. All the required results are being stored in an output files for further analysis. Iterations are finished when all the requested DOE analyses are performed or the convergence criteria is achieved.

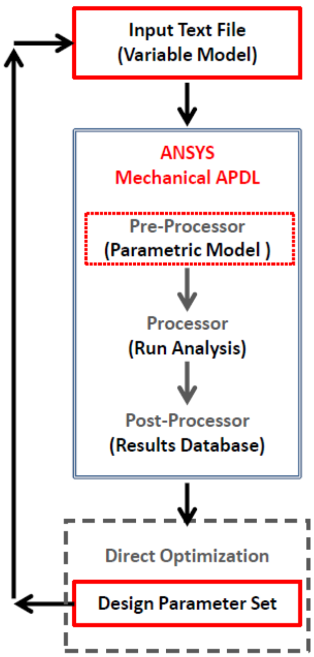

Figure 2-2: Analysis algorithm for design optimization, seeking the maximum steerability of the active needle.

2.2. Constitutive model: formulation and numerical integration

SMAs show two different behaviors known as (i) shape memory and (ii) pseudoelastic effects. The shape memory is its ability to recover a large residual strain by rising up the temperature whereas pseudoelasticity is its ability to resume a high amount of strain upon unloading in a hysteresis loop. These effects are observed in different temperatures and loading conditions. Two major phases exist in these alloys which are known as austenite and martensite. Austenite is known as the parent phase, which only exists at high temperatures. Only by decreasing the temperature will result in a phase change into the martensite. The martensite phase exists in two different orientations which are known as twined and detwined, with respect to its multiple variants and twins. The phase transformation between martensite and austenite generally empower the SMA to recover a large amount of strain which is used for activating the needle device. The constitutive Brinson model is used to model the active needle and it is described in this section. Prior to Brinson, Liang and Rogers (Liang & Rogers, 1990) suggested the stress (σ) to be related to three material functions: the modulus of SMA, $D(\varepsilon,\xi,T)$, the transformation tensor, $\Omega(\varepsilon,\xi,T)$ and the thermal coefficient of expansion, $\theta(\varepsilon,\xi,T)$ as shown in Equation 2-1. In this equation ε, ξ and T are the green strain, the martensite fraction and temperature respectively.

$$d\sigma = D(\varepsilon,\xi,T)d\varepsilon + \Omega(\varepsilon,\xi,T)d\xi + \theta(\varepsilon,\xi,T)d\theta \qquad 2\text{-}1$$

The material functions in Liang and Rogers (Liang & Rogers, 1990) formulation were assumed constant while the transformation kinetics was defined by a cosine function based on the Clausius-Clapeyron equation shown below. Equation 2-2 shows the relationship between temperature and transformation stress for an SMA material, where ε is the transformation strain and ΔH is the enthalpy change between martensite and austenite phases at temperature T_0. Both phases should be in equilibrium under the stress σ.

$$\frac{d\sigma}{dT} = -\frac{\Delta H}{T_0\varepsilon} \qquad 2\text{-}2$$

In Brinson model (Brinson, 1993), on the other hand, the martensite fraction was divided into two crystallographic shapes known as stress induced (ξ_s) and temperature induced (ξ_T) as shown below. The transformation function was modified accordingly.

$$\xi = \xi_s + \xi_T \qquad 2\text{-}3$$

Finally assuming non-constant material functions, Equation 2-4 was modified by Brinson to suggest the constitutive material behavior for SMAs as follows.

$$\sigma - \sigma_0 = D(\xi)\varepsilon - D(\xi_0) + \Omega(\xi)\xi_s - \Omega(\xi_0)\xi_{s0} + \theta(T - T_0) \qquad 2\text{-}4$$

Their mathematical definitions mean that they are functions of martensite volume fraction. Young's modulus, *D*, highly depends on the martensite fraction of the material (shown in Equation 2-5) where D_m and D_a represents the modulus of SMA with 100% martensite and 100% austenite, respectively.

$$D(\varepsilon, \xi, T) = D(\xi) = D_a + \xi(D_m - D_a) \qquad 2\text{-}5$$

The material function, $\theta(\varepsilon,\xi,T)$, is assumed to be constant due to its relatively small value, while the transformation function was described as a function of martensite fraction (Equation 2-6) where ε_L is the maximum residual strain of the wire.

$$\Omega(\xi) = -\varepsilon_L D(\xi) \qquad 2\text{-}6$$

Equation 2-4 and the transformation cosine function were used to find the behavior of our SMA wires in this study.

Input parameters to the Brinson model such as transformation temperatures and Clausius-Clapeyron coefficients (which are the slopes of the lines where transformation starts and ends) and the Young's modulus of austenite and martensite were obtained from experiments described in next section. The transition points on the strain-temperature response are the transformation temperatures at a particular level of stress. These tests were done at ten different constant-stress levels; thereby, the rate of change of transformation temperatures with stress gives the Clausius-Clapeyron coefficients. Finally all these parameters were gathered to form the stress-temperature diagram (shown in Figure 2-3), describing the regions in which the transformation happens. Also a constant-strain experiment was also developed to have a reliable prediction on the response of the SMA by the model (chapter 3.1.2). Having the phase transformation diagram formed, we were able to define an external function in MATLAB for the phase transformation kinetics. The material properties for each diameters of the SMA wires were provided to the code from experiments. Then a marching approach was followed based on Equation 2-4 to fill the stress, strain and temperature matrices while the martensite fraction at each step was predicted by the external function. For our finite element model the constant stress, constant strain and isothermal stress-strain responses were desired. Therefore, while iterating on equation 2-4 our convergence criteria was to have one of these parameters to remain constant at all steps. The isothermal stress-strain curves then was used as material properties of SMAs for the finite element model as illustrated in Figure 2-1.

Understanding the resistance heating of the SMA wires is important because they are being used as actuators in our system. An iterative approach to estimate the variation of temperature in the SMA wires considering the major heat mechanisms such as environmental convection, resistance heating and latent heat difference due to the phase transformation can be found in studies by Terriault and Brailovski (Terriault & Brailovski, 2011). The energy generated in the wire is contributed by Joule heating and latent energy of transformation. Our experimental results at room temperature on a single SMA wire showed that 10 to 15 seconds was required to cool down from 70ºC to room temperature (22ºC) for different wire diameters.

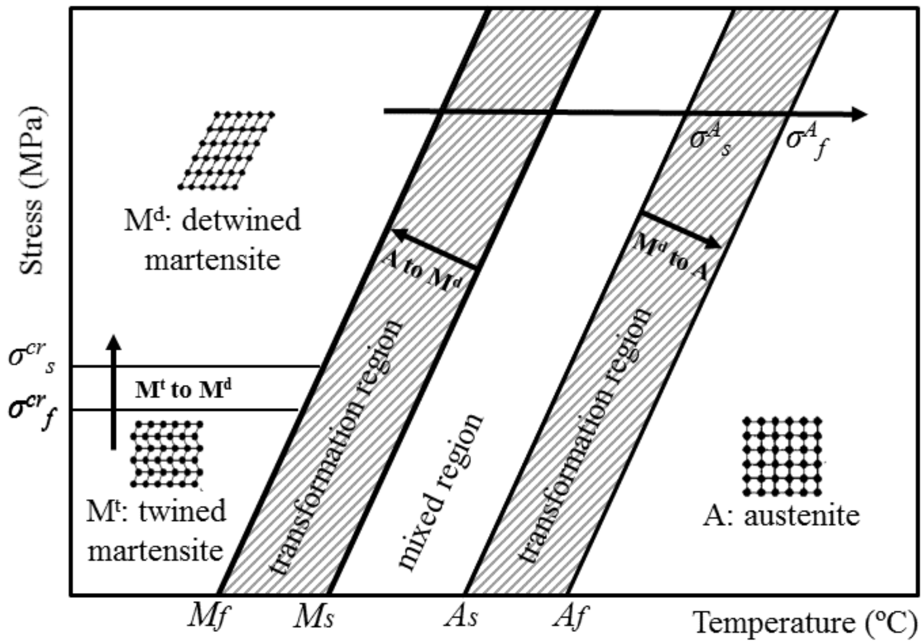

Figure 2-3: Typical phase transformation diagram of SMA wires.

CHAPTER 3

MATERIALS AND METHODS

3.1. Experimental setups for finding the material constants of shape memory alloy wires

3.1.1. Constant stress experiment

The configuration set up for the constant-stress experiment is shown in Figure 3-1a. The SMA wire was hung vertically under uniaxial tensile loading by attaching a weight hanger. The movements of the weight hanger were tracked by an attached Linear Variable Differential Transducer (LVDT) (HSD 750-500, Macro Sensor, Pennsauken, NJ) with a nominal range of ±12mm. The SMA wire was thermally activated, therefore contracting and moving the weight hanger upward. The SMA wire was activated thermally by Joule heating. The current was supplied as a ramp function using a programmable DC power supply (BK Precision 1696, Yorba Linda, CA). A bare 0.0762mm k-thermocouple (Omega Engineering, Stamford, CT) was attached to the top of SMA wire. The output signals of both the thermocouple and the LVDT were collected using SCXI-1321 terminal block (National Instrument, Austin, TX). To ensure complete austenitic transformation, the wires were heated up to 90°C. For each constant-stress level of each wire, three repetitive measurements were performed to ensure material stable behavior. Ten constant-stress levels were tested for each wire diameter to ensure sufficient data.

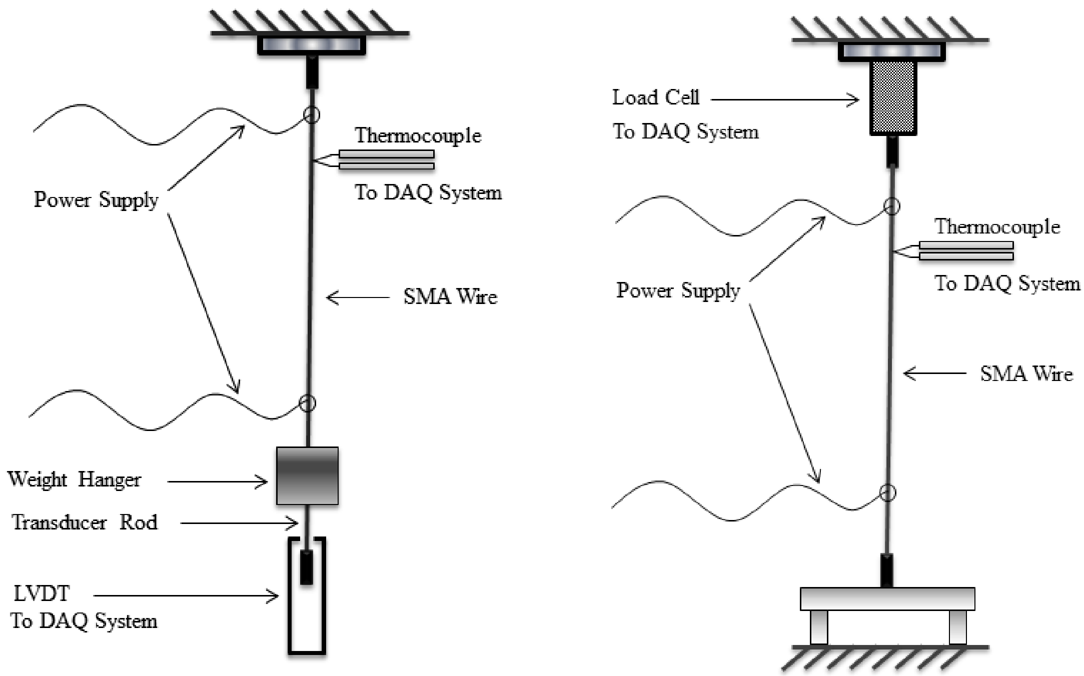

(a) (b)

Figure 3-1: Schematic pictures of the experimental setup for (a) the constant stress and (b) the constant strain experiments.

3.1.2. Constant strain experiment

In our active needle design SMA wires were used for their actuation purposes. The actuation capability can be described analogously as a fixed end cantilever beam. When thermally activated, the actuator contracts due to its higher temperature and shorter length. As the actuator would be fixed at both ends by a collet in the design, a reaction (actuation) force would be generated. Therefore, a constant-strain experiment was conducted to simulate the "actuation force" response of SMA wires. The experimental setup is illustrated in Figure 3-1b. The SMA wire was activated using Joule heating by applying current as a ramp function. Force response of the SMA wire was measured using a 22.7N load cell

(Futek Advance Sensor Tech, Irvine, CA). The load cell signal was collected using SCXI-1314 DAQ system. Similar to the constant-stress experiment, wire temperature was measured using the k-thermocouple. A linear stage (Edmund Optics, Barrington, NJ) was used to set a specific pre-strain on SMA wires. The pre-strain was measured by setting a fixed distance between the two holders located at each end.

3.1.3. Isothermal stress-strain experiment

Parameters required for the Brinson model such as transformation temperatures and Clausius-Clapeyron coefficients (the slopes of the lines where transformation starts and ends) were obtained from a constant stress experiment, described in chapter 3.1.1. The transformation temperatures at a particular stress level were determined from the transition points on the strain-temperature plots. These tests were done at ten different constant stress levels; thereby, the rate of change of transformation temperatures with stress gives the Clausius-Clapeyron coefficients. Also a Differential Scanning Calorimetry (DSC) test was performed to find the transformation temperatures at zero stress (chapter 3.1.4). Finally all these parameters were gathered to form the stress-temperature diagram which illustrates the regions at which the phase transformation happens. Further a constant strain experiment was developed to evaluate the model by comparing the SMA's force response (chapter 3.1.2). The other parameters needed for Brinson model are the critical stresses and the austenite and martensite Young's modulus which were found using the isothermal tensile tests. Also the critical stresses at which the transformation from martensite to austenite happens along with the Young's modulus of martensite and austenite were obtained from the isothermal tensile experiments. An Instron Mini-55 (Artisan Technology Group, Champaign, IL, USA) tensile machine was used to obtain the stress-strain response of the wires at room temperature (22ºC). A 10N load cell was used to capture the force response while the wires were loaded under a displacement control with a constant strain rate of 0.004mm/s. Before testing, the wires were ensured to be in detwined martensite through a heating and cooling cycle at a low stress.

Once the phase transformation diagram was constructed, our MATLAB model can simulate the stress-strain curves at different temperatures. These curves were implemented in finite element software using multilinear material properties. Loading and unloading part of each isothermal curve was defined by two separate material models. The loading part was used in the first step of the solution when the wire was under tension and then switched to the unloading part in the second and third steps when the tension pressure was removed and the wire was heated. As expected, transformation from martensite twinned to detwinned happened in the first two steps while martensite to austenite transformation was happening in the last step (wire contraction).

3.1.4. Measurement of stress free transformation temperatures

Differential Scanning Calorimetry (DSC) is the most common method to obtain the true zero stress transformation temperatures of Shape Memory Alloys. Samples are put into a small aluminum pan, then heated and cooled down at a constant rate. During these periods, DSC measures the heat flow of the samples due to material phase transformations. The experiments were performed using a DSC 2920CE machine (TA Instrument, New Castle, DE, USA). In these experiments, liquid Nitrogen was used as both the cover and purge gas. There were two sets of experiments performed. The first set of experiments was performed on wires in their as-received conditions. The second set of experiments was performed on wires that were previously annealed. ASTM-F2004-05 standard suggests that the SMA wire samples are annealed in an inert environment to avoid oxidation of the samples. Therefore, the wire was first cut up into smaller samples less than 5mm in length.

These pieces then were put into a small pre-made quartz tube (5mm x 7mm IDxOD). The pre-made quartz tube was sealed at one end. A vacuum pump, Maxima C Plus manufactured by Fisher Scientific (Waltham, MA, USA) was used to pump air and moisture out of the tube. The tubes with samples inside had to be vacuumed for a few minutes to ensure complete air removal. The pump suction hose had to pass through a buret submerged in liquid nitrogen to ensure complete moisture removal. The tube was then sealed using a high temperature glass burner.

3.2. Shape memory alloy modeling in MATLAB

Brinson model, one of the robust one dimensional constitutive models, was chosen to simulate the SMA wire behavior. This model is based on previous efforts of Tanaka (Tanaka et al., 1986) and Liang and Rogers (Liang & Rogers, 1990). Tanaka (Tanaka et al., 1986) first derived the constitutive relation for shape memory alloys using thermodynamic principles, Clausius-Duham inequality and Helmholtz free energy:

$$\sigma - \sigma_o = E(\xi)(\varepsilon - \varepsilon_o) + \Omega(\xi)(\xi - \xi_o) + \beta(T - T_o) \qquad 3\text{-}1$$

where σ, ε and T denote the current stress, strain and temperature, respectively. $E(\xi)$, $\Omega(\xi)$ and β are the Young's modulus, phase transformation tensor and thermoelastic coefficient, respectively. Their mathematical definitions mean that they are functions of martensite volume fraction, ξ. The subscript o indicates the initial values of each variable. Tanaka also proposed a phase transformation kinetic rule by using exponential functions. To overcome the limitation of Liang and Rogers model in describing shape memory effect at low temperatures, Brinson proposed to separate the martensite volume fraction into stress induced (ξ_s) and temperature induced (ξ_t) as follows:

$$\xi = \xi_s + \xi_T \qquad 3\text{-}2$$

Due to the introduction of separation of different types of martensite, Equation 3-1 by Tanaka had to be re-defined. Following the same thermodynamics approach of Tanaka, Brinson derived a new constitutive relation, as mathematically defined in Equation 3-3.

$$\sigma - \sigma_o = E(\xi)\varepsilon - E(\xi_o)\varepsilon_o + \Omega(\xi)\xi_s - \Omega(\xi_o)\xi_{so} + \beta(T - T_o) \quad 3\text{-}3$$

where the Young's modulus and the transformation tensors were defined as:

$$E(\xi) = E_A + \xi(E_M - E_A) \quad 3\text{-}4$$

$$\Omega(\xi) = -\varepsilon_{max}E(\xi) \quad 3\text{-}5$$

E_A denotes the Young's modulus of austenite and E_M the Young's modulus of martensite while ε_{max} is the maximum transformation strain, which was assumed to be constant for simplicity in implementation. Based on the kinetic transformation cosine function of Liang and Rogers, as well as the critical stress definition, Brinson redefined the kinetic phase transformation to accommodate newly defined ξ_T and ξ_s (Brinson, 1993). Other additive inputs in her model were σ_s^{cr} and σ_f^{cr} which are the start and finish critical stresses for detwinning process. The phase transformation kinetic was mathematically defined as:

For $T<M_s$ and $\sigma^{cr}_s < \sigma < \sigma^{cr}_f$:

$$\xi_s = \frac{1-\xi_{so}}{2}\cos\left(\frac{\pi}{\sigma_s^{cr}-\sigma_f^{cr}}\left(\sigma - \sigma_f^{cr}\right)\right) + \frac{1+\xi_{so}}{2} \quad 3\text{-}6$$

$$\xi_T = \xi_{TO} - \frac{\xi_{TO}}{1-\xi_{so}}(\xi_s - \xi_{so}) + \Delta T_\xi \quad 3\text{-}7$$

where, if $M_f < T < M_s$ and $T < To$:

$$\Delta T_\xi = \frac{1-\xi_{TO}}{2}\left(\cos\left(a_M\left(T - M_f\right)\right) + 1\right) \quad 3\text{-}8$$

else:

$$\Delta T_\xi = 0 \quad 3\text{-}9$$

For T>M_s and $\sigma^{cr}_s + C_M(T-M_s) < \sigma < \sigma^{cr}_f + C_M(T-M_s)$:

$$\xi_s = \frac{1-\xi_{so}}{2} cos\left(\frac{\pi}{\sigma_s^{cr}-\sigma_f^{cr}}\left(\sigma - \sigma_f^{cr} - C_M(T-M_s)\right)\right) + \frac{1+\xi_{so}}{2} \quad 3\text{-}10$$

$$\xi_T = \xi_{TO} - \frac{\xi_{TO}}{1-\xi_{so}}(\xi_s - \xi_{so}) \quad 3\text{-}11$$

For T> A_s and $C_A(T-A_f) < \sigma < C_A(T-A_s)$::

$$\xi = \frac{\xi_o}{2}\left(cos\left(a_A\left(T - A_s - \frac{\sigma}{C_A}\right)\right) + 1\right) \quad 3\text{-}12$$

$$\xi_s = \xi_{so} - \frac{\xi_{so}}{\xi_o}(\xi_o - \xi) \quad 3\text{-}13$$

$$\xi_T = \xi_{TO} - \frac{\xi_{TO}}{\xi_o}(\xi_o - \xi) \quad 3\text{-}14$$

where a_M and a_A are mathematically defined as:

$$a_M = \frac{\pi}{M_s - M_f} \quad 3\text{-}15a$$

$$a_A = \frac{\pi}{A_f - A_s} \quad 3\text{-}15b$$

3.3. Temperature profile of the SMA wires

Since the actuators are activated using the resistance heating, it is important to study the actuators heat transfer mechanisms. Terriault and Braislovski (Terriault & Brailovski, 2011) proposed an iterative scheme to predict the variation of temperature in the actuators by considering the dominant heat transfer mechanism such as environmental convection, resistance heating and latent heat difference due to the phase transformation. The formulation is briefly summarized here. The energy generated in the wire (E_G) is contributed by resistance Joule heating (E_{JE}) and latent energy of transformation (E_{LH}):

$$E_G = E_{JE} + E_{LH} \quad 3\text{-}16$$

with the resistance Joule heating defined as:

$$E_{JE} = Ri^2 \Delta t \quad 3\text{-}17$$

where i is the average current applied during the time increment and R is the resistance of the wire. R is a given by the mixing law of the global phase volume fraction based on the electrical resistivity of austenite and martensite.

The latent heat of transformation can be calculated using the increment of the global volume fraction of martensite ($\Delta\Xi_M$), the latent heat of transformation (Q_{PT}), and the actuator volume. The actuator volume is a product of the wire cross sectional area (S) and its length (L).

$$E_{LH} = Q_{PT}SL\Delta\Xi_M \qquad 3\text{-}18$$

The energy generated can be lost due to the convection (E_C) or the energy stored in the wire (E_s).

$$E_G = E_C + E_S \qquad 3\text{-}19$$

The convection energy can be described as a function (Equation 3-20) of the actuator convection coefficient (h), the length of the wire (L) and also the perimeter of the wire (P).

$$E_C = hLP(T_w + T_{AMB})\Delta t \qquad 3\text{-}20$$

where T_{AMB} and T_W is the average ambient air temperature and the average wire temperature during a time increment (Δt), respectively. Therefore, the wire temperature change during the time increment can be derived as Equation 3-21.

$$\Delta T_w = \frac{Ri^2\Delta t + Q_{PT}SL\Delta\Xi_M - hLP(T_w - T_{AMB})\Delta t}{\frac{hLP\Delta t}{2} + C_{pdLS}} \qquad 3\text{-}21$$

3.4. Finite element analysis for structural behavior of the active needle

A 3D FE model of the active cannula (see Figure 3-2) was developed in ANSYS to predict the cannula's deflection while actuated by attached SMA wires. This model was also used to investigate the effect of various design parameters on the cannula's deflection. The structure consists of two identical sections each 50mm long. The SMA wires were attached to the cannula through an 18mm diameter, 0.83mm thick stainless steel collet. The cannula's inner and outer diameter was D_{in}=0.88mm and D_{out}=1.59mm, respectively. Both cannula and actuator were modeled using SOLID65 elements. Material properties of the cannula were chosen to be linear elastic steel which is a usual material for surgical cannulas; though titanium and carbon-fiber are also used. This model was validated with the experiments done with a developed prototype which will be described in chapter 3.5.

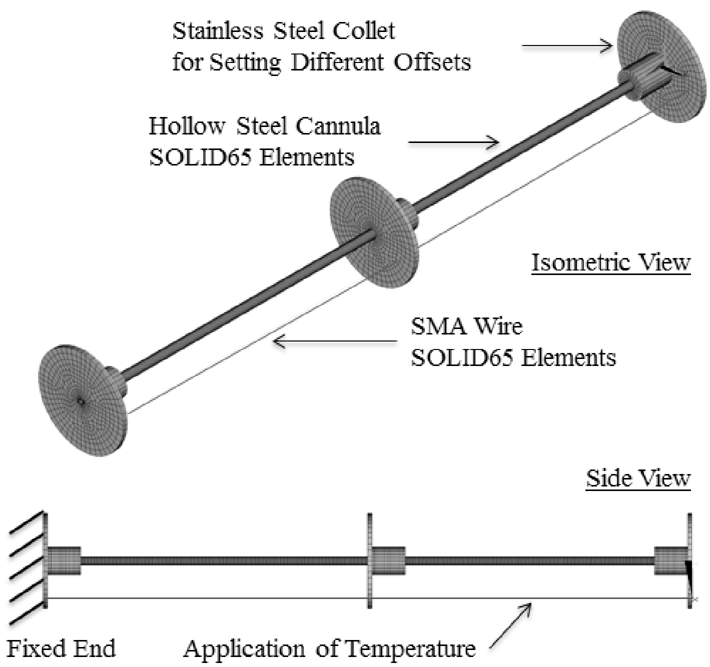

Figure 3-2: Geometry and mesh of a two-section active cannula modeled in ANSYS.

The maximum contraction (or the stroke length) of the SMA wire depends on its initial pre-strain condition prior to the actuation step. This pre-strain condition on SMA elements was achieved using the birth and death capability of ANSYS, which was implemented in three steps. First, a tensile pressure load was applied to the collet while all cannula elements were killed (removed from the structure) that resulted in tensile stress in the cannula. Then the cannula elements were made alive (inserted back to the structure) and the tensile load was removed. The equilibrium position after the second step consists of tensile stress in the SMA wire and a small compressive stress in the cannula. Lastly, to actuate the SMA wire, the wire temperature was increased from room temperature (22ºC) to 80ºC (above the austenite finish temperature) that contracts the SMA wire and consequently bends the cannula.

Defining an appropriate constitutive material model for the SMA wire was a challenging part of this study due to the complex relationship between stress, strain and temperature. This complex behavior is due to the crystallographic transformation that happens under different loading conditions. Furthermore, since none of the commercial FE software supports the shape memory behavior of SMAs, the material model was simulated using isothermal stress-strain curves obtained from a MATLAB implementation of the Brinson model.

3.5. Prototype development

Figure 3-3 shows the prototype of the cannula that was developed to validate the FE model. The structure consisted of a hollow steel cannula with inner and outer diameter of D_{in}=0.88mm and D_{out}=1.59mm, actuated by two FLEXINOL SMA wires (Dynalloy Inc., Tustin, CA, USA) attached to an 18mm diameter stainless steel collet in two sections. Additionally, five other prototypes were developed with different dimensions as shown in Table 3-1. The FE model was validated using the six manufactured prototypes. These prototypes also brought the privilege of investigating the real-time response of active cannulas with different geometries, stiffness and actuations.

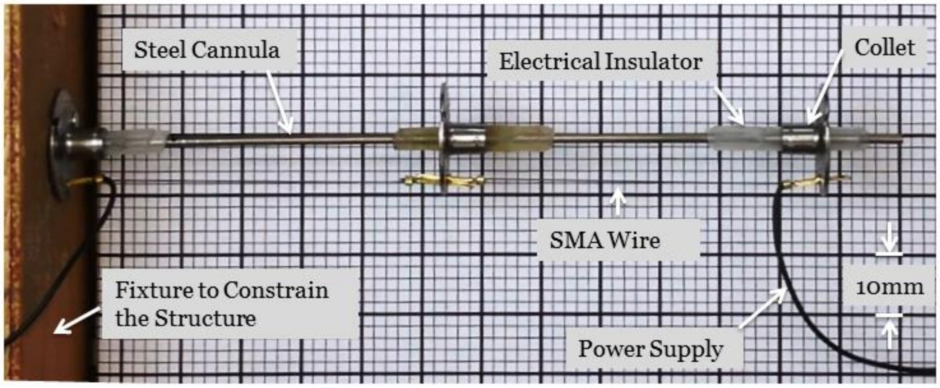

Figure 3-3: Experimental setup for measuring the deflection of the prototype.

SMA wires with diameters of 0.24 and 0.29mm were used for actuation purposes. The offset between the SMA wire and the neutral axis of cannula was set to 7.0mm for all the prototypes using a drilled hole on the holder. This offset was chosen as it was a convenient location on the holder to set the SMA's pre-strain condition and also to force the actuator to follow the desired loading path. This offset distance, however, is much larger than the allowable limit for clinical use, to address this point another design of prototype was developed with a much smaller offset distance; this new design will be introduced in chapter 3.8. The Joule heating method similar to the one described in the constant strain experiment was used here to actuate the SMA wire. The amount of deflection was quantified by taking pictures of the deflection with the background of a graph sheet, which was placed below the structure. The pictures were captured using a high speed camera (Fastec inline camera, Fastec Imaging, San Diego, CA, USA) and are then processed using the ImageJ software 1.45s (National Institutes of Health, Bethesda, MD, USA). The resolution of the image was 0.20mm/pixel. The stabilization of the actuator in the cannula's lumen is important as the positioning can cause an uncontrollable behavior. The out of plane movement of the cannula was minimized by having completely fixed and precise attachment of the actuators on the holders. In this work, pictures taken from sideways showed negligible out of plane deflections, while the deflection of the active cannula was controlled by the amount of current applied. Also the same prototypes of active needles were repeatedly tested in a closed-loop control system, explained in (Orlando et al., 2014) to show a precise and consistent response of our design.

Table 3-1: Different prototypes used in this study (all dimensions are in mm).

Prototype	Cannula D_{in}/D_{out}	SMA Diameter/Length	# of Sections	Total Length	Cannula Moment of Inertia
P1	0.88/1.59	0.24/100	1	100	0.284
P2	1.67/2.38	0.24/100	1	100	1.192
P3	2.46/3.18	0.24/100	1	100	3.220
P4	0.88/1.59	0.29/100	1	100	0.284
P5	0.88/1.59	0.24/50	2	100	0.284
P6	0.88/1.59	0.24/50	1	50	0.284

To improve the maneuverability of the actuated cannula it was necessary to consider the effects of various influencing parameters such as the cannula's Young's modulus, the SMA wire's pre-strain and its offset from the neutral axis of the cannula. The FE model described above was used to study the effect of the design parameters on cannula's deflection. Parametric studies were done with various FE models, where the range of 70 to 200GPa was selected for the cannula's Young's modulus while actuated by SMA wire of diameters of 0.20, 0.24 and 0.29mm, 1 to 6% for SMA's pre-strain and 3 to 7mm for the offset values.

3.6. Design parameter study

Figure 3-4 shows the variation in the deflection of the cannula (D_{in}=0.88mm and D_{out}=1.59mm) actuated by 0.20, 0.24 and 0.29mm SMA wires as a function of cannula's Young's modulus. These diameters of the SMAs were selected because the amount of force generated by them was enough to bend the structure. Since transformation temperatures and Clausius-Clapeyron coefficient vary with wire diameter, for studying each wire these parameters were determined experimentally and then used to obtain the appropriate isothermal curves. On the other hand, the actuation response time of the prototype was found to differ using different wires.

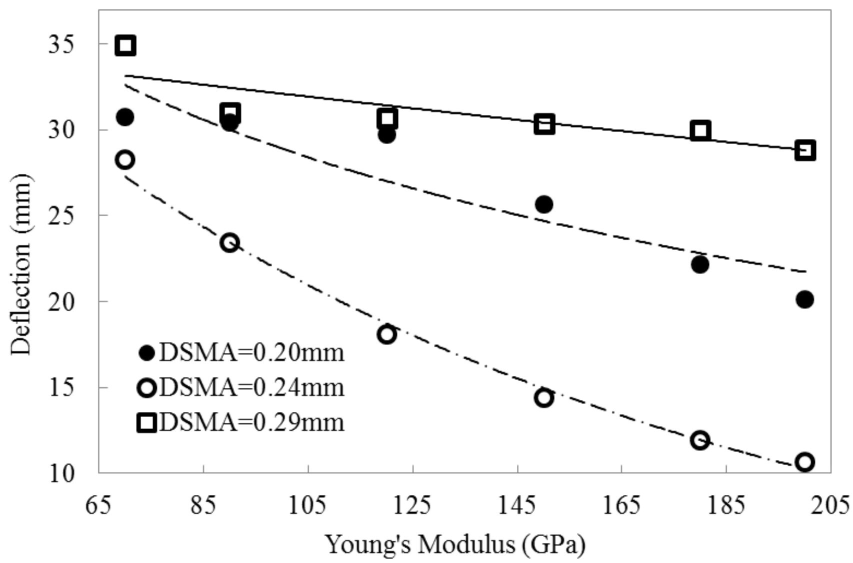

Figure 3-4: Deflection of cannulas of different Young's modulus.

Figure 3-5 shows how the cannula deflection is affected by SMA's pre-strain and its offset from the neutral axis of the cannula. The aluminum cannula with D_{in}=0.88mm and D_{out}=1.59mm actuated by 0.29mm SMA wire was used here. It can be seen that, as expected, as pre-strain on the wire prior to the actuation increased the deflection increased. Increasing pre-strain provides the SMA wire the capability to contract more when actuated with applied current. Figure 3-5 also shows the effect of offset between the SMA wire and the cannula on the deflection. It was observed that the deflection increased as the offset and the applied moment increased. The observed nonlinear relationship between the deflection and the applied moment was the nonlinear path that the SMA wire was following in the isothermal curves while placed at different offsets from the cannula. Increased resistance on the SMA wire caused higher stress on the wire and consequently lower strain.

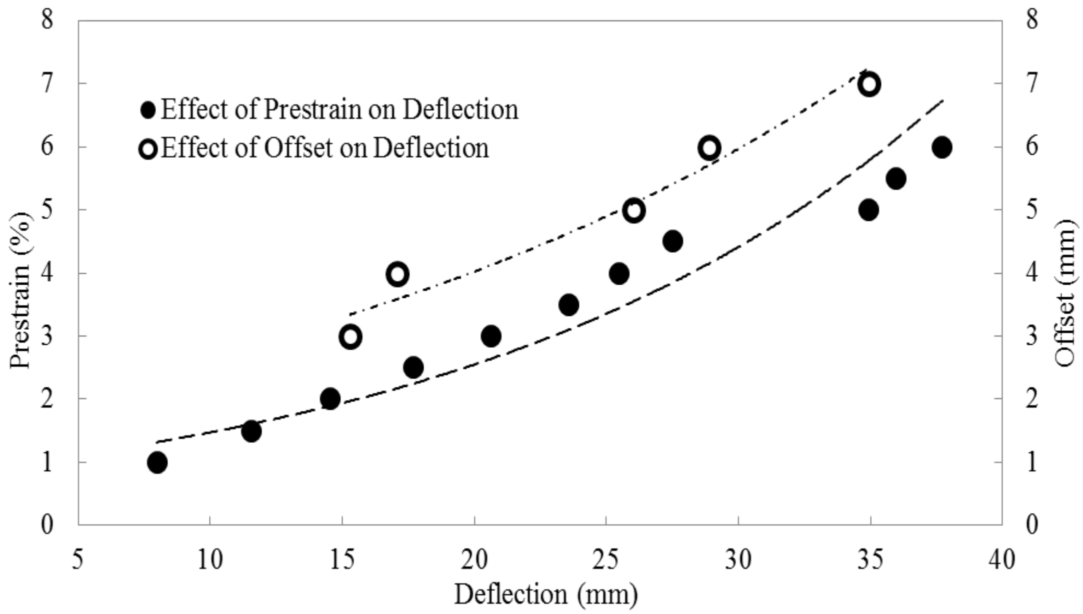

Figure 3-5: The effect of SMA's pre-strain and its offset from the neutral axis of the cannula on the maximum deflection.

3.7. Optimization process

3.7.1. Optimization of the active needle design

Design optimization of structures with active materials can be a challenging endeavor. Iterative analysis tools presented in chapter 2.1 (as illustrated in Figures 2-1 and 2-2) were utilized here to aid the design process. Several design variables were taken into consideration to accomplish this task. A 100mm long SMA wire attached to the needle with a stainless steel holder was considered as the initial configuration. In order to have a lower computational time in the structural iterative assessments, the simplified model (presented in chapter 3.7.2) was used instead of the complete FE model (presented in chapter 3-4). Moreover, the simplified model provides global results of deflections and forces with reasonable accuracies. Table 3-2 lists the deflection of the active needle predicted by the simplified model compared with the first prototype. It is also shown that the results of the FE model with nonlinear stress-stress curves are very close (with less than 3% deviation) to the simplified model. It should be noted that only the final deflection of the structure can be trusted with the simplified model since the nonlinear hysteresis response of SMAs cannot be predicted by the thermal expansion coefficient defined in this method. Assigning one dimensional element to SMA wire can lead to some degree of errors on the amount of stress; therefore a 100% safety factor was considered to avoid the plastic deformation. The objective in our design study was to achieve the maximum possible needle tip deflection to ensure the maximum flexibility while constraining the stress of SMA wire to be less than a critical level. The input design variables selected were as follow:

ε_L: maximum residual strain of SMA wires with different diameters

D_{SMA}: SMA wire diameter

$D_{outcannula}/D_{incannula}$: cannula's outer/inner diameter

offset: the offset distance between the neutral axis of cannula and SMA wire

$D_{outholder}/D_{inholder}$: outer/inner diameter of the holder

th: the thickness of the holder

L: total length of the cannula

L_1: holder length

The total deflection of the needle tip (δ_{tip}) and the maximum stress (σ_{max}) of all elements were taken as desired output variables. The baseline design point and the range of variation of each parameter which were used in our goal driven optimization study are stated in Table 3-2. Starting from the initial baseline design point we sought the maximum needle tip deflection with the constraint that the SMA's maximum stress must be lower than 150MPa. This optimization task was done using two approaches: Design of Experiments (DOE) and Multi-Objective Genetic Algorithm (MOGA). It should be noted that the selected bond for the offset makes the overall scale of the needle much larger than the conventional needles (which are in the range of 18 Gauges ~ OD=1.27mm). In order to have a needle this small, another method for attaching SMA wires is preferable. Therefore another design was introduced by the same authors (Datla, Konh, & Hutapea, 2014a) to eliminate the collet component completely. In this work however, the effect of offset along with the other effective design parameters is discussed.

Table 3-2: Parameters used for optimization study.

Input Parameter	Initial Design Point	Lower Bound	Upper Bound
ε_L (%)	5.00	4.50	5.50
D_{SMA} (mm)	0.20	0.08	0.30
$D_{outcannula}$ (mm)	1.50	1.30	2.00
$D_{incannula}$ (mm)	1.00	0.50	1.29
$D_{outholder}$ (mm)	15.0	10.0	20.0
$D_{inholder}$ (mm)	5.0	4.5	6.0
offset (mm)	7.00	2.00	8.00
th (mm)	1.00	0.90	1.10
L (mm)	100	80	120
L_1 (mm)	1.00	0.90	1.10

The DOE task, which is a non-iterative direct sampling method, was performed by choosing 100 random possible configurations by ANSYS. Once this task was accomplished, a large collection of samples and a response surface based on the objectives and constraints was obtained providing a global overview.

The MOGA study, available in ANSYS, was also performed that provided a more refined approach to find the best design configuration. This optimization algorithm started with the initial design point (shown in Table 3) and iterated through the whole domain with the samples evolving genetically until the best case was found.

3.7.2. Thermal expansion method as a simplified FE model

A simplified approach was used to develop a FE model of the SMA actuated needle. In this approach the strain response of the SMA wire was approximated while thermally actuated above austenite start temperature. To have a good approximation the constant-stress experiment described above was repeated for different stress levels to find the contraction range of the wire (shown in Figure 3-6 for 0.20mm diameter SMA wire). This strain response of the wire was estimated by defining the thermal expansion coefficient, α, as shown in the Equations 3-22 and 3-23. This value of α was producing the same strain response as the wire temperature rises from A_s to A_f. FE model with the same geometry and dimension as described above was used in this approach. Element BEAM188 and SOLID185 were used for the wire and the cannula, respectively.

$$\alpha = \frac{H}{A_s - A_f} \qquad 3\text{-}22$$

$$\alpha = -\,0.0096^{\circ}C^{-1} \qquad 3\text{-}23$$

The negative sign in Equation 3-23 shows that by increasing the temperature above A_s the material goes through the transformation to austenite phase which leads to the negative strain because of the smaller crystallographic shape.

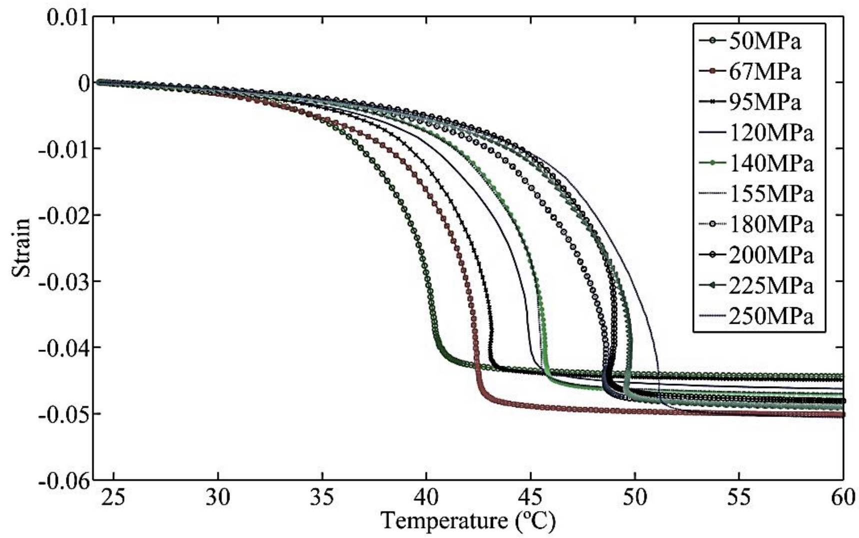

Figure 3-6: Strain response of 0.20mm SMA wire under different constant stresses.

3.8. Real size prototype of the active needle

Our proposed design of the active needle includes two concentric steel tubes, which are connected by a flexible component. Figure 3-7 shows the active needle of outer and inner diameter of 2.05mm and 1.70mm, respectively. The tube outer diameter is equivalent to 14G devices used in prostate brachytherapy procedures. The shape memory alloy wire (our actuator in the design) was attached to the needle by passing through drilled holes on the body of the needle at one end, and fixed by using a crimp at the other end. Shrinking plastic tubes and super glue (Loctite 415, Henkel, EU) were used to prevent the SMA wire from sliding during its contractions due to the applied current. Contraction of about 5% of the SMA wire (Flexinol from Dynalloy Inc., Tustin, CA, USA) along with its biocompatible properties make it a suitable candidate for our actuator component. The SMA wire with the diameter of 0.20mm was selected.

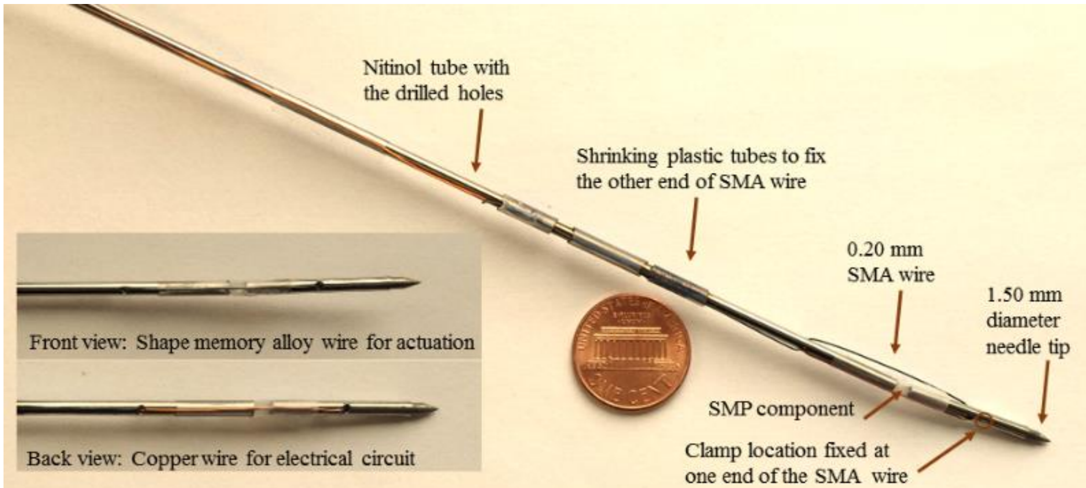

Figure 3-7: Prototype of the active needle using activation force of both SMA and SMP.

There are two major tasks expected from the flexible connector: (i) to provide an electrical insulation between the two segments of the needle to prevent a short cut circuit, and (ii) to act like a joint type connection in the needle system. The nylon connector, if chosen as the connector component, would be unable to recover its original shape after each trial therefore it had to be manually altered to be brought back to its initial shape. Using the SMPs as suggested by this work would help recover the structure after each round of activation. The SMP's recovery is due to an applied heat above its glass transition temperature (Tg).

3.8.1. Shape memory polymer as an additional active component

In this work, it is specifically aimed to incorporate an additional active component made of shape memory polymer (SMP) for the prototype. The unique capability of the

SMP to recover its shape at temperatures higher than its glass transition temperature is aimed to be used to get the needle structure back to its original shape after each actuation stage.

SMPs could be made by different chemical structures and crosslinking densities. A challenging task incorporating SMPs in active needle is to control its temperature while heated. Different concentrations of SMPs show different glass transition temperatures and thereby requires in depth investigations. In the current work, accurate temperature measurements have been presented, while the force measurements of different types of SMPs are left for future studies.

The primary actuation component in our design is the shape memory alloy wire, where the main bending forces are provided for the needle. However, we are aiming to utilize the shape memory polymer as a secondary active component. Two different types of SMP were used in this work for the joint connection with different concentrations: (i) containing approximately 70% butyl methacrylate (BMA) 30% Poly(ethylene glycol) dimethacrylate (PEGDMA), and (ii) 50%BMA and 50% PEGDMA. These two types were selected for our needling system for their considerably high stiffness and suitable glass transition temperatures. However, the glass transition temperatures, for the SMP, is tunable to some extent. The glass transition temperature is the most significant characteristic parameter that has to be found prior to performing the SMP's actuation capabilities. A Differential Scanning Calorimetry (DSC) test was performed to obtain the transition glass temperatures of the SMP component. Samples were put into a small aluminum pan, then heated and cooled at a constant rate. During heating and cooling, the heat flow of the samples due to phase transformations was measured. The experiments were performed using a DSC 2920CE machine (TA Instrument, New Castle, DE). Liquid Nitrogen was used as both the cover and the purge gas. Also, as another way to determine the glass transition temperature, while heating the SMP component, its temperature was captured carefully using attached thermocouples and an infra-red camera; then the real-time videos were analyzed to determine the moment of actuation as will be described later on.

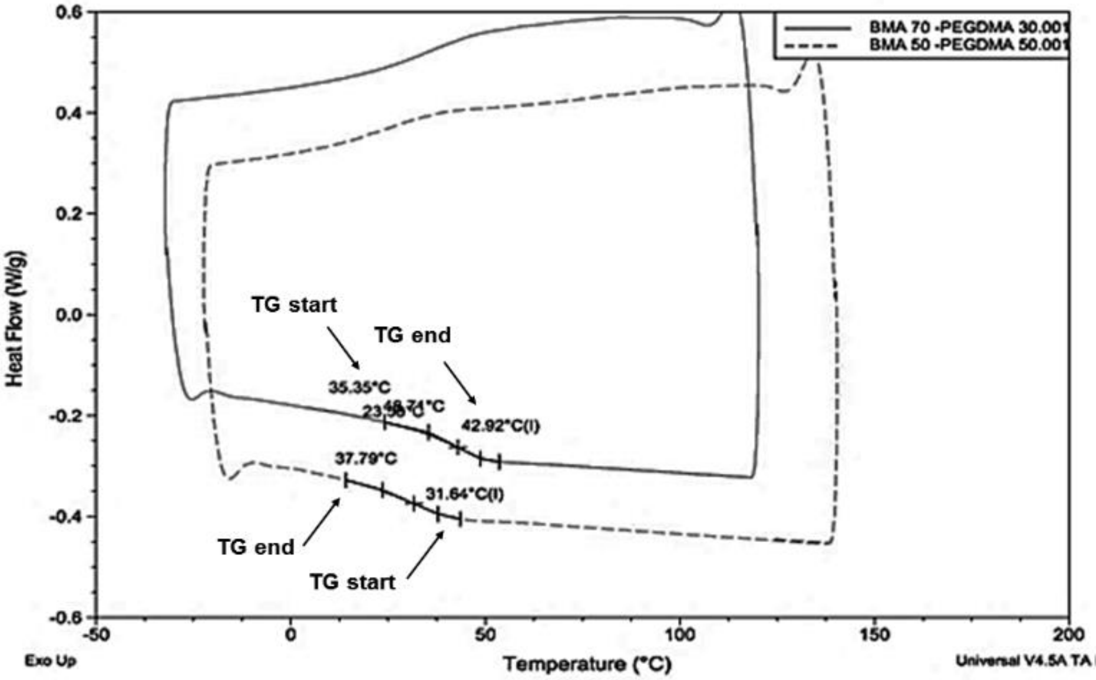

Figure 3-8: DSC results for the SMPs with BMA:PEGDMA concentrations of 70:30 and 50:50.

Results of the DSC test is shown in Figure 3-8 for SMPs with BMA:PEGDMA ration of 70:30 and 50:50. The transition temperatures for the SMP of BMA:PEGDMA ratio of 50:50 was starting and ending at 31.64ºC and 37.79ºC, respectively; while for the SMP with ratio of 70:30 the transition temperatures of 35.35º and 42.92ºC were reported.

An active prototype shown in Figure 3-9 was then made in order to evaluate the feasibility of incorporating the SMP as another actuation component for the needle structure. The prototype consists of two steel tubes with inner and outer diameter of 1.70mm and 2.05mm, respectively connected with a SMP component of the matching size.

To heat the SMP element, a partially stripped copper wire was wrapped around the joint as to pass an electrical current using a DC power supply (BK Precision 1696, Yorba Linda, CA, USA). Figure 3-9 shows the recovery of the SMP structure after an induced deformation with an applied current of 0.70A. The temperature of the SMP during actuation was captured by using an infra-red camera (FLIR Systems, Inc., Wilsonville, OR, USA) and an attached k-thermocouple (Omega Engineering, Stamford, CT, USA).

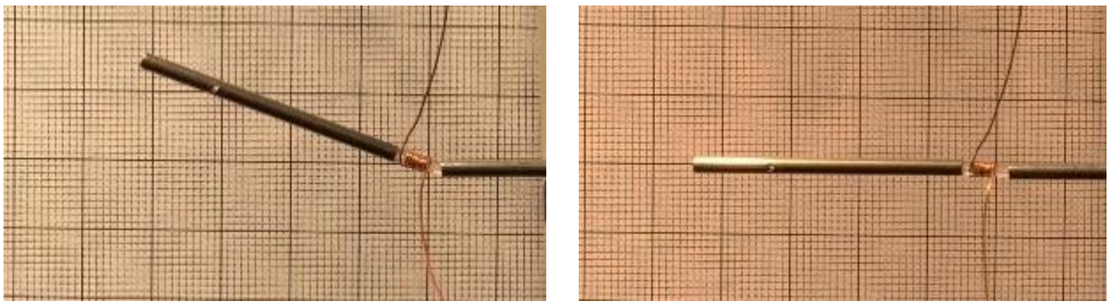

(a) (b)

Figure 3-9: Active needle prototype built by the connected steel tubes using the 70:30 SMP: (a) the bent position by the angle of 25º and (b) the recovered initial configuration after heating above Tg.

3.8.2. Measurements of the glass transition temperatures

Figure 3-10 shows the temperature of the SMP captured by the infra-red camera while heat was supplied though the copper wires. The top row shows the 70:30, while the bottom row shows the 50:50 SMP. The prototypes were bent by 25º (Figures 3-10a and c) and were recovered to its initial position after a complete shape recovery of the SMP component (Figures 3-10b and d). The maximum temperature in the square box, shown in the figure, was detected and considered as the SMP's temperature. For the 70:30 SMP component 0.70A of current was sufficient for the complete recovery of the structure, while for 50:50 component 0.50A of current was enough. It should be noted that application of higher currents should be avoided as the SMPs reduce stiffness and thereby not strong enough to hold on to the structure. However, this behavior is aimed to achieve a higher, more flexible deflection during actuation by the SMA wire.

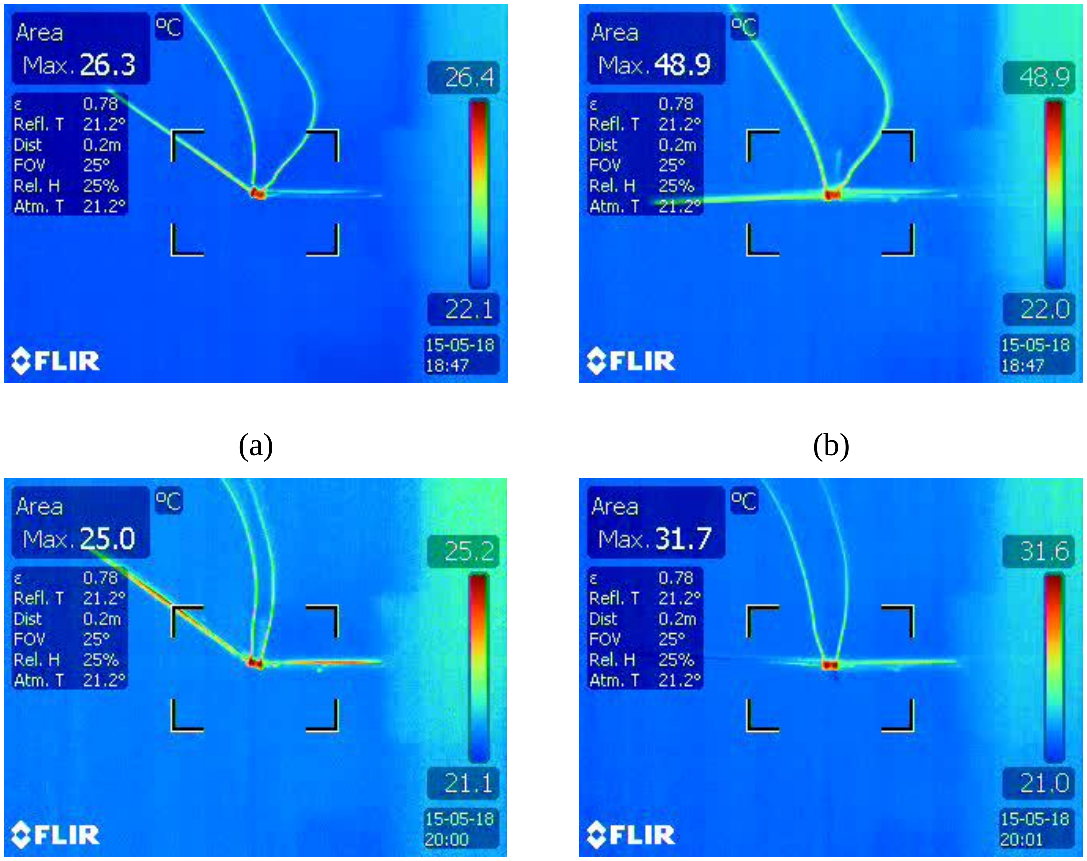

(a) (b)

(c) (d)

Figure 3-10: Temperature of the SMP captured by the infra-red camera for ((a) and (c)) the bent position prior to the actuation, and ((b) and (d)) the recovered position after applying heat. The BMA:PEGDMA concentrations for top row is 70:30, and bottom row is 50:50.

The initial movement of the structure was also recorded by analyzing real-time videos obtained by the infra-red camera (shown in Figure 3-11a and b for 70:30 and 50:50

SMPs, respectively). The glass transition temperatures were found to be 28.4ºC and 36.2ºC for 70:30 and 50:50 SMPs. These values were found comparable with the transition temperature predicted by the DSC results.

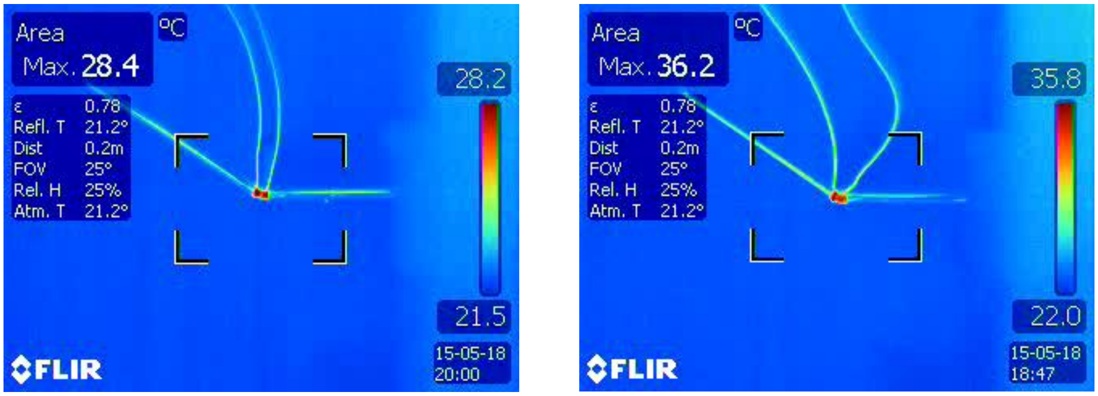

(a) (b)

Figure 3-11: The SMP temperatures at which the actuation starts for BMA:PEGDMA concentrations of: (a) 70:30, and (b) 50:50.

3.8.3. Prototype experimentations

The deflection of the prototype is shown in Figure 3-12. The SMP was heated above its transition temperature to provide a more flexible joint. By using this method the amount of force required to get the needle deflected by some amount would be less and therefore a more dexterous response would be seen. Compared with the Nylon connector, the deflection was much higher since the flexibility of the reduced stiffness SMP was higher. Figure 3-12a shows the deflected active needle due to the application of 0.80A current to the SMA wire, while Figure 3-12b shows the recovered configuration after the SMA is cooled to room temperature. For a total recovery SMP was cooled and heated in an additional cycle to get to the exact initial position. The curved shape of the active needle prior to the actuation is due to the pre-strain condition of the SMA wire.

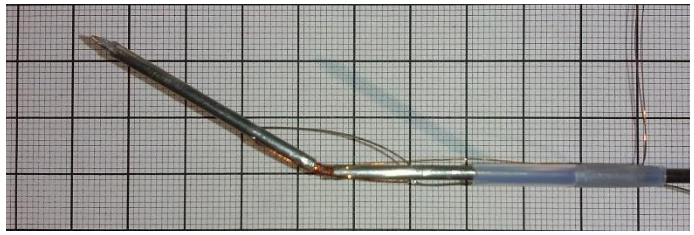

(a)

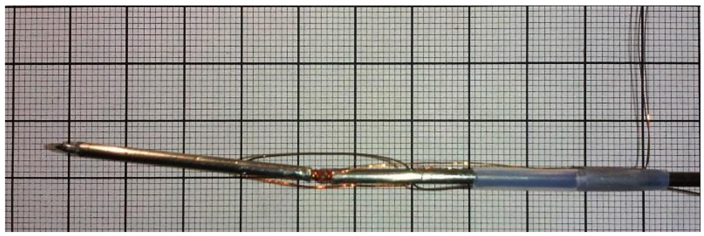

(b)

Figure 3-12: (a) Deflected shape of the active needle due to the actuation of the SMA wires while the SMP component is heated above its glass transition temperature, and (b) the recovered initial position of the active needle.

3.9. Needle insertion experiment

Figure 3-13 shows the needle insertion setup developed to validate the FE simulations. The phantom material was made of Plastisol gel (M-F Manufacturing Co., Ft. Worth, TX, USA), where the elastic modulus of the phantom could be controlled by the compositions of polyvinylchloride suspension and softener. As it was shown in studies of Misra et al. (Misra, Reed, Schafer, Ramesh, & Okamura, 2010) changes in the volume ratio of plastic to softener from 3:1 to 8:1 increases the elastic modulus from 22.29 to 45.24kPa. In this study, Plastisol was prepared with 3:1 ratio of plastic to softener. The elastic modulus of the phantom was measured by an indentation test shown in Figure 3-13. The load frame was made to have the spherical 10mm diameter indenter normal to the surface of the phantom which was laid unconstrained on the table. The indentation test was done to the depth of 4mm and speed of 1mm/s followed by unloading to the original position at the same speed. The initial moment of contact was captured prior to running the test by tracking the force response using a 5N load cell while the indenter was advancing by increments of 4µm. Then the elastic modulus was calculated using Oliver-Pharr method (Oliver & Pharr, 1992) from the slope of fourth degree polynomial fit at the start of the unloading curve by the equation below.

$$dP/dh = \frac{2}{\sqrt{\pi}}\sqrt{A}\frac{E}{(1-\vartheta^2)} \qquad 3\text{-}23$$

In this equation υ is the Poisson's ratio that is assumed to be 0.49, E is the Young's modulus and A is the area of contact based on the equation below suggested by Herzian (Hertz H. R., 1882).

where δ is the indentation depth and R is the indenter's radius.

Insertion tests were done with bevel-tipped needles made of spring steel having bevel angles of 29.25°, 32.73°, and 32.04° for needle diameters of 0.38, 0.51, and 0.64mm, respectively. A sharp bevel-tip free of burrs was achieved by embedding the spring steel wire at an angle in CrystalbondTM (Aremco Products, Inc., Valley Cottage, NY, USA) mounting adhesive followed by polishing the assembly. After polishing, the needle was removed from the adhesive and then cleaned with CrystalbondTM stripper.

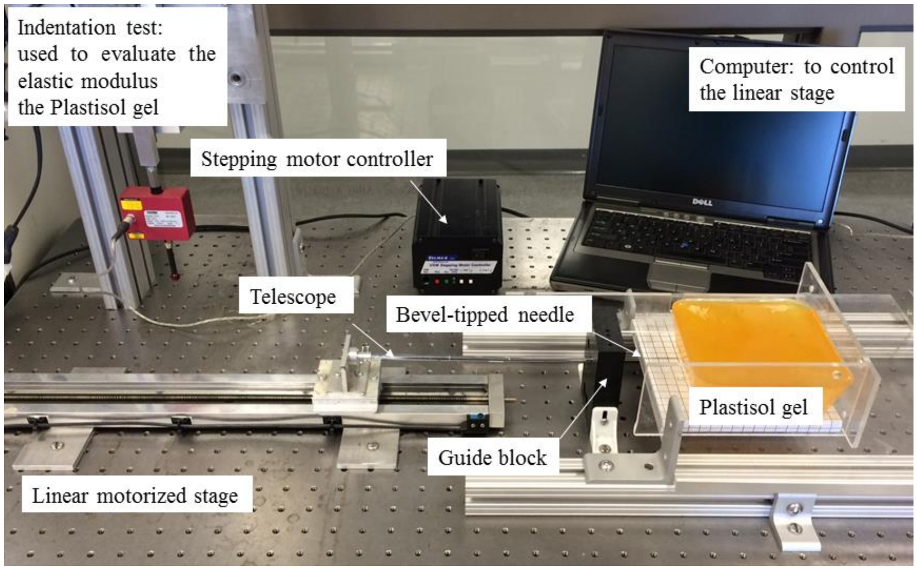

Figure 3-13: The experimental setup used: (i) to measure the elastic modulus of the phantom, and (ii) to robotically insert the needle inside the phantom.

Needles were fixed at one end to the linear stage where the motion was controlled and at the other end next to the tissue using a guide block. Similar to what was seen in the model, buckling was very probable in the experiment as well. Even before insertion a small buckle was observable due to the needle's weight. The buckling was very likely to happen at the early stage of insertion when the needle tends to puncture the tissue. So additional support was provided using a telescope support that kept the needle straight during the whole insertion period. These needles were inserted into the plastisol gel at a constant typical insertion speed of 2.5mm/s by attaching the needle to a motorized linear stage (Velmex Inc., Bloomfield, NY, USA) of 6µm resolution.

3.9.1. Effect of needle geometry on final deflection

Three cases including three different diameters of the needle each with five different bevel tip angles were developed to study the effects of needle diameter and its bevel angle on the final deflection. Needles of diameters 0.38, 0.51 and 0.64mm were selected with the bevel angle ranging from 20° to 60°. The effect of having various interacting areas at the tip was studied through this parametric study. The study can also be used for optimization purposes where the maximum flexibility of the needle is aimed or in the applications for selecting a suitable design of the needle for a certain task. The results of this study are presented in section 4.8.2.

3.10. Needle insertion simulation

3.10.1. Fluid-structure interaction formulation

As of the preliminary step of the needle insertion simulation, the appropriate fluid-structure interaction formulation has to be explored. The main challenge in this category of simulations is to carefully consider the solid elements of the needle penetrating the fluid elements of the tissue. In this study the geometry and mesh of the needle and tissue was generated in LS-DYNA (LSTC, Livermore, CA, USA) software. The cylindrical shape of the needle modeled by rectangular elements increases the complexities due to large number of required elements. The tissue was modeled as a rectangular cube to allow the overall insertion depth that is desired. Surrounding the tissue, a void part was modeled to provide an empty space for the transferred mass of the tissue while pushed by the needle movement. The needle was considered penetrating and bending inside the tissue with a constant velocity.

In this category of simulations where elements of small size and of high Young's modulus are incorporated, the computational time is expected to be high. In our penetration model a very stiff material was used for the needle along with a soft material for the tissue. In the meantime, the size of element representing needle had to be chosen much smaller than the tissue elements because of the small cross-section and the high length of the needle. Therefore, in this model we have needle elements of high aspect ratio and stiffness along with the soft elements of the tissue. These are among the factors that make the simulation computationally expensive, especially when modeling for a long insertion depth. In order to reduce the computation time without sacrificing the results, minimum possible number of needle elements was modeled.

Tissue-needle interactions were simulated using a Lagrangian method with a penalty contact algorithm (*LSTC. LS-DYNA Theory Manual Version 970. r:6030*, n.d.). The coupling algorithm is the communication between the solid elements of the needle and the fluid elements of the tissue. Needle insertion in tissue was simulated using the Arbitrary-Lagrangian-Eulerian (ALE) formulation available in LS-DYNA. The elements that represent the soft tissue were the ALE elements. Using this method, penetration or deformation of the needle does not result in large distortion and instability of the soft tissue elements. The reason is that in ALE type of formulation, nodes do not follow the material flow and instead the elements are being shaped in a way to avoid the highly twisted elements. On the other hand due to the flux of material between elements, the governing equations are in more complicated forms. The hourglass option was turned on to avoid zero energy modes on elements while solving for the internal forces. The time step was selected smaller than a particular value selected by the software for the defined geometry and material properties. Strain increment was also defined equal to the strain rate times the time step size. Using these parameters for formulation the results of needle insertion were obtained.

3.10.2. Real-size insertion model

By setting all the parameters to control the ALE formulation as explained in section 3.10.1, the needle insertion model was developed to simulate the whole insertion depth.

The goal here is to demonstrate that the model represents the needle insertion experiment with reasonable accuracy. This model will be used to study several parameters involved, which for reasons such as limitations in ex-vivo and in-vivo experiments, might be difficult or costly to investigate.

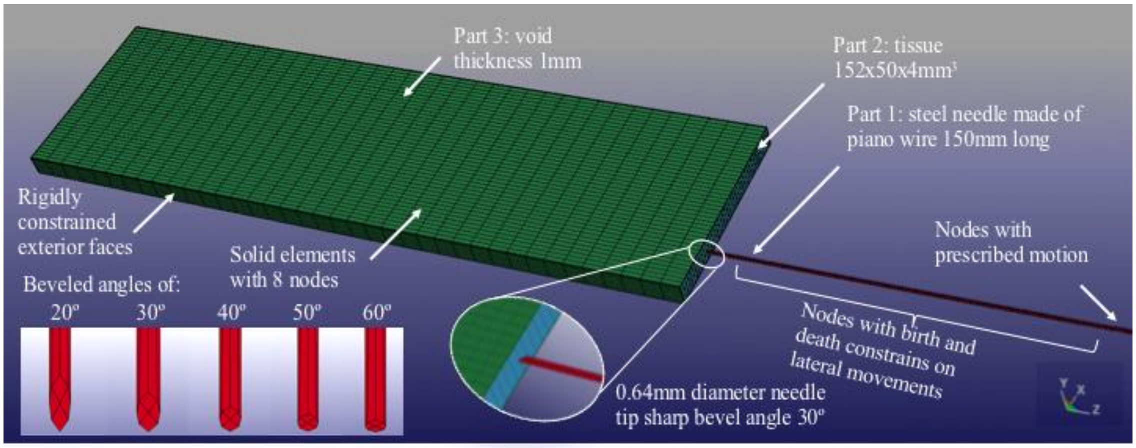

Figure 3-14: Geometry, mesh, initial and boundary conditions for the needle insertion simulation.

A 0.64mm diameter, 150mm long needle with a bevel tip angle of 30° was selected to penetrate a tissue modeled as a box of 50x152x4mm^3. The 8-nodes Solid elements were chosen for both tissue and needle. A void part of the thickness of 1mm was also modeled surrounding the tissue as shown in Figure 3-14 (part 3). The total number of elements of 244, 12464, and 4914 was used in the needle, the tissue, and the void part, respectively. All nodes located on the exterior face of the void part were rigidly constrained. For this model the unit system of Kg-mm-ms was chosen. The needle was inserted from the apex end of the tissue, in the middle of the transverse plane. A motion function with a constant velocity was assigned to the set of nodes located at the ending element of the needle. The prescribed motion curve was defined as a ramp function varying from zero to 15mm/s in 10s. In order to restrict the translational movement of the tissue in space, all the nodes located on the external boundaries of the void part were constrained to move in x, y and z directions. For the total insertion depth of 150mm, a total simulation time of 10s was required. The results were written to a separate database file in every 0.1s of insertion.

The material properties of the tissue were selected based on the published literatures. Because of the common utilization of needle insertion techniques in prostate brachytherapy it was intended here to model the tissue close to the prostate properties. The normal prostate tissue was considered as a linear elastic material with elastic modulus of 24.1+14.5kPa and Poisson's ratio of υ=0.49 (Ahn, Kim, Ian, Rha, & Kim, 2010). Since the variability of elastic moduli is relatively small, in the preliminary model presented here, the soft tissue was considered as a homogeneous material. The void part was chosen to have the similar properties of the tissue.

Buckling was very probable in our simulation because of the needle's high slenderness ratio. Even the small amount of axial force applied to the needle tip from the tissue could buckle the needle, as the calculated critical force was in the range of 0.4N for this size of the needle. In order to prevent buckling, all needle elements located outside of the tissue were constrained from lateral movements using the birth and death constraint option available in LS-DYNA. This constrain was removed from the elements as they were penetrating into the tissue. The birth and death option was representing the telescope support used in the insertion experiment. While the alive, the nodes were prevented from out of axis movement, and while dead the nodes were free to move in any direction.

To decrease the computational time, some assumptions were made to achieve a reasonable convergence time and accuracy. Attempts to refine the mesh in the areas away from the needle did not result in lower computational time. As the needle's stiffness and mesh size were found as two main factors for the expensive computational time, both needle and tissue were modeled as linear materials with Young's Modulus of $1.0\text{x}10^6$ smaller than real values. This provides less computatisonal costs per each time step. To justify this assumption two case studies were modeled through which the scaled Young's Modulus was aimed to be assessed. The results of this case study is presented in section 4.8.2.

CHAPTER 4

RESULTS AND DISCUSSIONS

4.1. Prediction of shape memory alloy wire behavior from the experiments and the model

In this section the obtained transformation temperatures of each SMA wire will be described followed by a brief discussion on the SMA's phase transformation diagram. The validation and comparison between the model and the experiment will also be shown.

4.1.1. Transformation temperatures

A typical strain-temperature response from the constant stress experiment is shown in Figure 4-1a. As shown in the figure, the four transformation temperatures were obtained from the intersection points between tangential lines of the plateau and the transformation curve. At each constant stress level, for each wire diameter, three repetitions were performed to ensure the stability of the material and also to perform the statistical analysis. It was observed that during the first loading cycle a biased strain could remain unrecovered in some wires. This amount of biased strain would be eliminated in the next cycle and therefore a consistent actuation response was being observed in the following loading cycles. The results used to generate the transformation were gathered while the material was showing a stable response. The detailed discussion can be found in the studies of Honarvar et al. (Honarvar et al., 2014). For this reason, in Figure 4-1b only the third repetition was shown. As can be seen, this figure compares strain-temperature response of the 0.20mm SMA wire under various constant stress levels. Zero strain in the figures refers to the initial position of the wire after the weight hanger-transducer rod was first hung. Although ten stress levels were adopted here, only five are shown here for clarity. It can be seen that a higher positive strain is observed at higher stress levels. This is plausible because the initial room temperature strain of each stress level was different due to the mechanical loading of the wire. The higher the stress level, the more it stretches the wire. Therefore, when the wire was heated it reversed back to its shorter, high temperature shape, hence decreasing strain in the heating curve.

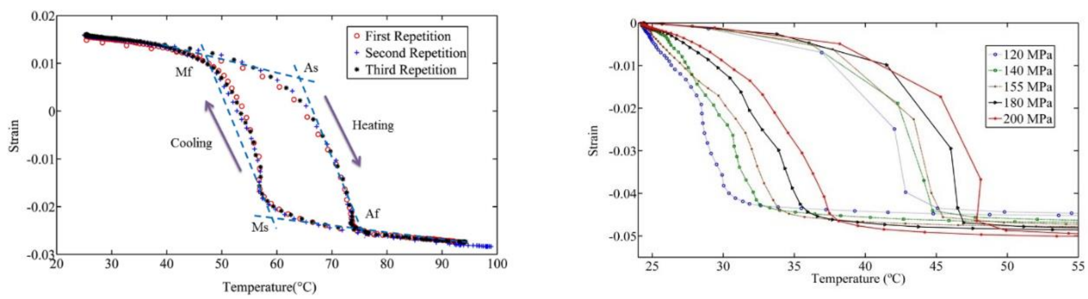

(a) (b)

Figure 4-1: Strain-temperature response of a SMA wire: (a) typical curve to determine the transformation temperatures and (b) curves from a 0.20mm diameter wire under different stress levels.

4.1.2. Phase transformation diagram

Figure 4-2 shows the stress levels plotted against transformation temperatures using the average values of the three repetitions. Average values were used because of relatively low standard deviation. In the figure, the transformation temperatures at zero level of stress were obtained from the DSC test.

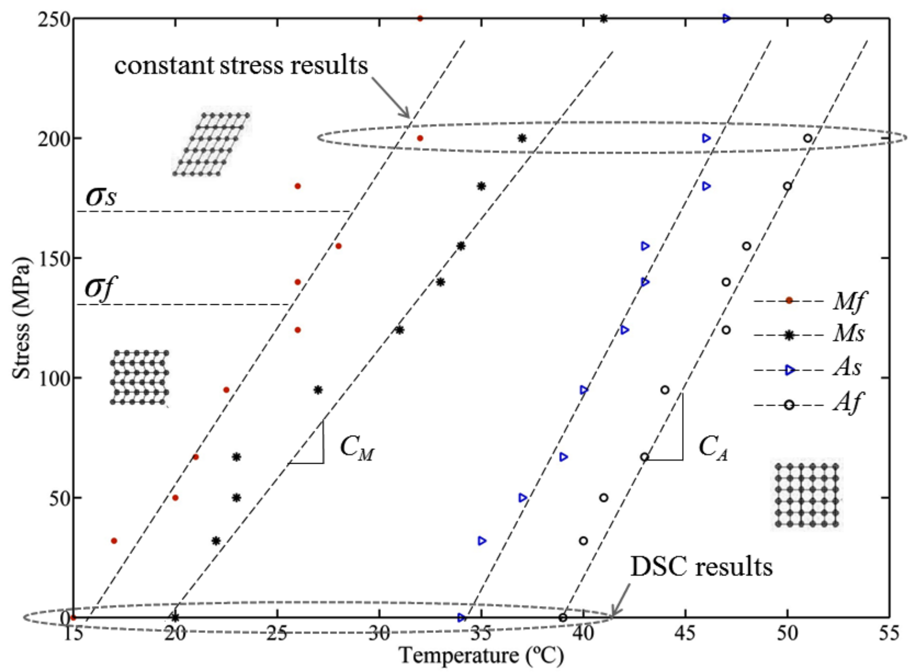

Figure 4-2: Transformation temperatures at different levels of stress for SMA wires of 0.20mm diameter. This figure shows the regions where each phase exist and the regions in which the transformation happens.

The Clausius-Clapeyron coefficients were determined from the slopes of the fitted linear curves, which are 13.5, 10.5, 16.7 and 16.7MPa/°C for M_f, M_s, A_s and A_f, respectively. Average slopes were taken as martensitic (C_M) and austenitic (C_A) Clausius-Clapeyron coefficients. Therefore, C_M and C_A were determined to be 12.0 and 16.7MPa/°C, respectively. Moreover, based on the linear curve fits, the zero stress values of transformation temperatures were extrapolated to be 16.5, 19.4, 34.2 and 38.4ºC for M_f, M_s, A_s and A_f, respectively. As illustrated by Brinson (Brinson, 1993) M_s and M_f should be taken at the stress level where the detwinning process starts (at the stress level of σ_s shown in the figure), so these values should be considered as 25.0 and 31.0ºC respectively. To simulate the actuator mechanical response, other material properties were also needed that were obtained from the room temperature tensile test (shown in Figure 4-2) and tabulated in Table 4-1. The stress levels where the detwinning process start and end are denoted by σ_s and σ_f, respectively. Critical stresses were determined from the intersection points to the tangential lines to the elastic and the transformation parts of the curves, and Young's modulus of austenite or martensite was determined as the slopes of the tangential lines to the elastic part of the curve.

Table 4-1: Additional material properties obtained from the stress-strain response of the SMA wire. These properties were used as input to the Brinson model.

Material Properties	Values
Critical start transformation stress (σ_s)	130 MPa
Critical finish transformation stress (σ_f)	170 MPa
Martensite Young's modulus (E_M)	32.5 GPa
Austenite Young's modulus (E_A)	90 GPa
Maximum residual strain (ε_{max})	0.05

The phase transformation diagram with all the critical stresses could be formed at this point by having the gathered four transformation temperatures plotted vs. temperature at each level of stress (Figure 4-2). This diagram would enable us to predict the areas in which each phase exists and would show when the transformation happens under certain loading conditions. Table 4-2 shows the stress free transformation temperatures and Clausius-Clapeyron coefficients obtained following the same method for other wire diameters. It can be seen that due to the manufacturing process, different wire diameters showed different characteristics.

Table 4-2: Transformation temperatures at zero level of stress and Clausius-Clapeyron coefficients for different wire diameters.

Wire Diameter	M_f (ºC)	M_s (ºC)	A_s (ºC)	A_f (ºC)	C_M (MPa/ºC)	C_A (MPa/ºC)
0.20mm	25.0	31.0	34.2	38.4	12.0	16.6
0.23mm	18.0	23.0	24.0	32.0	8.1	5.7
0.29mm	30.0	35.0	38.0	56.0	6.9	8.3
0.48mm	40.0	45.0	50.0	60.0	6.0	9.3

4.2. Validation of SMA's behavior predicted by Brinson model

The experimental stress-strain response of the SMA wire (shown in Figure 4-3) was also compared with the Brinson model. It can be seen that the simulated response of the wire was in a good agreement with the experimental results, thereby showing the reliability of our model. For more verification the stress-temperature and the strain-temperature of the wires obtained from the constant strain and constant strain experiments respectively is also compared with the Brinson model in the next two sections.

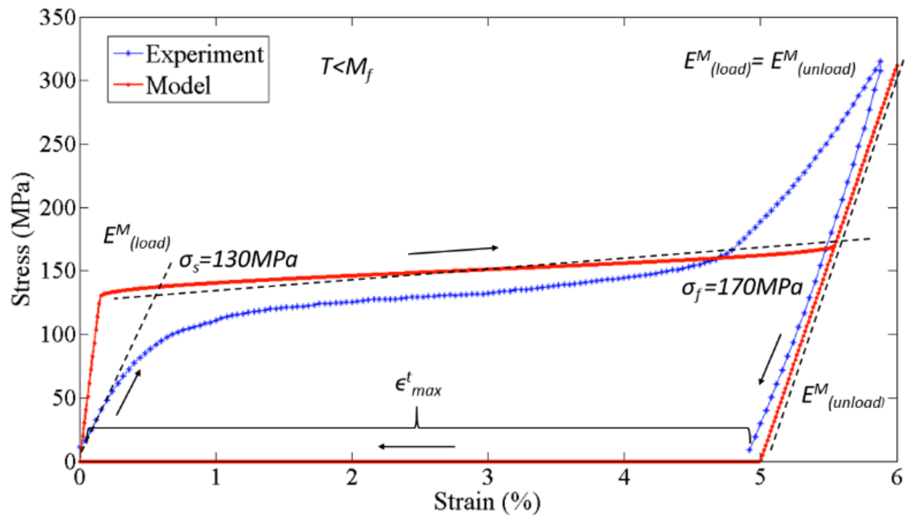

Figure 4-3: Comparison of stress-strain response obtained from the Brinson model and the isothermal test for 0.20mm SMA wire. The stress levels at which the transformation starts and ends, along with the maximum residual strain are shown.

4.2.1. Stress-temperature response

Figure 4-4a compares the stress-temperature response of 0.48mm SMA wire simulated using the Brinson model and that determined from the constant strain experiment. The mismatches could be explained by the errors encountered in measuring the transformation temperatures and Clausius-Clapeyron slopes, primarily resulting from improper crimping and thermocouple attachments.

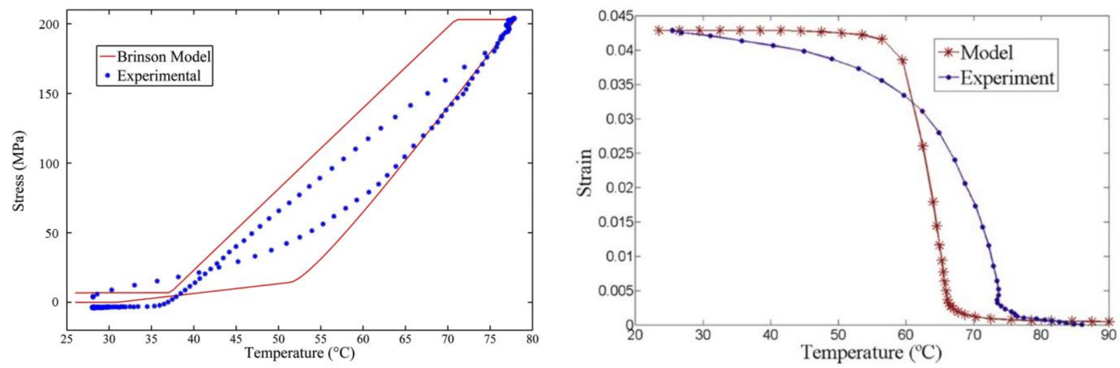

(a) (b)

Figure 4-4: Comparison of (a) stress-temperature and (b) strain-temperature response of SMA wires obtained using the Brinson model and from experiments.

4.2.2. Strain-temperature response

The FE model was compared with experimental results and is shown in Figure 4-4b. It can be seen that the model closely predicted the final strain in the wire, but a mismatch was observed in the slope of the transformation region. The mismatch could be explained by different response time of wires during the experiment. The small size of the wire and the thermocouple and their poor connection introduced difficulties in temperature measurement, thereby could lead to deviation from the numerical prediction.

4.3. Prediction of SMA behavior using Brinson model and temperature model

4.3.1. The isothermal stress-strain curves

To examine the thermomechanical characteristics of SMA wire the isothermal response of the 0.20mm diameter SMA wire predicted by the model at various temperatures is presented in Figure 4-5. At almost all temperatures, the material shows a linear response to the applied stress until it reaches a critical stress after which the SMA goes through a phase transformation, where stiffness decreases and a high amount of strain was observed in the material, in which similar to plastic yielding. After transformation, the material gets stiffer again (due to the presence of complete austenite phase) and a linear response with higher distinctive slope was observed.

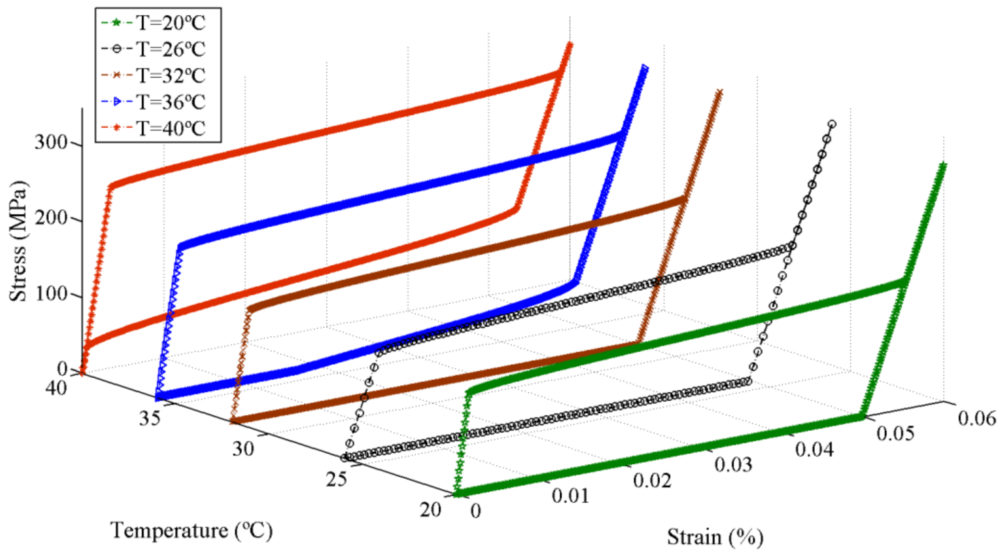

Figure 4-5: Isothermal stress-strain curve for the SMA wire diameter of 0.20mm obtained from the MATLAB code.

At low temperatures ($T<A_s$) applying stress would cause the transformation from the temperature-induced (twinned) martensite to the stress-induced (detwinned) martensite. This transformation enforces the habit planes to align with the direction of the applied force and consequently a large amount of residual strain. This large amount of strain at higher temperatures ($T>M_s$) is caused by the transformation from austenite to martensite phase. Upon unloading, a partial or a complete recovery of strain could be seen due to the different reverse transformation process in the material at different temperatures. For lower temperatures a large residual strain can be observed due to an incomplete transformation to austenite. The material should be heated above A_f to recover this residual strain. For temperatures lower than A_f there would be a partial recovery due to the existence of both austenite and detwinned martensite after unloading. For the temperatures above A_f on the other hand the material can recover the whole amount of strain which is known as the superelasticity effect (Brinson, 1993).

4.3.2. Temperature profile

Figure 4-6 shows negligible differences between the predicted and experimentally measured temperature profiles. These negligible differences suggest that the Terriault and Brailoski (Terriault & Brailovski, 2011) resistance formulation accurately simulated the heat transfer mechanism of Nitinol actuator mechanism. Most of the thermal values (tabulated in Table 4-3) used in this resistance heating simulation were obtained from the manufacturer.

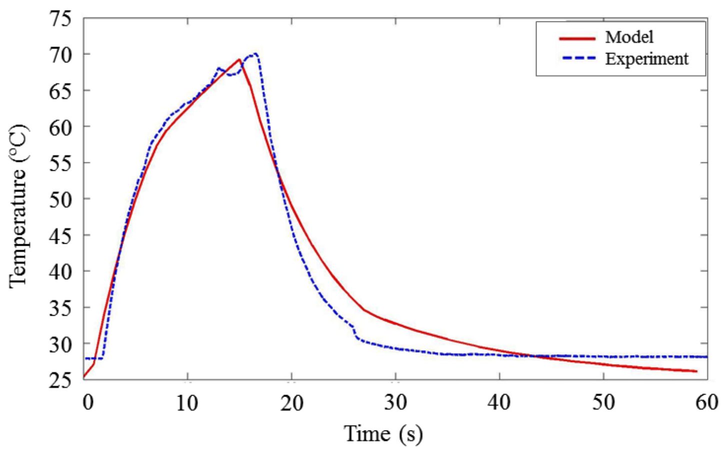

Figure 4-6: Temperature response using Terriault and Brailosvki resistance heating formulation. 1.5A was applied for 15s followed by ambient cooling, D=0.48 mm.

Table 4-3: Thermal properties of the Flexinol wires.

Resistivity of austenite (Ω_A)	1.0e-6 Ω.m
Resistivity of martenite (Ω_M)	8.0e-5 Ω.m
Density of the wire (D)	6450 kg/m^3
Latent heat of phase transformation (Q_{PT})	156e6 J/m^3
Specific heat (C_p)	837.17 J/kg/^{o}C
Convection coefficient (h)	85 W/m^2/^{o}C

4.4. Active needle deflection

4.4.1. Deflection prediction using the finite element model and the prototype

Figure 4-7 shows the cannula's deflection with 0.20mm SMA actuators obtained by the FE models and prototypes both with one (P1) and two (P5) sections. The cannula bends due to the SMA wire's contraction upon increasing the wire temperature, achieved using conventional Joule heating. The maximum deflection of the cannula was ensured by setting the highest pre-strain condition and by applying sufficient amount of current. For the one-section and the two-sections active cannula (D_{in}=0.88mm, D_{out}=1.59mm) the maximum deflection of 24±0.24 and 27±0.33mm was observed (Figure 4-7a and 4-7b), while it was predicted to be 23.45 and 28.58mm by the FE model, respectively. Six prototypes of different configurations as described in section 3.5 were used to validate the FE model.

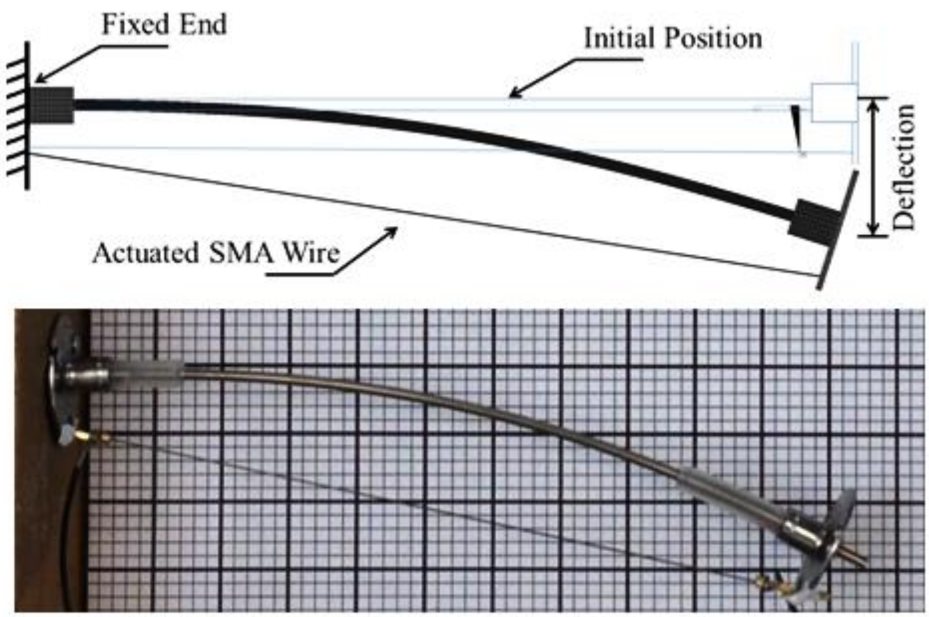

(a)

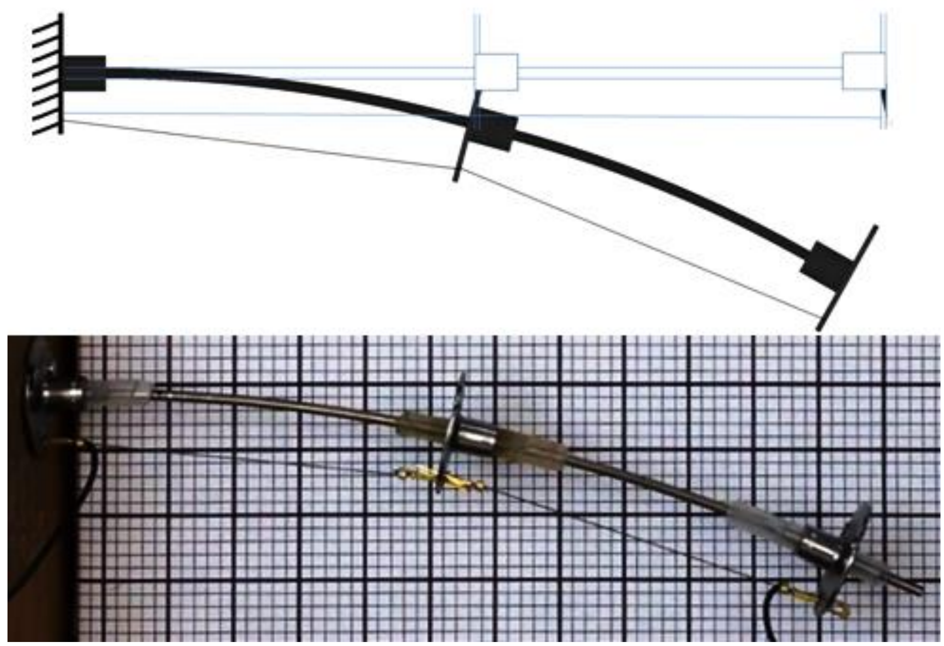

(b)

Figure 4-7: Verification of the FE model using the corresponding prototype for (a) one-section (P1) and (b) two-section models (P5).

Table 4-4 compares the deflection of different cannulas actuated by different SMA wires with the FE model predictions. The difference of less than 10% was observed and therefore validated our FE model.

Table 4-4: The maximum deflection of aluminum prototypes predicted by both experimental test and FE model.

Prototype	Experimental test	Finite Element Model	Error (%)
P1	20±0.22	19.76	1.21
P2	9.5±0.17	9.81	3.16
P3	4±0.25	4.34	7.83
P4	24±0.24	23.45	2.34
P5	27±0.33	28.58	5.52
P6	9±0.19	9.87	8.81

Figure 4-8 shows the real-time deflection of the six prototypes of Table 3-1 actuated by the current input applied as a ramp function. The vision based measurement like the one described before was used to evaluate the deflection. The current was kept constant for 6 seconds to show the stabilized values of deflection at 1.0A. Also it was found that by applying 1.0A all the prototypes reached their maximum repeatable deflections, while applying more current did not increase the deflection and in some cases caused the wires to fail; for example, the wires were burned and in many occasions lost their shape memory properties. The amount of allowable current was different for different wire diameters; for example, 0.20mm SMA wires failed at 2.20A and the results were not repeatable at 1.50A. The quickest response time was achieved by the prototype with two sections of actuations

(P5). The maximum deflection was reached by prototypes numbered P4 and P5 because of their relatively lower moment of inertia and higher SMA actuation forces. These results suggest that having multiple sections of actuations would enhance the maneuverability of the active cannula.

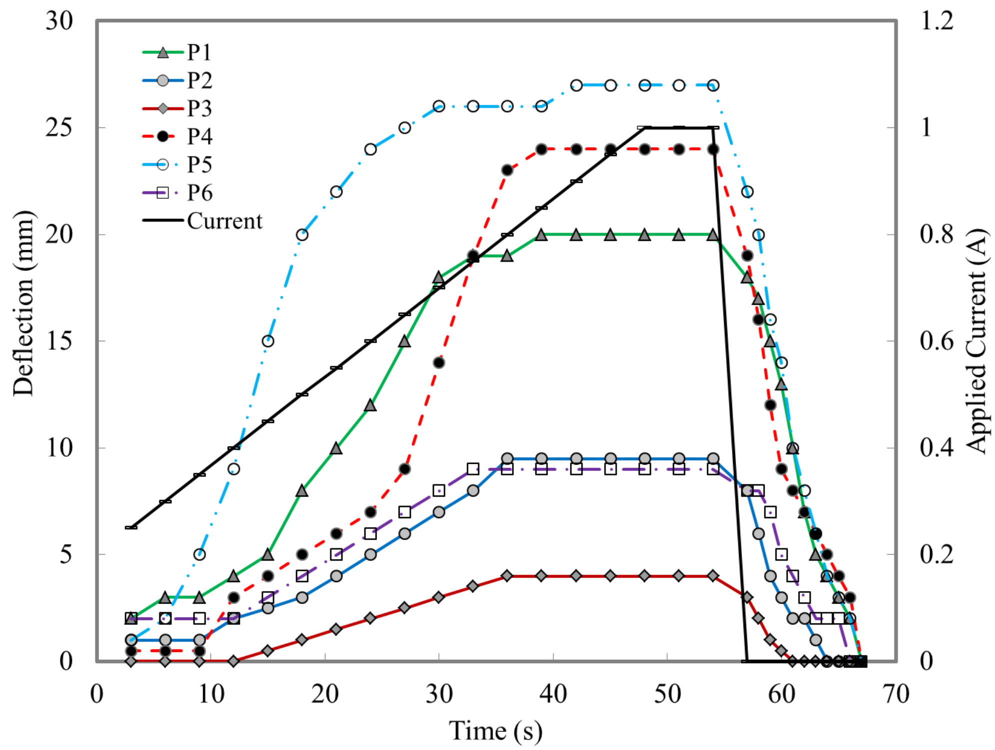

Figure 4-8: Real-time deflection of different cannulas due to the applied current as a ramp function for the prototypes developed in chapter 3.5.

4.4.2. Design parameter study

It could be seen that with all three actuators, as expected, the deflections were smallest for stiffer cannulas. It was also observed that as modulus increased the deflection of cannula decreased nonlinearly, which can be explained as follows. When SMA wires are actuated (contracts), stresses are generated in the wire due to the resistance to bend the cannula. This amount of stress makes the wire follow a different path in the transformation diagram reaching higher stresses. With the stiffer cannulas, the incomplete transformation to austenite is expected which prevents the SMA wire from reaching the maximum contraction and therefore noticeable decrease in the deflection. The earlier transformation to austenite in the wires (with the higher values of CA) caused the transformation to happen at lower stress level, meaning faster response.

For clinical use, the lowest amount of offset is always preferable as it diminishes the size of the device. To date, significant efforts have been made to develop the SMA actuated needles in the smallest dimensions possible using variety of advanced techniques; for instance, Ryu et al. (Ryu, Renaud, Black, Daniel, & Cutkosky, 2011) developed a prototype of 1.37mm needle diameter (18G needle tip) where all actuators and heating optical fibers were mounted inside the cannula. Moreover, prototypes were developed by Ayvali et al. (Ayvali, Liang, Ho, Chen, & Desai, 2012b) and Datla et al. (Datla, Konh, & Hutapea, 2014a, 2014b) where the needle diameter was in a comparable range of 3.17mm (~11G) and 2.20mm (~14G), respectively. Furthermore, several other challenges need to be thoroughly considered while incorporating the SMA wire in the cannula. The method of setting the SMA's pre-strain condition and the electrical insulation between the wire and the cannulas which are mostly made of conductive materials are among these challenges. It is reported that tissue necrosis is happening at temperatures greater than 50.4^{o}C (Mcdannold, King, Jolesz, & Hynynen, 2000). Since most of our actuators are being heated above this range, the thermal insulation is essential to be investigated. In our previous studies (Datla, Konh, Koo, et al., 2014), the probable thermal damage to the prostate tissue was reported using a heated SMA wire embedded in a phantom material that mimics the tissue's thermal damage properties. In depth investigations are being done in our research group for a proper thermal insulation of the heated elements with appropriate biocompatible materials prior to the development of the active needles for the realistic clinical use. As a solution, the SMA wires could be encapsulated by an insulating polymer layer with low thermal conductivity. For example, polyimides have low thermal conductivities in the order of 0.1 W/m-K. The thickness of this polymer layer should be carefully selected to minimize the temperature rise on the outer surface of the device. An in situ photon-initiated polymerization method could be utilized with the photosensitive polymers of low cytotoxicity (Myllymaa et al., 2010) as for the candidate materials. Furthermore, it has been demonstrated that polyimides can be used to coat the wires' surfaces (Allen, Leong, Lim, & Kohl, 1997; Shah & Gordon, 2003).

4.5. Optimization of the active needle

The analysis showed that, among all input parameters, the length of the cannula and the offset distance are the most influencing parameters on the needle tip deformation.

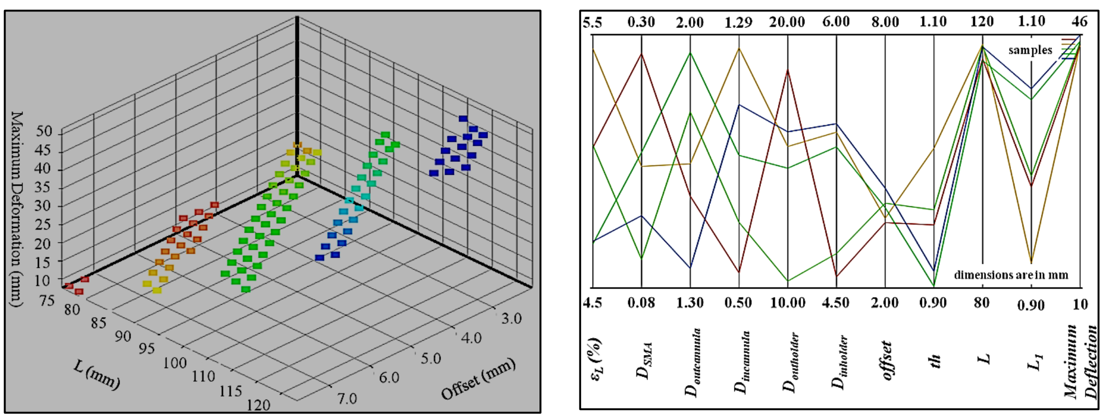

(a) (b)

Figure 4-9: Optimization results from the DOE method. (a) Visualization of the objective parameter (needle tip deflection) with variation of cannula's length and offset distance and (b) five best candidate design points.

Figure 4-9a shows the variation of needle tip deflection (the objective parameter) based on these two sensitive parameters for all the 100 design points. Of these, the five best configurations having the maximum deflection are shown in Figure 4-9b.

The convergence achieved after 11 total iterations and 594 evaluations resulted in 10 best candidates for the active needle design which are shown in Figure 4-10b. Also among all input parameters the offset, the cannula's length and the cannula's outer diameter were shown to be the most influential parameters on the needle tip deflection. The variation of the tip deflection based on variations of the two sensitive parameters (the total length and the offset) is shown in Figure 4-10a.

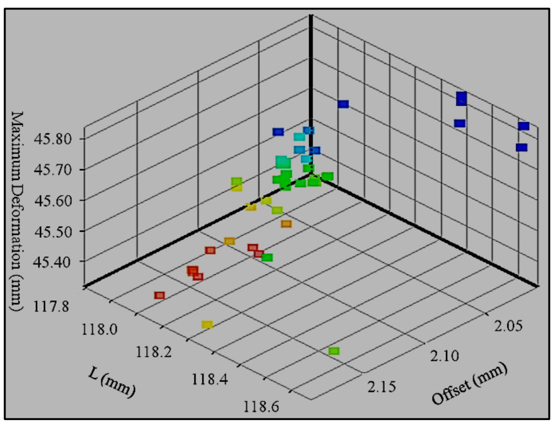

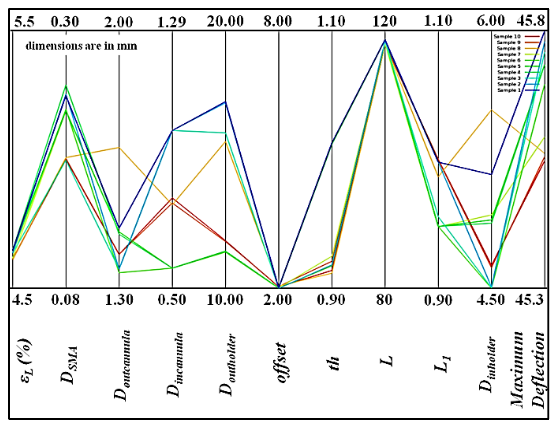

(a) (b)

Figure 4-10: Optimization results from the MOGA method. (a) Visualization of the objective parameter (needle tip deflection) with variation of cannula's length and offset distance and (b) ten best candidate design points.

Table 4-5 compares the best candidate design points obtained from DOE and MOGA methods. It was observed that almost similar results were obtained using the two methods. The offset and the DSMA values show deviations of 41 and 39%, respectively. It was observed that the values of the five best candidates suggested by the DOE method do not show a specific trend so that a certain converged value can be interpreted.

Comparing the best five candidates of DOE and MOGA method leads to a more or less deviations within different parameters. The calculation time using MOGA was less since the iterations were done using genetic algorithm and therefore less number of assessments/iterations. This suggests that MOGA is a preferred optimization method over DOE, because similar optimized solution was reached in a shorter time period.

Table 4-5: Comparison of the optimized design points obtained from DOE and MOGA methods (all dimensions are in mm).

	ε_L (%)	D_{SMA}	*Cannula*		*Holder*		*offset*	*th*	*L*	L_1	*Max Def.*
			D_{out}	D_{in}	D_{out}	D_{in}					
DOE	4.68	0.15	1.36	1.09	16.44	5.46	4.37	0.92	118.54	1.06	45.93
MO GA	4.65	0.24	1.46	0.98	17.02	5.08	2.01	1.01	118.64	0.99	45.84

A clinical aspect that needs to be addresses in the needle design is to minimize tissue rupture while inserting the needle. The amount of rupture is directly proportional to the maximum distance between the SMA wire and the cannula, which happens at the needle's mid length. Therefore, minimizing this gap will reduce the amount of rupture. This can be achieved by dividing the length into several sections. To demonstrate this, a case study with two sections having half length of the SMA wire was designed to investigate how much this gap can be decreased. The optimization study showed 44.06mm deflection assuming two sections compared to 45.84mm deflection of the past one section model. However the gap decreased from 2.56mm to 1.47mm. This clearly illustrated that the more the number of section is, the less destructive the active needle would be. Also, the tissue damage due to existence of heated elements of actuators has to be investigated thoroughly. The degree to which real tissue is damaged due to the heated SMA wires is very similar to that of the phantom since it shares the tissue's thermal properties. This aspect has been reported in our previous work (Datla, Konh, Koo, et al., 2014). In most cases the tissue necrosis occurs at temperatures above 50.4ºC as was reported in (Mcdannold et al., 2000). The thermal damage can be avoided by actuating the wires for a very short period of time or by thermally insulating the wires which is being investigated by our research group.

4.6. Advanced prototype of the active needle with shape memory polymer

Figure 4-11 shows the temperature of SMPs captured by the attached thermocouples while subjected to the current of 0.70A and 0.5A for 70:30 and 50:50 SMPs for an overall time of 50s. Three repetitions were done to ensure the repeatability of the results. The average temperature of SMP has also been shown in the figure. The fluctuations in the temperature profile were due to the movement of the structure that makes the connection between the thermocouple and the SMP was not as perfect as the stationary position. This happens when the SMP reaches its glass transition temperature (~30ºC for 70:30, and ~35ºC for 50:50 SMP).

The maximum temperature and the average temperature of the SMP were sensed to be 48.0ºC and 42.5ºC, respectively for the 70:30 SMP. These values were found to be 32.2ºC and 30.5ºC for the 50:50 SMP. According to the DSC result the complete phase transformation was expected at 42.92ºC and 37.79ºC for the 70:30 and 50:50 SMPs, respectively. The values confirm that the amount of power supplied was sufficient for the shape recovery.

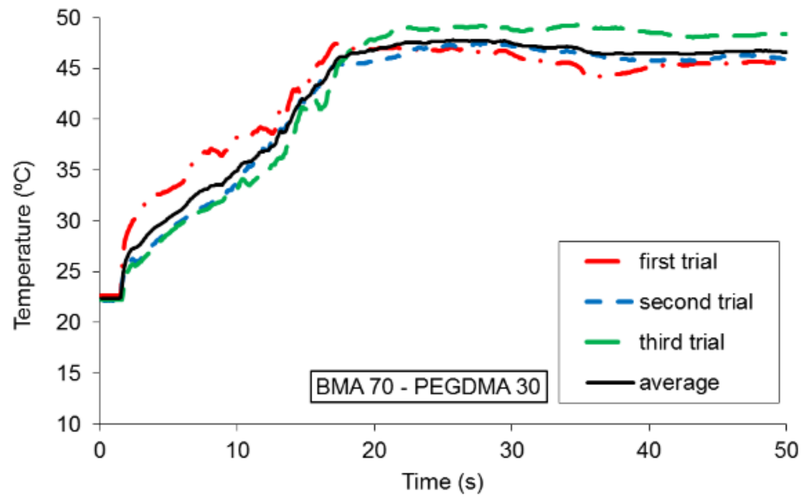

(a)

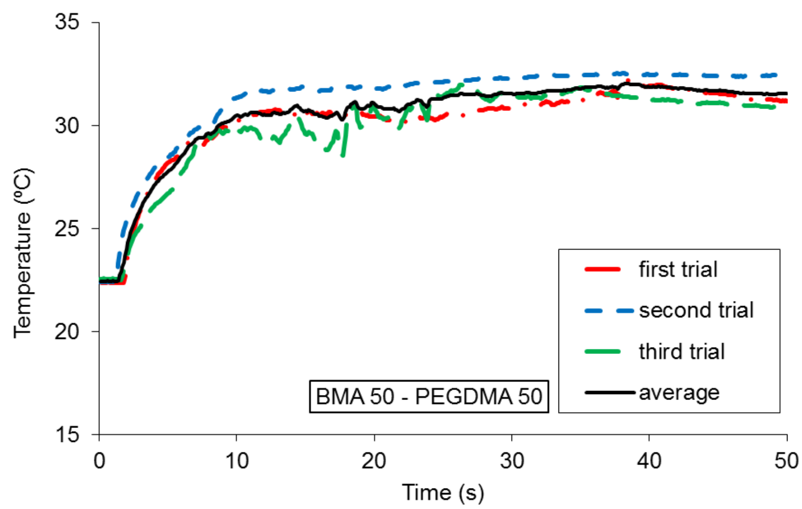

(b)

Figure 4-11: SMP’s temperature captured by the attached thermocouples for BMA:PEGDMA concentrations of (a) 70:30, and (b) 50:50.

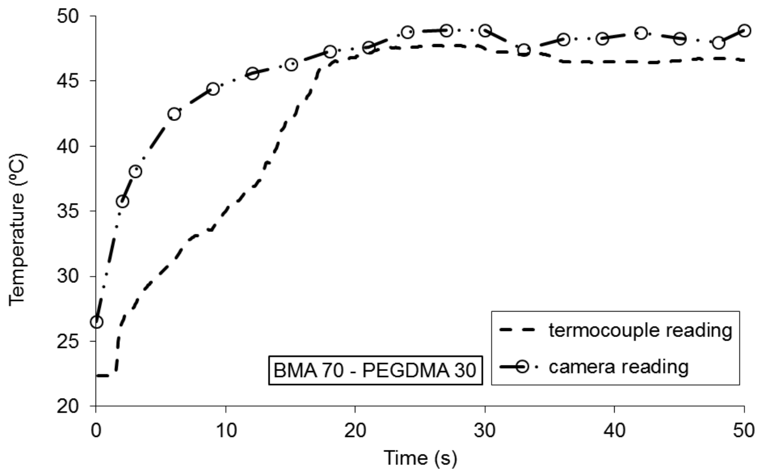

(a)

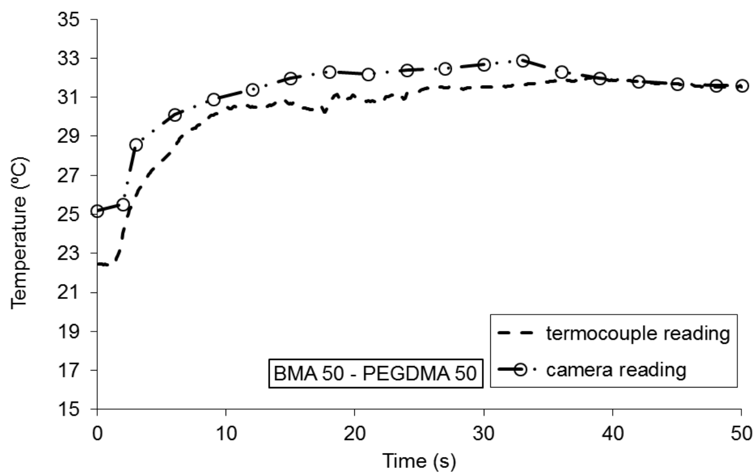

(b)

Figure 4-12: SMP's temperature profile measured by the infra-red camera, and the attached thermocouples for BMA:PEGDMA concentrations of (a) 70:30, and (b) 50:50.

The SMPs' temperature profile obtained by the infra-red camera is shown in Figure 4-12 while also compared with the thermocouple measurements. Only the average temperature is shown in this figure. It was seen that the readings of the temperatures are almost the same using both methods. While heating, the measurements of the camera and the thermocouple were showing a bigger difference; however, after 20s of heating the readings were close with less than 10% difference. However, the infra-red camera has the privilege of displaying real-time temperatures on the structure which better assist us in collecting the glass transition temperatures of the SMP.

SMAs' unique characteristics such as robust actuation, high energy density and biocompatible properties make them suitable candidates to be used as actuators in many devices, especially in medical instruments. This study aims to show the feasibility of activating surgical needles utilizing two way actuations of both SMAs and SMPs. Incorporation of the additional actuation of SMP elements in the design introduces more dexterity and actuation. Privileging from this actuating system, surgeons would be able to compensate for their probable misplacements and errors. Controlling the actuation system would make it even possible to guide the needle in a desired trajectory, away from sensitive organs, reaching target locations. Therefore, the procedure's outcome would be improved drastically. Deflection of the active needle was evaluated in air while the SMA wire was subjected to different amount of current. The amount of heat required for the SMP element to get the structure back to its initial position was studied. The SMP's temperature was captured using and infra-red camera and an attached thermocouple. A different method of heating was also used with the attached electrical wires. It was shown that a higher deflection could be achieved using SMPs at higher temperatures. A promising approach to incorporate SMP as a flexure joint component was shown through the results. Thermal insulation of the SMP and the SMA component is inevitable as thermal damage to the tissue is very probable while actuated. In our previous study [4] the thermal tissue damage while subjected to the heated SMA wires has been reported. The proper thermal insulation of the heated elements with appropriate biocompatible materials is currently under investigation in our laboratory. The amount of force that can be generated through SMPs of different concentrations of BMA:PEGDMA is still under investigation to achieve the best SMP suitable for the design.

4.7. Needle insertion tests

Figure 4-13 shows the experimental deflection of the needle inside the phantom. The experiment was repeated three times to ensure the repeatability of results. The final tip deflection of 22.2 ± 0.3mm was observed which was comparable to the deflection of 20.8mm predicted by the simulation. The standard deviation values was found by performing three experimental repetitions. The error of 6.3% suggests that our simulation can predict the bending of the needle with a reasonable accuracy in spite of our modeling assumptions of ignoring friction and planar movement of the needle.

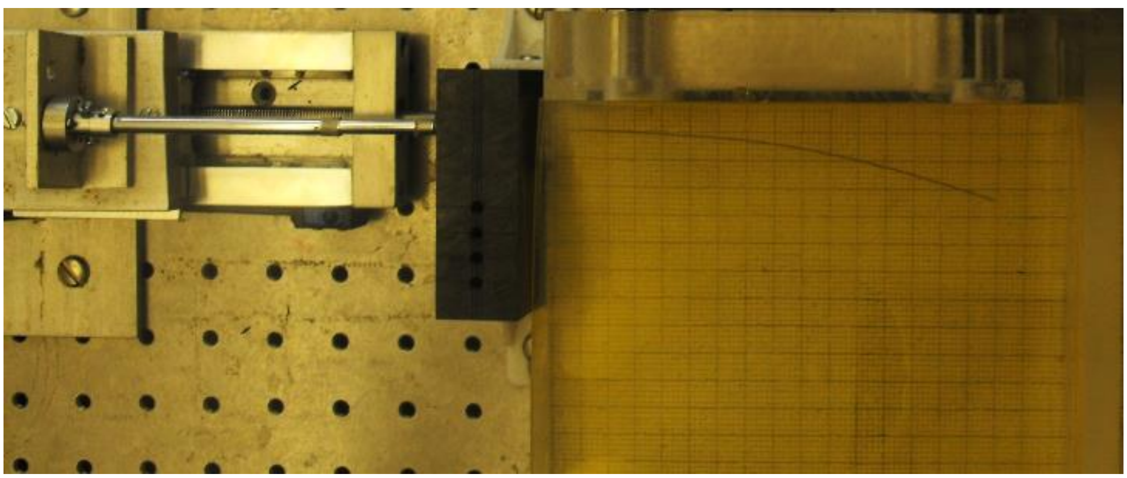

Figure 4-13: Deflection of the needle in the tissue mimicking phantom.

4.8. Needle insertion simulation

The final deflected shape of the needle inside the tissue obtained from simulation and the experiment is shown in Figure 4-14. Also the difference of the predicted deflection and the experimental results is shown. It can be seen that for a higher depth the error between the prediction by the simulation and the experiment goes higher. The required model accuracy for needle insertion inside the soft tissue is not known yet. However, the difference of less than 3mm at all time is considered as a good estimation for 150mm of insertion depth. This simulation while validated with experiment is desirable to be used in system optimization, path planning and real time control. Our simulation has also the capability of matching with image-guide control algorithms to improve the outcome of the robotic steering needles inside biological tissues.

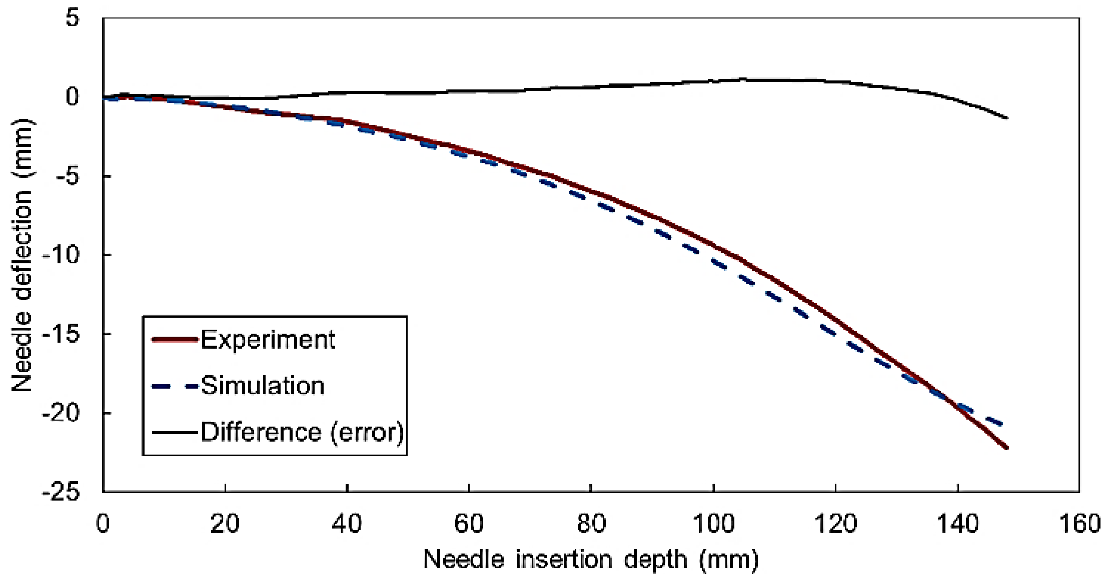

Figure 4-14: Comparison of the simulation and experimental results of the needle deflection vs. the insertion depth.

4.8.1. Validation of the simulation with experiments

According to the literatures (Ahn et al., 2010) the healthy and cancerous prostate tissue has the elastic modulus of 24.1+14.5kPa and 17.0+9.0kPa, respectively. Figure 4-15 shows the measured indentation force for the Plastisol phantom developed for the needle insertion tests. The pure elastic behavior was observable since the loading and unloading curves are overlapping. The elastic modulus was found to be 25.6±0.6kPa which was close to the reported values of real prostate tissue (Ahn et al., 2010).

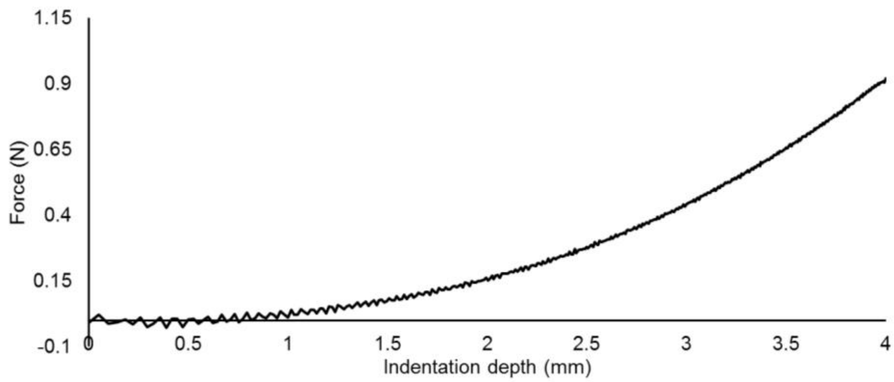

Figure 4-15: Indentation data: the measured force vs. displacement.

In our needle insertion experiment, the needle was inserted at an offset distance varying between 50 to 70mm, where offset distance was the transverse distance between the line of action of needle insertion and the tissue boundary. The insertion test was performed repeatedly with 0.51mm needle for offset distances of 14 and 50mm and it was shown that despite the changes in offset distances, the needle-tip deflections differed by 4.5% (28.2 and 27.0mm deflections for 14 and 50mm offsets, respectively), thereby showing negligible effects of offset and boundary constraints. Therefore, the experimental results showed negligible effect on the final deformation of the needle due to the offset distance between the needle and the tissue boundaries. Our simulation, on the other hand, showed similar results as well. The tip deflection of 24.6 and 25.9mm was found for 0.51mm needle diameter, setting two different offset distances of 5 and 10mm. the difference of less than 5% was observed and thereby showed a negligible effect of offset distance on the total deflection. In all of our simulations, a gap of 10.0mm between the boundary and the insertion point was adopted.

Two cases were developed for needle diameter of 0.64mm and bevel tip angle of 20º. The only difference between these two cases was the Young's modulus of tissue and needle which were scaled down with the factor of 1.0×10^6 in one case and not scaled in the other one. The results showed a 4.7% difference (25.5mm for the scaled model and 24.3mm for the real values) between the two cases, while the computation time was hugely cheaper in case of the scaled Young's modulus. Therefore, justified our previous assumption to scale down both the Young's modulus of needle and tissue by the same ratio.

Figure 4-16 shows the deflection of the real size needle inside the tissue with the contours of fluid density shown. It can be seen that the mass translation at the tip of the needle is high. It should also be noticed that the mass of the elements that is pushed by the needle was moved to some elements of the void part. This is due to the capability of the ALE formulation that include the option of having multiple materials inside elements. The same trend was observed on the von Misses stress showing the interacting forces that are applied to the needle tip from tissue resistance.

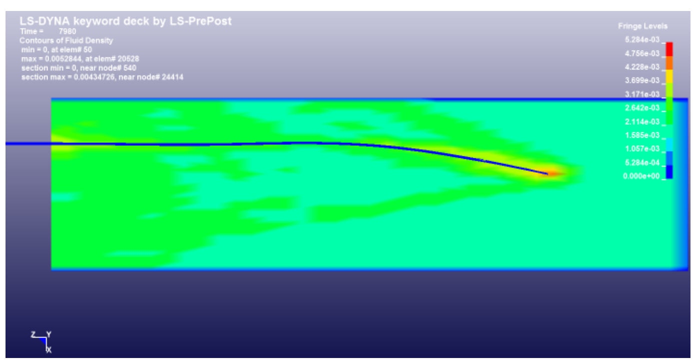

Figure 4-16: Contours of the fluid density for the 0.64mm needle diameter inserted 150mm into the phantom.

There are numerous factors influence the needle interactions such as needle type, insertion speed, and tissue characteristics. However, the influence of these factors on the final deflection in not clear. The simulation here could explain many of these questions while validated. Figure 4-17 shows the deflected shape of needles with diameters of 0.64, 0.51 and 0.38mm and bevel tip angle of 30º while inserted 150mm into the phantom. The difference between the numerical predictions and the experimental results was observed higher for deeper penetrations. However, since this difference was less than 5mm in the total insertion depth of 150mm, the simulation could be trusted with reasonable accuracy. The less amount of deflection for thicker needles could be explained by their higher resistance to bending. Although the overall forces acting on thicker needle's tip is higher because of the bigger interacting area but it is not high enough to cause high deflections as shown also by our experimental results.

Table 4-6: Comparison between the deflection prediction by the LSDYNA model and the insertion experimental results. The standard deviations were obtained by three repetitions of the tests.

Bevel angle	Needle Deflection (mm)		
	LSDYNA model	Insertion test	% Error
20	25.50	26.47±0.3	3.66
30	20.80	24.92±0.4	16.53
40	14.80	23.96±0.4	38.23
50	10.40	19.51±1.1	46.69
60	7.30	18.61±0.7	60.77

Table 4-6 compares the final needle tip deflection of three different diameters of needle obtained by the needle insertion test and the simulation. It is shown that the deflection predicted by model has small difference (maximum error of less than 10%) with the experimental results and therefore validates our simulation. In our simulation, an octagonal prism represented the cylindrical shape of needle with 4 nodes at the cross-section. This meshed shape reduces the interacting bevel area of the needle by 4% compared to the real cylindrical shape. Therefore considering same amount of stress applied to a smaller area some portion of the error could be explained.

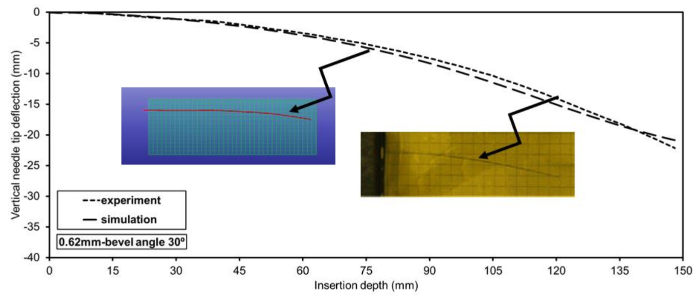

(a)

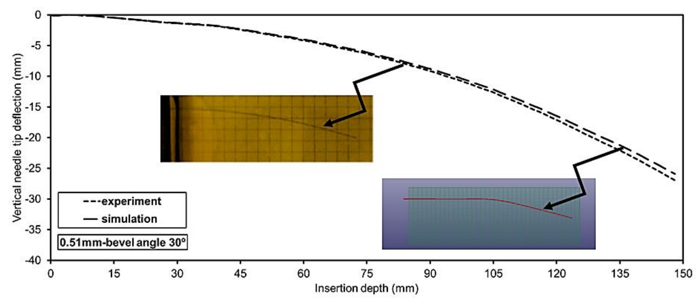

(b)

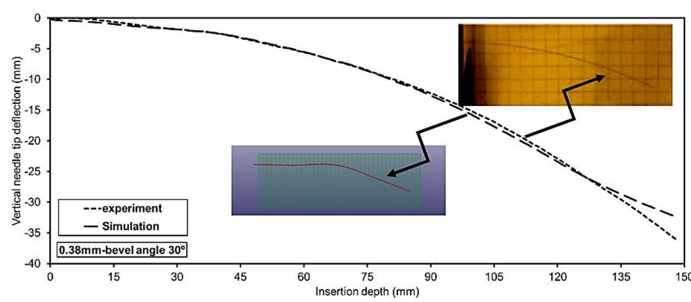

(c)

Figure 4-17: Numerical and experimental predictions for the deflected shape of (a) Ø 0.62mm, (b) Ø 0.51mm, and (c) Ø 0.38mm needles after 150mm of insertion.

4.8.2. Deflection of needles of various diameters and bevel angles inside the tissue

The primary function of having a bevel tip is to create a path way inside the tissue. Figure 4-18 shows the parametric studies to investigate the effect of having different bevel angles on the needle's tip.

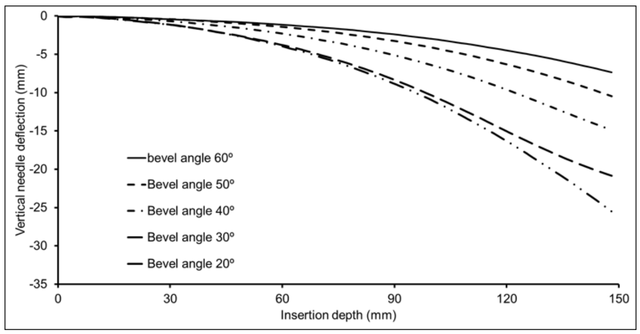

(a)

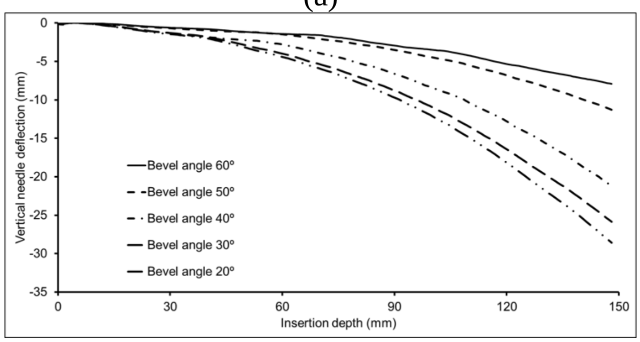

(b)

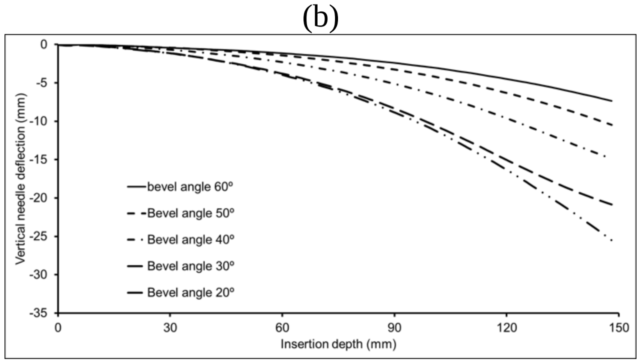

(c)

Figure 4-18: Simulated deflected shape of needles of (a) Ø 0.38mm, (b) Ø 0.51mm, and (c) Ø 0.64mm with different bevel tip angles.

Three different needles with diameters of 0.38, 0.51 and 064mm were selected for this aim. It was seen that the higher the bevel angle is the more deflection is achieved. This can be explained by the fact that a straight trajectory is expected with needles of symmetrical tip.

While inserting a thin needle with small bevel angle, the large deflection of the needle would align its bevel tip nearly perpendicular to the line of insertion. The amount of the exerted force in such cases becomes so effective that makes bucking very probable. Our simulations showed that increasing stiffness of both needle and tissue by a same ratio could prevent this probable buckling which was not observed in the experiments.

Figure 4-19 lists the summary of the final position of needles of various design configurations. The figure suggests that the effect of the bevel tip angle was aggravated for bigger diameters of needle. It can be seen that different shapes of the needle can be achieved by choosing the appropriate needle size and bevel tip angle. This study would be helpful for reaching a target location robotically when a certain radius of curvature is needed.

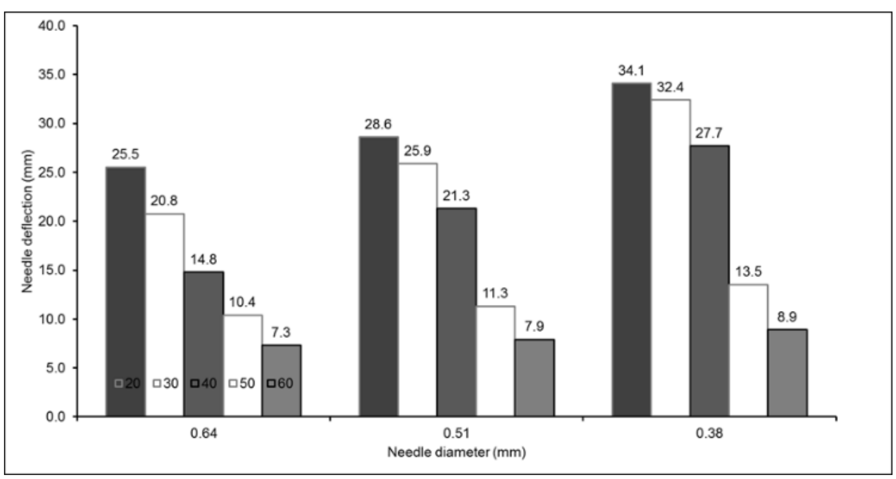

Figure 4-19: Needle deflection estimated for different needle diameters with different bevel tip angles.

CHAPTER 5

CONCLUSIONS

This study has looked into many areas all with the focus of demonstrating the feasibility of developing an active needle with incorporation of smart materials. First a 3D finite element model of an actuated steerable needle was developed in ANSYS to study the structural response of the device. The shape memory alloy behavior was modeled by defining the isothermal stress-strain curves using the multilinear capability of ANSYS. These isothermal curves were formed using implementation of the Brinson model in MATLAB. Stress and strain responses of SMAs predicted by this model were compared by experimental results to show the reasonable accuracy of this model. Birth and death method was used in the solution procedure to get the pre-strain condition on the SMA wire. The FE model was validated by a developed prototype of the actuated steerable needle. This model was found suitable for capturing the actuation characteristics of SMAs. Several design parameters, such as needle's diameter, SMA's pre-strain and its offset from the needle were studied using the FE model to help optimize the design of a surgical needle. Through different designed models and prototypes it was found that the maximum flexibility could be obtained using multiple sections of actuations. This study can serve as a basis for the optimization study which would eventually lead to a more practical design of the active needle closer to the practical use. Also this study demonstrates the modeling, analysis and optimization of a shape memory alloy actuated needle using finite element approach. The accuracy of the finite element model was established by validating with experiments done on a developed prototype of the active needle. A design optimization study was performed with the objective of maximizing the needle tip deflection to ensure the highest steerability of the active needle. Suitable design parameters that maximize the needle deflection were presented using two different methods: Design of Experiments (DOE) with random choices of design points and Multi-Objective Genetic Algorithm (MOGA) with evolving choices of design points in the domain. The length of the SMA wire as well as the offset distance between the needle and the SMA wire were found to be the most effective parameters on the needle deflection. The optimized design resulted in a maximum deflection of 45.84mm with a 118.64mm long SMA wire. This amount is much larger than the clinical requisite; the amount of deflection could be controlled based on need by applying appropriate amount of current. Based on the optimization study a physical advanced prototype of the active needle was developed. This prototype was tested in air and inside a phantom material to substantiate the enhancements that are provided by the active elements. Along with the shape memory alloy wires as the primary active components of the device, shape memory polymers were also incorporated in the design to provide additional actuation capabilities. It was shown that by heating shape memory polymers above their glass transition temperatures, a higher deflection could be achieved while supplying the same amount of electrical energy. Having a feasible prototype developed, there was a need to investigate the response of the device inside the tissue. Several factors appear to be of a great importance for a precise path planning and developing a control algorithm for the active needle that is interacting within the tissue. A finite element model was developed in LSDYNA to simulate the deflection of a passive needle inside a tissue. This model used a Arbitrary-Lagrangian-Eulerian (ALE) formulation to consider the penetration of a passive needle inside the tissue. This model was validated by needle insertion experiments, and a reasonable accuracy was achieved.

This study provides a table that could assist surgeons choosing the suitable configuration of needle if a certain radius of curvature has to be achieved. The methodology and studies introduced in this work could be followed for design and development of any other innovative medical devices in which the smart materials play a major role.

CHAPTER 6

FUTURE WORKS

There are several areas that has the potential to be investigated as future works. First to improve the performance, dividing the overall length of the active needle into a number of sections could be explored to minimize the tissue puncture. The amount of tissue damage due to the heating elements of actuators depend on two factors: the actuator's temperature and also the time the tissue is subjected to heat. The propagation of the damage zone inside a thermal sensitive phantom due to the heated wires could be studied. Also insulation of the SMA wires with a low conductive polymer could be studied to minimize the thermal damage to the tissue via the heating elements. Also the needle insertion model could be modified to present a real-time simulation. Future work will focus on modeling the tissue as a quasilinear viscoelastic material having a hyperelastic instantaneous elastic function and a linear relaxation function in the form of Prony series to take into account the complete viscoelastic characteristics of the tissue. In this model the relaxation of the tissue after puncture and friction effects will be considered. Mechanics of active needle with SMA actuators inside the tissue will be investigated where rather than choosing the size and bevel-tip angle of the needle surgeons can also utilize the actuation forces to control the needle. This simulation could be used to train surgeons in their needle-based tasks. The insertion force and speed applied by the user could be captured using a haptic device, and then provided to the finite element model as boundary and initial conditions. The surgeons could practice several times until they develop a feel to maintain the best speed and force required to form the desired curvature of the needle path.

BIBLIOGRAPHY

Ahn, Kim, Ian, Rha, & Kim. (2010). Mechanical property characterization of prostate cancer using a minimally motorized indenter in an ex vivo indentation experiment. *Urology*, *76*(4), 1007–1011. http://doi.org/10.1016/j.urology.2010.02.025

Allen, Leong, Lim, & Kohl. (1997). Photofabrication of the third dimension of NiTi shape memory alloy microactuators. In *SPIE Microlithography and Metrology in Micromachining III* (Vol. 3225, pp. 126–132). Forschungszentrum Karlsruhe (Germany). Retrieved from http://dx.doi.org/10.1117/12.284549

Auricchio, Taylor, & Lubliner. (1997). Shape-memory alloys: macromodelling and numerical simulations of the superelastic behavior. *Computer Methods in Applied Mechanics and Engineering*, *146*, 281–312.

Ayvali, Liang, Ho, Chen, & Desai. (2012a). Towards a discretely actuated steerable cannula for diagnostic and therapeutic procedures. *The International Journal of Robotics Research*, *31*(5), 588–603.

Ayvali, Liang, Ho, Chen, & Desai. (2012b). Towards a discretely actuated steerable cannula for diagnostic and therapeutic procedures. *The International Journal of*

Robotics Research, *31*(5), 588–603. http://doi.org/10.1177/0278364912442429

Brinson. (1993). One-dimensional constitutive behavior of shape memory alloys: thermomechanical derivation with non-constant material functions and redefined martensite internal variable. *Journal of Intelligent Material Systems and Structures*, *4*(2), 229–242. http://doi.org/10.1177/1045389X9300400213

Crews, & Buckner. (2012). Design optimization of a shape memory alloy-actuated robotic catheter. *Journal of Intelligent Material Systems and Structures*, *23*(5), 545–562. http://doi.org/10.1177/1045389X12436738

Datla, Konh, Honarvar, Podder, Dicker, Yu, & Hutapea. (2013). A model to predict deflection of bevel-tipped active needle advancing in soft tissue. *Medical Engineering & Physics*, *36*(3), 258–293. http://doi.org/10.1016/j.medengphy.2013.11.006

Datla, Konh, & Hutapea. (2014a). A flexible active needle for steering in soft tissues. In *40th Annual Northeast Bioengineering Conference* (pp. 1–2). Boston, MA, Apr.

Datla, Konh, & Hutapea. (2014b). Studies with SMA actuated needle for steering within tissue. In *ASME Conf. on Smart Material, Adaptive Structures and Intelligent Systems (SMASIS)*. Newport, RI, Sep.

Datla, Konh, Koo, Daniel, Yu, Dicker, … Hutapea. (2014). Polyacrylamide phantom for self-actuating needle-tissue interaction studies. *Medical Engineering & Physics*, *36*(1), 140–145. http://doi.org/10.1016/j.medengphy.2013.07.004

Dumont, & Kühl. (2005). Finite element simulation for design optimisation of shape memory alloy spring actuators. *International Journal of Engineering Computations*, *22*(7), 835–848.

Eaton-Evans, Dulieu-Barton, Little, & Brown. (2007). Observations during mechanical testing of nitinol. *Journal of Mechanical Engineering Science*, *222*(C), 97–106. http://doi.org/10.1243/09544062JMES797

Haga, Tanahashi, & Esashi. (1998). Small diameter active catheter using shape memory alloy coils. In *Micro Electro Mechanical Systems* (pp. 419–424). Heidelberg, Germany, 25-29 Jan 1998. http://doi.org/10.1541/ieejsmas.120.509

Hagmann, Noelke, Rau, Kaierle, Overmeyer, Wesling, & Wolkers. (2015). Design, processing and characterization of Nickel Titanium micro-actuators for medical implants. *Journal of Laser Applications*, *27*. http://doi.org/DOI: 10.2351/1.4906381

Hartl, Lagoudas, & Calkins. (2011). Advanced methods for the analysis, design, and optimization of SMA-based aerostructures. *Journal of Smart Materials and Structures*, *20*(9), 094006–26. http://doi.org/10.1088/0964-1726/20/9/094006

Heintze, Seelecke, & Bueskens. (2003). Modeling and optimization control of microscale SMA actuators. In *SPIE Smart Structures and Materials: Modeling, Signal Processing, and Control* (Vol. 5049, pp. 495–505). San Diego, CA, Jul 31, 2003. http://doi.org/10.1117/12.484065

Hertz H. R. (1882). *On the contact of rigid elastic solids and on hardness*. Newyork, NY: McMillan.

Honarvar, Datla, Konh, Podder, Dicker, Yu, & Hutapea. (2014). Study of unrecovered strain and critical stresses in one-way shape memory Nitinol. *Materials Engineering and Performance*, *23*(8), 2885–2893. http://doi.org/10.1007/s11665-014-1077-6

Honarvar, Konh, Datla, Devlin, & Hutapea. (2013). Size effect on the critical stress of Nitinol wires. In *ASME Conf. on Smart Material, Adaptive Structures and Intelligent Systems, (SMASIS)* (pp. 1–5). Snowbird, UT, Sep 16-18.

Kohl, Skrobanek, & Miyazaki. (1999). Development of stress-optimised shape memory microvalves. *Journal of Sensors and Actuators A: Physical*, *72*(3), 243–250. http://doi.org/10.1016/S0924-4247(98)00221-0

Konh, Datla, & Hutapea. (2014). Feasibility of SMA wire actuation for an active steerable cannula. *Journal of Medical Devices*, doi: 10.1115/1.4029557. http://doi.org/10.1115/1.4029557

Konh, Honarvar, & Hutapea. (2013). Application of SMA wire for an active steerable cannula. In *ASME Conf. on Smart Material, Adaptive Structures and Intelligent Systems (SMASIS)* (pp. 1–5). Snowbird, UT, Sep 16-18.

Konh, & Hutapea. (2013). Finite element simulation of an active surgical needle for prostate brachytherapy. In *1st Annual frontiers in medical devices: applications of computer modeling and simulation* (pp. 1–2). Washington, DC, Sep 11-13.

Kota, Hetrick, Li, & Saggere. (1999). Tailoring unconventional actuators using compliant transmissions: design methods and applications. In *IEEE/ASME Transactions on Mechatronics* (Vol. 4, pp. 396–408). Dec 1999.

Liang, & Rogers. (1990). One-dimensional thermomechanical constitutive relations for shape memory materials. *Journal of Intelligent Material Systems and Structures*, *1*(2), 207–234. http://doi.org/10.1177/1045389X9000100205

LSTC. LS-DYNA Theory Manual Version 970. r:6030. (n.d.). Livermore, CA: Livernire Software Technology Corporation (LSTC).

Main, Garcia, & Howard. (1994). Optimal placement and sizing of paired piezoactuators in beams and plates. *Journal of Smart Materials and Structures*, *3*(3), 373–381. http://doi.org/10.1088/0964-1726/3/3/013

Masuda, & Noori. (2002). Optimization of hysteretic characteristics of damping devices based on pseudoelastic shape memory alloys. *International Journal of Non-Linear Mechanics*, *37*(8), 1375–1386. http://doi.org/10.1016/S0020-7462(02)00024-0

Mcdannold, King, Jolesz, & Hynynen. (2000). Usefulness of MR imaging – derived thermometry and dosimetry in determining the threshold for tissue damage induced by thermal surgery in rabbits. *Radiology*, *216*(11), 517–523.

Meier, Czechowicz, & Haberland. (2009). Control loops with detection of inner electrical resistance and fatigue-behaviour by activation of NiTi -Shape Memory Alloys. *ESOMAT 2009 - 8th European Symposium on Martensitic Transformations*, *05006*(2009), 0–7. http://doi.org/10.1051/esomat/200905006

Misra, Reed, Schafer, Ramesh, & Okamura. (2010). Mechanics of flexible needles robotically steered through soft tissue. *The International Journal of Robotics Research*, *29*(13), 1640–1660. http://doi.org/10.1177/0278364910369714

Morgan. (2004). Medical shape memory alloy applications—the market and its products.

Materials Science and Engineering: A, 378(1-2), 16–23. http://doi.org/10.1016/j.msea.2003.10.326

Myllymaa, Myllymaa, Korhonen, Lammi, Tiitu, & Lappalainen. (2010). Surface characterization and in vitro biocompatibility assessment of photosensitive polyimide films. *Colloids and Surfaces. B, Biointerfaces*, *76*(2), 505–11. http://doi.org/10.1016/j.colsurfb.2009.12.011

Oliver, & Pharr. (1992). An improved technique for determining hardness and elastic modulus using load and displacement sensing indentation experiments. *Journal of Materials Research*, *7*(6), 1564–1583. http://doi.org/http://dx.doi.org/10.1557/JMR.1992.1564

Orlando, Joseph, Kumar, Franz, Konh, Hutapea, … Podder. (2014). Control of shape memory alloy actuated flexible needle using multimodal sensory feedbacks. In *3rd International Conference on Control, Robotics and Informations (ICCRI)*. HongKong.

Ozbulut, Roschke, Lin, & Loh. (2010). GA-based optimum design of a shape memory alloy device for seismic response mitigation. *Journal of Smart Materials and Structures*, *19*(6), 065004. http://doi.org/10.1088/0964-1726/19/6/065004

Pfeiffer, DeLaurentis, & Mavroidis. (1999). Shape memory alloy actuated robot prostheses: initial experiments. In *IEEE International Conference on Robotics and Automation* (Vol. 3, pp. 2385 – 2391). Detroit, MI, 10-15 May 1999: Ieee. http://doi.org/10.1109/ROBOT.1999.770462

Ryu, Quek, Renaud, Black, Daniel, & Cutkosky. (2012). An optical actuation system and curvature sensor for a MR-compatible active needle. In *IEEE International Conference on Robotics and Automation* (pp. 1589–1594). (Saint Paul, MN, May). http://doi.org/10.1109/ICRA.2012.6224964

Ryu, Renaud, Black, Daniel, & Cutkosky. (2011). Feasibility study of an optically actuated MR-Compatible active needle. In *IEEE/RSJ International Conference on Intelligent Robots and Systems (IROS)* (pp. 2564–2569). Ieee. http://doi.org/10.1109/IROS.2011.6094945

Seeley, & Chattopadhyay. (1993). The development of an optimization procedure for the design of intelligent structures. *International Journal of Smart Materials and Structures*, *2*, 135–146.

Shah, & Gordon. (2003). Polyimide coated shape-memory material and method of making same.

Shu, Lagoudas, Hughes, & Wen. (1997). Modeling of a flexible beam actuated by shape memory alloy wires. *Journal of Smart Materials and Structures*, *265*(6), 265–277.

Tanaka, Kobayashi, & Sato. (1986). Thermomechanics of transformation pseudoelasticity and shape memory effect in alloys. *International Journal of Plasticity*, *2*, 59–72.

Tang, Chen, & He. (2007). Magnetic force aided compliant needle navigation and needle performance analysis. In *IEEE International Conference on Robotics and Biomimetics* (pp. 612–616). Sanya, China, Dec 2007.

Terriault, & Brailovski. (2011). Modeling of shape memory alloy actuators using

Likhachev's formulation. *Journal of Intelligent Material Systems and Structures*, *22*(4), 353–368. http://doi.org/10.1177/1045389X11401450

Troisfontaine, Bidaud, & Larnicol. (1999). Optimal design of micro-actuators based on SMA wires. *Journal of Smart Materials and Structures, 8*(2), 197–203. http://doi.org/10.1088/0964-1726/8/2/004

APPENDIX 1

CONSTITUTIVE MODEL FOR SHAPE MEMORY ALLOY WIRES

Brinson Model algorithm used to simulate the force response of Nitinol wire.

```
function [T,sig]=brinson(N,ep,Tstart,Tend)


% Necessary inputs are
% N: number of space the stress, strain, temperature matrix should have
% ep: The amount of prestrain the wire should have. This is kept constant
% throughout the calculation
% Tstart: Initial temperature, usually for convection (room) temperarture
% Tend:  Maximum temperture that the wire reach
% Several material constants must first be defined
% ---------------------- Material constants ---------------------------
% Young's Modulus
Ea=69.643e9;              % Austenite Young's Modulus [Pa]
Em=33.14e9;               % Martensite Young's Modulus [Pa]
theta= 0.7e6;             % Coefficient of thermo expansion [Pa/C]
ep_l=0.07;                % Maximum residual strain

% ----------------- Stress related constants ---------------------------
Cm= 5.91e6;          % Clausius-Clapeyron coefficient of Martensite [Pa/C]
Ca=8.78e6;           % Clausius-Clapeyron coefficient of Austenite [Pa/C]
sig_s=5e5;           % Critical start stress below Ms temperature [Pa]
sig_f=40e6;          % Critical finish stress below Ms temperature [Pa]

% --------------------- Temperature related constants -------------------
Mf=28.02;            % Martensite Finish Temperature [C]
Ms=37.23;            % Martensite Start Temperature [C]
As=49.73;            % Austenite Start Temperature [C]
Af=60.17;            % Austenite Finish Temperture [C]

% --------------------- Heating curve ----------------------------------
% -------------------- Initialize all the vectors --------------
T_lo=linspace(Tstart,Tend,N);   % Temperature profile
sig_lo=zeros(size(T_lo));       % Stress profile
ep_lo=ep*ones(size(sig_lo));    % Strain profile
```

```
ep_temp=zeros(size(sig_lo));    % Trial strain
D_lo= zeros(size(sig_lo));      % Young's Modulus profile
Ohm_lo=zeros(size(sig_lo));     % Transformation profile
exci_tlo=zeros(size(sig_lo));   % Temperature induced martensite
exci_slo=zeros(size(sig_lo));   % Stress induced martensite
exci_lo=zeros(size(sig_lo));    % Global martensite
% -------------------- Initial Conditions ------------------------------

T_lo(1)=Tstart;                  % Initial temperature
ep_lo(1)=ep;                     % Initial strain
sig_lo(1)=0;                     % Initial stress
exci_tlo(1)=0.85;                % Iniital temperature induced martensite
                                 % Initial temperature induced martensite
exci_slo(1)=0.12;                % Initial stress induced martensite
exci_lo(1)=exci_slo(1)+exci_tlo(1); % Initial martensite volume fraction
D_lo(1)=Ea+exci_lo(1)*(Em-Ea);      % Initial young modulus
Ohm_lo(1)=-ep_l*D_lo(1);            % Initial transformation tensor
Cons=D_lo(1)*ep_lo(1)+Ohm_lo(1)*exci_slo(1);

% -------------------- Calculation of the model -------------------------

for jj=2:length(T_lo)
   sig_temp=sig_lo(jj-1);
   while abs(ep_temp(jj)-ep_lo(jj)) >1e-4
      [exci_lo(jj),exci_tlo(jj),exci_slo(jj)]=kinetic1(sig_temp, ...
         T_lo(jj),T_lo(1),exci_slo(1),exci_tlo(1),exci_lo(1), ...
         exci_slo(jj-1),exci_tlo(jj-1),exci_lo(jj-1),Cm,Ca, ...
         sig_s,sig_f,Mf,Ms,As,Af);
      D_lo(jj)=Ea+exci_lo(jj)*(Em-Ea);
      Ohm_lo(jj)=-ep_l*D_lo(jj);
      ep_temp(jj)=1/D_lo(jj)*(sig_temp-sig_lo(1)-Ohm_lo(jj)*exci_slo(jj) ...
        -theta*(T_lo(jj)-T_lo(1))+Cons);
      sig_temp=sig_temp+0.01e5;
   end
   sig_lo(jj)=sig_temp;
end

% -----------------------------------------------------------------

% Since the constitutive equations are based on initial condition
% calculation of the cooling and heating curve has to be seperated
% ---------------------- Cooling curve ----------------------------------
% --------------------- Initialize all the vectors  --------------
T_un=linspace(Tend,Tstart,N);          % Temperature profile
sig_un=sig_lo(end)*ones(size(T_un));    % Stress profile
```

```
ep_un=ep*ones(size(sig_un));          % Strain profile
ep_t=zeros(size(sig_un));             % Trial strain
D_un= zeros(size(sig_un));            % Young's Modulus profile
Ohm_un=zeros(size(sig_un));           % Transformation profile
exci_tun=zeros(size(sig_un));         % Temperature induced martensite
exci_sun=zeros(size(sig_un));         % Stress induced martensite
exci_un=zeros(size(sig_un));          % Total martensite

% -------------------- Initial Conditions ------------------------------

T_un(1)=Tend;                        % Initial temperature
ep_un(1)=ep;                         % Initial strain
sig_un(1)=sig_lo(end);               % Initial stress
exci_tun(1)=exci_tlo(end);           % Initial temperature induced martensite
exci_sun(1)=exci_slo(end);           % Initial stress induced martensite
exci_un(1)=exci_sun(1)+exci_tun(1);     % Initial martensite volume fraction
D_un(1)=Ea+exci_un(1)*(Em-Ea);         % Initial young modulus
Ohm_un(1)=-ep_l*D_un(1);             % Initial transformation tensor
Cons_un=D_un(1)*ep_un(1)+Ohm_un(1)*exci_sun(1);% Initial term of cons. model
% -------------------- Calculation of the model -------------------------

for jj=2:length(T_un)
   sig_t=sig_un(jj-1);
   while abs(ep_t(jj)-ep_un(jj)) >1e-3
      [exci_un(jj),exci_tun(jj),exci_sun(jj)]=kinetic1(sig_t, ...
         T_un(jj),T_un(1),exci_sun(1),exci_tun(1),exci_un(1), ...
         exci_sun(jj-1),exci_tun(jj-1),exci_un(jj-1),Cm,Ca, ...
         sig_s,sig_f,Mf,Ms,As,Af);
      D_un(jj)=Ea+exci_un(jj)*(Em-Ea);
      Ohm_un(jj)=-ep_l*D_un(jj);

      ep_t(jj)=1/D_un(jj)*(sig_t-sig_un(1)-Ohm_un(jj)*exci_sun(jj) ...
         -theta*(T_un(jj)-T_un(1))+Cons_un);
      sig_t=sig_t-0.01e5;
   end
   sig_un(jj)=sig_t;
end

% Combine output temperature and stress response
T=[T_lo,T_un];
sig=[sig_lo, sig_un];

%
end
```

```
% Nested Phase Transformation Kinetic Formulation

function [exci,exci_t,exci_s]=kinetic1(sig,T,To,exci_so,exci_to,exci_o ...
   ,exci_st,exci_tt,exci_m,Cm,Ca,sig_s,sig_f,Mf,Ms,As,Af)


% -----------------Define material constants ----------------------------
aA=pi/(Af-As);
aM=pi/(Ms-Mf);

% ---------------------------------------------------------------------

% -------------------Conversion to austensite ----------------------------
if T>To
   if T>As && T<Af
      if sig > Ca*(T-As)
         exci=exci_m;
         exci_s=exci_st;
         exci_t=exci_tt;
      elseif sig < Ca*(T-As)
         exci=exci_o/2*(cos(aA*(T-As-sig/Ca))+1);
         exci_s=exci_so-exci_so/exci_o*(exci_o-exci);
         exci_t=exci_to-exci_to/exci_o*(exci_o-exci);
      end
   elseif T> Af
      if sig <Ca*(T-As) && sig >Ca*(T-Af)
         exci=exci_o/2*(cos(aA*(T-As-sig/Ca))+1);
         exci_s=exci_so-exci_so/exci_o*(exci_o-exci);
         exci_t=exci_to-exci_to/exci_o*(exci_o-exci);
      elseif sig<Ca*(T-Af)
         exci=exci_m;
         exci_s=exci_st;
         exci_t=exci_tt;
      end
   elseif T<As
      exci=exci_m;
      exci_s=exci_st;
      exci_t=exci_tt;
   end
end
%----------------------------------------------------------------------
%-------------------- Conversion to martensite ---------------------------
if T<To
   if T>Ms
      if sig <sig_s+Cm*(T-Ms)
```

```
        exci=exci_m;
        exci_s=exci_st;
        exci_t=exci_tt;

    elseif sig_s+Cm*(T-Ms)< sig && sig < sig_f+Cm*(T-Ms)
        if sig_s==0 && sig_f==Cm*(Ms-Mf)
            exci_s=(1-exci_so)/2*cos(aM*(T-Mf-sig/Cm)) ...
                + (1+exci_so)/2;
        else
            exci_s=(1-exci_so)/2*cos(pi()/(sig_s-sig_f)*(sig ...
                -sig_f-Cm*(T-Ms)))+ (1+exci_so)/2;
        end
        exci_t=exci_to-exci_to/(1-exci_so)*(exci_s-exci_so);
        exci=exci_t+exci_s;
    elseif sig > sig_f+Cm*(T-Ms);
        exci=exci_m;
        exci_s=exci_st;
        exci_t=exci_tt;
    end
 elseif T < Ms
    if  sig >sig_f
        exci=exci_m;
        exci_s=exci_st;
        exci_t=exci_tt;
    elseif sig < sig_s
        exci=exci_m;
        exci_s=exci_st;
        exci_t=exci_tt;

    elseif sig>sig_s && sig<sig_f
        exci_s=(1-exci_so)/2*cos(pi()/(sig_s-sig_f)*(sig-sig_f))...
            + (1+exci_so)/2;
        if Mf<T && T<Ms
            deltaT=(1-exci_to)/2*(cos(aM*(T-Mf))+1);
        else
            deltaT=0;
        end
        exci_t=exci_to-exci_to/(1-exci_so)*(exci_s-exci_so) ...
            +deltaT;
        exci=exci_t+exci_s;

    end
end
```

```
end
end
%----------------------------------------------------------------------
```

APPENDIX 2

ANSYS MODEL OF THE ACTIVE NEEDLE

```
/BATCH
/COM,ANSYS RELEASE 14.5    UP20120918       10:24:00    05/02/2013
/input,menust,tmp,''
/GRA,POWER
/GST,ON
/PLO,INFO,3
/GRO,CURL,ON
/CPLANE,1
/REPLOT,RESIZE
WPSTYLE,,,,,,,,0
/REPLOT,RESIZE
!
FINISH
/CLEAR
/COM,ANSYS RELEASE 14.5    UP20120918       10:24:07    05/02/2013
/input,start145,ans,'C:\Program Files\ANSYS Inc\v145\ANSYS\apdl\'
/PREP7
ET,1,solid65
MP,EX,1,60E9  !STEEL HOLDER
MP,PRXY,1,.3
MP,EX,2,60E9  !ALUMINUUM CANULA 1
MP,PRXY,2,.3
TB,MELA,3,1,3,
TBTEMP,20
!TBPT,,3.183231575841485e-4,20e6
TBPT,,0.068771,50e6
TBPT,,.1,866e6
MPTEMP,,,,,,,,
MPTEMP,1,0
MPDATA,EX,3,,90e9
MPDATA,PRXY,3,,0.3
TB,MELA,4,5,3,
TBTEMP,20
TBPT,,0.066934,2E+006
TBPT,,0.1,866E+006
TBTEMP,55
```

```
TBPT,,0.033,3E+006
TBPT,,0.068738,4.475E+007
TBPT,,0.1,8.66E+008
TBTEMP,60
TBPT,,0.0703,8.85E+007
TBPT,,0.1,8.6625E+008
TBTEMP,70
TBPT,,0.0014025,8.8118E+007
TBPT,,0.07375,1.75E+008
TBPT,,0.1,8.66E+008
TBTEMP,90
TBPT,,0.004,2.6355E+008
TBPT,,0.0805,3.545E+008
TBPT,,0.1,8.66E+008
MPTEMP,,,,,,,,
MPTEMP,1,0
MPDATA,EX,4,,90e9
MPDATA,PRXY,4,,0.3
CYL4,0,0,9.015e-3
FLST,2,2,8
FITEM,2,0.7E-02,0,0
FITEM,2,0.7145E-02,0,0
CIRCLE,P51X
FLST,3,4,4,ORDE,2
FITEM,3,5
FITEM,3,-8
ASBL,       1,P51X
/REPLOT,RESIZE
KDIST,       7,       5
!
FINISH
/CLEAR
/COM,ANSYS RELEASE 14.5    UP20120918       10:26:41    05/02/2013
/input,start145,ans,'C:\Program Files\ANSYS Inc\v145\ANSYS\apdl\'
/PREP7
ET,1,solid65
MP,EX,1,60E9  !STEEL HOLDER
MP,PRXY,1,.3
MP,EX,2,60E9  !ALUMINUUM CANULA 1
MP,PRXY,2,.3
TB,MELA,3,1,3,
TBTEMP,20
!TBPT,,3.183231575841485e-4,20e6
TBPT,,0.068771,50e6
TBPT,,.1,866e6
```

```
MPTEMP,,,,,,,
MPTEMP,1,0
MPDATA,EX,3,,90e9
MPDATA,PRXY,3,,0.3
TB,MELA,4,5,3,
TBTEMP,20
TBPT,,0.066934,2E+006
TBPT,,0.1,866E+006
TBTEMP,55
TBPT,,0.033,3E+006
TBPT,,0.068738,4.475E+007
TBPT,,0.1,8.66E+008
TBTEMP,60
TBPT,,0.0703,8.85E+007
TBPT,,0.1,8.6625E+008
TBTEMP,70
TBPT,,0.0014025,8.8118E+007
TBPT,,0.07375,1.75E+008
TBPT,,0.1,8.66E+008
TBTEMP,90
TBPT,,0.004,2.6355E+008
TBPT,,0.0805,3.545E+008
TBPT,,0.1,8.66E+008
MPTEMP,,,,,,,
MPTEMP,1,0
MPDATA,EX,4,,90e9
MPDATA,PRXY,4,,0.3
CYL4,0,0,9.015e-3
FLST,2,2,8
FITEM,2,0.7E-02,0,0
FITEM,2,0.7145E-02,0,0
CIRCLE,P51X
FLST,3,4,4,ORDE,2
FITEM,3,5
FITEM,3,-8
ASBL,       1,P51X
FLST,2,2,8
FITEM,2,0,0,0
FITEM,2,0.79375E-03,0,0
CIRCLE,P51X
FLST,3,4,4,ORDE,2
FITEM,3,9
FITEM,3,-12
ASBL,       3,P51X
GPLOT
```

```
FLST,2,2,8
FITEM,2,0,0,0
FITEM,2,0.43815E-03,0,0
CIRCLE,P51X
FLST,3,4,4,ORDE,2
FITEM,3,13
FITEM,3,-16
ASBL,       1,P51X
ADELE,       3, , ,1
FLST,2,2,8
FITEM,2,0,0,0
FITEM,2,0.265E-02,0,0
CIRCLE,P51X
FLST,3,4,4,ORDE,2
FITEM,3,17
FITEM,3,-20
ASBL,       4,P51X
FLST,2,1,5,ORDE,1
FITEM,2,4
FLST,2,1,5,ORDE,1
FITEM,2,5
VEXT,P51X, , ,0,0,111.66e-3,,,,
FLST,2,1,5,ORDE,1
FITEM,2,2
VEXT,P51X, , ,0,0,111.66e-3,,,,
FLST,2,1,5,ORDE,1
FITEM,2,1
VEXT,P51X, , ,0,0,7.17e-3,,,,
FLST,2,1,5,ORDE,1
FITEM,2,3
VEXT,P51X, , ,0,0,.83e-3,,,,
! MESH
NUMMRG,KP,1e-008, , ,LOW
CM,_Y,VOLU
VSEL, , , ,       2
CM,_Y1,VOLU
CMSEL,S,_Y
!*
CMSEL,S,_Y1
VATT,       3, ,   1,       0
CMSEL,S,_Y
CMDELE,_Y
CMDELE,_Y1
!*
CM,_Y,VOLU
```

```
VSEL, , , ,       1
CM,_Y1,VOLU
CMSEL,S,_Y
!*
CMSEL,S,_Y1
VATT,       2, ,   1,       0
CMSEL,S,_Y
CMDELE,_Y
CMDELE,_Y1
!*
FLST,5,2,6,ORDE,2
FITEM,5,3
FITEM,5,-4
CM,_Y,VOLU
VSEL, , , ,P51X
CM,_Y1,VOLU
CMSEL,S,_Y
!*
CMSEL,S,_Y1
VATT,       1, ,   1,       0
CMSEL,S,_Y
CMDELE,_Y
CMDELE,_Y1
/VIEW,1,1,1,1
/ANG,1
/REP,FAST
! MESH
SMRT,6
SMRT,7
CM,_Y,VOLU
VSEL, , , ,       4
CM,_Y1,VOLU
CHKMSH,'VOLU'
CMSEL,S,_Y
!*
VSWEEP,_Y1
!*
CMDELE,_Y
CMDELE,_Y1
CMDELE,_Y2
!*
GPLOT
CM,_Y,VOLU
VSEL, , , ,       3
CM,_Y1,VOLU
```

```
CHKMSH,'VOLU'
CMSEL,S,_Y
!*
VSWEEP,_Y1
!*
CMDELE,_Y
CMDELE,_Y1
CMDELE,_Y2
!*
GPLOT
CM,_Y,VOLU
VSEL, , , ,       1
CM,_Y1,VOLU
CHKMSH,'VOLU'
CMSEL,S,_Y
!*
VSWEEP,_Y1
!*
CMDELE,_Y
CMDELE,_Y1
CMDELE,_Y2
!*
GPLOT
CM,_Y,VOLU
VSEL, , , ,       2
CM,_Y1,VOLU
CHKMSH,'VOLU'
CMSEL,S,_Y
!*
VSWEEP,_Y1
!*
CMDELE,_Y
CMDELE,_Y1
CMDELE,_Y2
/DIST,1,0.924021086472,1
/REP,FAST
/DIST,1,0.924021086472,1
/REP,FAST
/DIST,1,0.924021086472,1
/REP,FAST
/DIST,1,0.924021086472,1
/REP,FAST
/DIST,1,1.08222638492,1
/REP,FAST
/DIST,1,1.08222638492,1
```

```
/REP,FAST
/DIST,1,1.08222638492,1
/REP,FAST
/ZOOM,1,RECT,1.06962,0.867273 ,1.68068278516 ,0.324545439807
/ZOOM,1,RECT,1.03689,-0.0354545 ,1.32877661819 ,-0.321818167203
/ZOOM,1,RECT,-0.512593,0.504545 ,0.32488925816 ,0.0245454534308
/AUTO,1
/REP,FAST
/REPLOT,RESIZE
/REPLOT,RESIZE
/INPUT,'2','txt','E:\ANSYS Works\Parametric Study\SMAs Diameter\E60 SMA 0.29
mm\',, 0
/COM,ANSYS RELEASE 14.5    UP20120918       11:11:03    05/02/2013
/VIEW,1,1,1,1
/ANG,1
/REP,FAST
CM,_Y,VOLU
VSEL, , , ,       4
CM,_Y1,VOLU
CHKMSH,'VOLU'
CMSEL,S,_Y
!*
VSWEEP,_Y1
!*
CMDELE,_Y
CMDELE,_Y1
CMDELE,_Y2
!*
/INPUT,'2','txt','E:\ANSYS Works\Parametric Study\SMAs Diameter\E60 SMA 0.29
mm\',, 0
/COM,ANSYS RELEASE 14.5    UP20120918       11:11:34    05/02/2013
/VIEW,1,1,1,1
/ANG,1
/REP,FAST
SMRT,6
SMRT,7
CM,_Y,VOLU
VSEL, , , ,       4
CM,_Y1,VOLU
CHKMSH,'VOLU'
CMSEL,S,_Y
!*
VSWEEP,_Y1
!*
CMDELE,_Y
```

```
CMDELE,_Y1
CMDELE,_Y2
!*
/INPUT,'2','txt','E:\ANSYS Works\Parametric Study\SMAs Diameter\E60 SMA 0.29
mm\',, 0
/COM,ANSYS RELEASE 14.5    UP20120918       11:12:12    05/02/2013
/VIEW,1,1,1,1
/ANG,1
/REP,FAST
SMRT,6
CM,_Y,VOLU
VSEL, , , ,       4
CM,_Y1,VOLU
CHKMSH,'VOLU'
CMSEL,S,_Y
!*
VSWEEP,_Y1
!*
CMDELE,_Y
CMDELE,_Y1
CMDELE,_Y2
!*
/INPUT,'2','txt','E:\ANSYS Works\Parametric Study\SMAs Diameter\E60 SMA 0.29
mm\',, 0
/COM,ANSYS RELEASE 14.5    UP20120918       11:12:37    05/02/2013
/VIEW,1,1,1,1
/ANG,1
/REP,FAST
SMRT,6
SMRT,5
CM,_Y,VOLU
VSEL, , , ,       4
CM,_Y1,VOLU
CHKMSH,'VOLU'
CMSEL,S,_Y
!*
VSWEEP,_Y1
!*
CMDELE,_Y
CMDELE,_Y1
CMDELE,_Y2
!*
GPLOT
VPLOT
SMRT,6
```

```
CM,_Y,VOLU
VSEL, , , ,       3
CM,_Y1,VOLU
CHKMSH,'VOLU'
CMSEL,S,_Y
!*
VSWEEP,_Y1
!*
CMDELE,_Y
CMDELE,_Y1
CMDELE,_Y2
!*
VPLOT
CM,_Y,VOLU
VSEL, , , ,       2
CM,_Y1,VOLU
CHKMSH,'VOLU'
CMSEL,S,_Y
!*
VSWEEP,_Y1
!*
CMDELE,_Y
CMDELE,_Y1
CMDELE,_Y2
!*
VPLOT
CM,_Y,VOLU
VSEL, , , ,       1
CM,_Y1,VOLU
CHKMSH,'VOLU'
CMSEL,S,_Y
!*
VSWEEP,_Y1
!*
CMDELE,_Y
CMDELE,_Y1
CMDELE,_Y2
!*
/UI,MESH,OFF
!
LGWRITE,'try','lgw','E:\ANSYSW~1\PARAME~1\SMASDI~1\E60SMA~1.29M\',COMMENT
/INPUT,'2','txt','E:\ANSYS Works\Parametric Study\SMAs Diameter\E60 SMA 0.29 mm\',, 0
/COM,ANSYS RELEASE 14.5    UP20120918       12:32:16    05/02/2013
```

```
ALLSEL,ALL
EALIVE,ALL
ALLSEL,ALL
FLST,2,40,5,ORDE,2
FITEM,2,1
FITEM,2,-40
SFADELE,P51X,1,PRES
FLST,2,1,5,ORDE,1
FITEM,2,2
DADELE,P51X,ALL
VSEL,S, , ,       2
ESLV,S
MPCHG,4,ALL,
ALLSEL,ALL
TIME,2
SOLVE
*DEL,_FNCNAME
*DEL,_FNCMTID
*DEL,_FNCCSYS
*SET,_FNCNAME,'tt'
*SET,_FNCCSYS,0
! /INPUT,TEMPERATURE.func,,,1
*DIM,%_FNCNAME%,TABLE,6,5,1,,,,%_FNCCSYS%
!
! Begin of equation: {TIME}*2+20
*SET,%_FNCNAME%(0,0,1), 0.0, -999
*SET,%_FNCNAME%(2,0,1), 0.0
*SET,%_FNCNAME%(3,0,1), 0.0
*SET,%_FNCNAME%(4,0,1), 0.0
*SET,%_FNCNAME%(5,0,1), 0.0
*SET,%_FNCNAME%(6,0,1), 0.0
*SET,%_FNCNAME%(0,1,1), 1.0, -1, 0, 2, 0, 0, 1
*SET,%_FNCNAME%(0,2,1), 0.0, -2, 0, 1, 1, 3, -1
*SET,%_FNCNAME%(0,3,1),   0, -1, 0, 20, 0, 0, -2
*SET,%_FNCNAME%(0,4,1), 0.0, -3, 0, 1, -2, 1, -1
*SET,%_FNCNAME%(0,5,1), 0.0, 99, 0, 1, -3, 0, 0
! End of equation: {TIME}*2+20
!-->
VSEL,S, , ,       2
ESLV,S
FLST,2,1,6,ORDE,1
FITEM,2,2
BFV,P51X,TEMP, %TT%
ALLSEL,ALL
TIME,30
```

```
SOLVE
/REPLOT,RESIZE
FINISH
/POST1
PLDISP,0
/VIEW,1,,1
/ANG,1
/REP,FAST
/USER,  1
/VIEW,  1,  0.373409617403E-01,  0.846321398663    , -0.531362157800
/ANG,   1,   175.580236947
/REPLO
/ZOOM,1,RECT,0.447647,0.81 ,0.728626565999 ,0.583636337132
/ZOOM,1,RECT,-0.0870319,0.177273 ,0.319433348595 ,-0.3190908946
FLST,5,3,1,ORDE,3
FITEM,5,44703
FITEM,5,44705
FITEM,5,62532
NSEL,S, , ,P51X
!*
PRNSOL,U,COMP
ALLSEL,ALL
!*
PRNSOL,U,COMP
/VIEW,1,,1
/ANG,1
/REP,FAST
/AUTO,1
/REP,FAST
PLDISP,1
PLDISP,2
!*
PLESOL, S,Z, 0,1.0
/ZOOM,1,RECT,0.338529,0.807273 ,0.690435199041 ,0.449999979564
/ZOOM,1,RECT,-0.272533,0.766364 ,0.946862948614 ,-0.482727250805
/ZOOM,1,RECT,0.851385,-0.520909 ,1.00687795383 ,-0.662727242631
/DIST,1,1.37174211248,1
/REP,FAST
/DIST,1,1.37174211248,1
/REP,FAST
/DIST,1,1.37174211248,1
/REP,FAST
/DIST,1,1.37174211248,1
/REP,FAST
/DIST,1,1.37174211248,1
```

```
/REP,FAST
/DIST,1,1.37174211248,1
/REP,FAST
/DIST,1,1.37174211248,1
/REP,FAST
/FOC,1,,0.3,,1
/REP,FAST
/FOC,1,,0.3,,1
/REP,FAST
/FOC,1,,0.3,,1
/REP,FAST
/FOC,1,-0.3,,,1
/REP,FAST
/FOC,1,-0.3,,,1
/REP,FAST
/DIST,1,1.37174211248,1
/REP,FAST
!*
PLESOL, S,X, 0,1.0
!*
PLESOL, S,Y, 0,1.0
/VIEW,  1,  0.530782887760    ,  0.756158917116    , -0.382744324749
/ANG,   1,   123.483534134
/REPLO
/VIEW,  1,  0.591345423430    ,  0.703288209152    , -0.394583685745
/ANG,   1,   121.943486140
/REPLO
!*
PLESOL, S,EQV, 0,1.0
/AUTO,1
/REP,FAST
/VIEW,1,,1
/ANG,1
/REP,FAST
!*
PLDI, ,
ANTIME,10,0.5, ,1,1,0,3
!*
/ANFILE,SAVE,'deformation',' ',' '
SET,FIRST
!*
PLESOL, S,Z, 0,1.0
/ZOOM,1,SCRN,0.363081,0.668182,0.229411,0.812727
/DIST,1,0.729,1
/REP,FAST
```

```
/DIST,1,0.729,1
/REP,FAST
/FOC,1,,0.3,,1
/REP,FAST
/FOC,1,,0.3,,1
/REP,FAST
/FOC,1,,0.3,,1
/REP,FAST
SET,NEXT
!*
PLESOL, S,Z, 0,1.0
/AUTO,1
/REP,FAST
/ZOOM,1,RECT,0.172124,0.777273 ,0.483110635557 ,0.62181815358
/ZOOM,1,RECT,-0.610799,0.550909 ,1.40788730689 ,-0.436363616547
/FOC,1,,0.3,,1
/REP,FAST
SET,NEXT
PLDISP,2
/AUTO,1
/REP,FAST
/SHOW,TIFF,,0
TIFF,COMP,1
TIFF,ORIENT,HORIZ
TIFF,COLOR,2
TIFF,TMOD,1
/GFILE,3600,
!*
/CMAP,_TEMPCMAP_,CMP,,SAVE
/RGB,INDEX,100,100,100,0
/RGB,INDEX,0,0,0,15
/REPLOT
/CMAP,_TEMPCMAP_,CMP
/DELETE,_TEMPCMAP_,CMP
/SHOW,CLOSE
/DEVICE,VECTOR,0
!*
PLDISP,0
/SHOW,TIFF,,0
TIFF,COMP,1
TIFF,ORIENT,HORIZ
TIFF,COLOR,2
TIFF,TMOD,1
/GFILE,2400,
!*
```

```
/CMAP,_TEMPCMAP_,CMP,,SAVE
/RGB,INDEX,100,100,100,0
/RGB,INDEX,0,0,0,15
/REPLOT
/CMAP,_TEMPCMAP_,CMP
/DELETE,_TEMPCMAP_,CMP
/SHOW,CLOSE
/DEVICE,VECTOR,0
!*
PLDISP,1
/SHOW,TIFF,,0
TIFF,COMP,1
TIFF,ORIENT,HORIZ
TIFF,COLOR,2
TIFF,TMOD,1
/GFILE,2400,
!*
/CMAP,_TEMPCMAP_,CMP,,SAVE
/RGB,INDEX,100,100,100,0
/RGB,INDEX,0,0,0,15
/REPLOT
/CMAP,_TEMPCMAP_,CMP
/DELETE,_TEMPCMAP_,CMP
/SHOW,CLOSE
/DEVICE,VECTOR,0
!*
SET,FIRST
PLDISP,0
/SHOW,TIFF,,0
TIFF,COMP,1
TIFF,ORIENT,HORIZ
TIFF,COLOR,2
TIFF,TMOD,1
/GFILE,2400,
!*
/CMAP,_TEMPCMAP_,CMP,,SAVE
/RGB,INDEX,100,100,100,0
/RGB,INDEX,0,0,0,15
/REPLOT
/CMAP,_TEMPCMAP_,CMP
/DELETE,_TEMPCMAP_,CMP
/SHOW,CLOSE
/DEVICE,VECTOR,0
!*
/REPLOT,RESIZE
```

```
/REPLOT,RESIZE
/REPLOT,RESIZE
FINISH
! /EXIT,ALL
```

APPENDIX 3

LSDYNA NEEDLE INSERTION MODEL

```
$# LS-DYNA Keyword file created by LS-PrePost 4.0 - 28Jan2013(19:00)
$# Created on Dec-12-2014 (14:41:12)
*KEYWORD
*TITLE
$# title
LS-DYNA keyword deck by LS-PrePost
*CONTROL_ALE
$#     dct      nadv      meth      afac      bfac      cfac      dfac      efac
         3         1         2 -1.000000     0.000     0.000     0.000     0.000
$#   start       end     aafac     vfact      prit       ebc      pref   nsidebc
    0.0001.0000E+20  1.000000 1.0000E-6         0         0     0.000         0
$#    ncpl      nbkt    imascl    checkr
         1        50         0     0.000
*CONTROL_TERMINATION
$#  endtim    endcyc     dtmin    endeng    endmas
 7890.0000         0     0.000     0.000     0.000
*DATABASE_BINARY_D3PLOT
$#      dt      lcdt      beam     npltc    psetid
 10.000000         0         0         0         0
$#   ioopt
         0
*DATABASE_BINARY_FSIFOR
$#      dt      lcdt      beam     npltc    psetid
 10.000000         0         0         0         0
*DATABASE_FSI
$#      dt
  1.000000
$#dbsfi_id       sid     stype      swid    convid
         1         1         2         0         0
*BOUNDARY_PRESCRIBED_MOTION_SET_ID
$#      id                                                               heading
         1velocity
$#    nsid       dof       vad      lcid        sf       vid     death     birth
        26         3         0         1 -1.000000         01.0000E+28     0.000
*BOUNDARY_SPC_SET_ID
$#      id                                                               heading
```

```
      1fixed faces
$#    nsid      cid      dofx      dofy      dofz     dofrx     dofry     dofrz
        17        0         1         1         1         0         0         0
*SET_NODE_LIST_TITLE
fixed nodes
$#     sid       da1       da2       da3       da4    solver
        17     0.000     0.000     0.000     0.000MECH
$#    nid1      nid2      nid3      nid4      nid5      nid6      nid7      nid8
      9938      9940      9944      9945      9947      9948      9951      9955
      9956      9958      9961      9965      9966      9968      9971      9975
      9976      9978      9981      9985      9986      9988      9991      9995
      9996      9998     10001     10005     10006     10008     10011     10015
     10016     10018     10219     10223     10261     10265     10787     10793
     10797     10798     10801     10804     10807     10808     10811     10814
     10817     10818     10821     10824     10827     10828     10831     10834
     10837     10838     10841     10844     10847     10848     10851     10854
     10857     10858     10861     10864     10867     10868     10871     10874
     10877     10878     10883     10884     11085     11093     11095     11098
     11099     11104     11105     11108     11109     11114     11115     11118
     11119     11124     11125     11128     11129     11134     11135     11138
     11139     11144     11145     11148     11149     11154     11155     11158
     11159     11164     11165     11168     11169     11174     11175     11178
     11181     11184     11187     11193     11197     11198     11200     11204
     11207     11208     11211     11214     11217     11218     11220     11222
     11224     11225     11227     11231     11234     11235     11237     11241
     11244     11245     11247     11249     11251     11252     11254     11256
     11258     11259     11261     11265     11268     11269     11271     11275
     11278     11279     11281     11283     11285     11286     11288     11290
     11292     11293     11295     11299     11302     11303     11309     11313
     11315     11317     11319     11320     11324     11327     11330     11333
     11336     11337     11339     11341     11343     11344     11347     11350
     11353     11354     11356     11358     11360     11361     11363     11365
     11367     11368     11370     11372     11374     11375     11377     11379
     11381     11382     11384     11386     11388     11389     11391     11393
     11395     11396     11398     11400     11402     11403     11405     11407
     11409     11410     11412     11414     11416     11417     11419     11421
     11423     11424     11428     11431     11433     11435     11437     11438
     11442     11445     11448     11451     11454     11455     11457     11459
     11461     11462     11465     11468     11471     11472     11474     11476
     11478     11479     11481     11483     11485     11486     11488     11490
     11492     11493     11495     11497     11499     11500     11502     11504
     11506     11507     11509     11511     11513     11514     11516     11518
     11520     11521     11523     11525     11527     11528     11530     11532
     11534     11535     11537     11539     11541     11542     11546     11549
     11551     11553     11555     11556     11560     11563     11566     11569
```

11572	11573	11575	11577	11579	11580	11583	11586
11589	11590	11592	11594	11596	11597	11599	11601
11603	11604	11606	11608	11610	11611	11613	11615
11617	11618	11620	11622	11624	11625	11627	11629
11631	11632	11634	11636	11638	11639	11641	11643
11645	11646	11648	11650	11652	11653	11655	11657
11659	11660	11664	11667	11669	11671	11673	11674
11678	11681	11684	11687	11690	11691	11693	11695
11697	11698	11703	11704	11707	11708	11710	11712
11714	11715	11717	11719	11721	11722	11725	11726
11729	11730	11732	11734	11736	11737	11739	11741
11743	11744	11747	11748	11751	11752	11754	11756
11758	11759	11763	11766	11769	11770	11774	12944
12945	12956	12957	12962	12963	12964	12965	12970
12971	12972	12973	12978	12979	12980	12981	12985
12986	12987	13362	13363	13374	13375	13380	13381
13382	13383	13388	13389	13390	13391	13396	13397
13398	13399	13403	13404	13405	13780	13781	13792
13793	13798	13799	13800	13801	13806	13807	13808
13809	13814	13815	13816	13817	13821	13822	13823
14198	14199	14210	14211	14216	14217	14218	14219
14224	14225	14226	14227	14232	14233	14234	14235
14239	14240	14241	14616	14617	14628	14629	14634
14635	14636	14637	14642	14643	14644	14645	14650
14651	14652	14653	14657	14658	14659	15088	15089
15096	15099	15101	15103	15105	15107	15109	15111
15113	15115	15117	15119	15121	15123	15125	15127
15129	15131	15133	15193	15215	15237	15259	15281
15682	15683	15690	15693	15695	15697	15699	15701
15703	15705	15707	15709	15711	15713	15715	15717
15719	15721	15723	15725	15727	15787	15809	15831
15853	15875	16276	16277	16284	16287	16289	16291
16293	16295	16297	16299	16301	16303	16305	16307
16309	16311	16313	16315	16317	16319	16321	16381
16403	16425	16447	16469	16870	16871	16878	16881
16883	16885	16887	16889	16891	16893	16895	16897
16899	16901	16903	16905	16907	16909	16911	16913
16915	16975	16997	17019	17041	17063	17318	17319
17324	17325	17326	17327	17328	17329	17330	17331
17332	17333	17334	17335	17336	17337	17338	17339
17340	17527	17528	17533	17534	17535	17536	17537
17538	17539	17540	17541	17542	17543	17544	17545
17546	17547	17548	17549	17736	17737	17742	17743
17744	17745	17746	17747	17748	17749	17750	17751
17752	17753	17754	17755	17756	17757	17758	17945

17946	17951	17952	17953	17954	17955	17956	17957
17958	17959	17960	17961	17962	17963	17964	17965
17966	17967	18154	18155	18160	18161	18162	18163
18164	18165	18166	18167	18168	18169	18170	18171
18172	18173	18174	18175	18176	18410	18421	18432
18443	18454	18476	18487	18498	18509	18520	18542
18553	18564	18575	18586	18608	18619	18630	18641
18652	19149	19150	19153	19155	19156	19157	19158
19159	19160	19161	19162	19163	19164	19165	19166
19167	19168	19169	19170	19171	19172	19202	19213
19224	19235	19246	19312	19323	19334	19345	19356
19853	19854	19857	19859	19860	19861	19862	19863
19864	19865	19866	19867	19868	19869	19870	19871
19872	19873	19874	19875	19876	19906	19917	19928
19939	19950	20016	20027	20038	20049	20060	20557
20558	20561	20563	20564	20565	20566	20567	20568
20569	20570	20571	20572	20573	20574	20575	20576
20577	20578	20579	20580	20610	20621	20632	20643
20654	20720	20731	20742	20753	20764	21261	21262
21265	21267	21268	21269	21270	21271	21272	21273
21274	21275	21276	21277	21278	21279	21280	21281
21282	21283	21284	21314	21325	21336	21347	21358
21424	21435	21446	21457	21468	21965	21966	21969
21971	21972	21973	21974	21975	21976	21977	21978
21979	21980	21981	21982	21983	21984	21985	21986
21987	21988	22018	22029	22040	22051	22062	22128
22139	22150	22161	22172	22669	22670	22673	22675
22676	22677	22678	22679	22680	22681	22682	22683
22684	22685	22686	22687	22688	22689	22690	22691
22692	22722	22733	22744	22755	22766	22832	22843
22854	22865	22876	23373	23374	23377	23379	23380
23381	23382	23383	23384	23385	23386	23387	23388
23389	23390	23391	23392	23393	23394	23395	23396
23426	23437	23448	23459	23470	23536	23547	23558
23569	23580	24077	24078	24081	24083	24084	24085
24086	24087	24088	24089	24090	24091	24092	24093
24094	24095	24096	24097	24098	24099	24100	24130
24141	24152	24163	24174	24240	24251	24262	24273
24284	10022	10024	10028	10029	10031	10032	10035
10039	10040	10042	10046	10048	10052	10053	10055
10056	10060	10062	10067	10069	10073	10075	10077
10078	10082	10084	10088	10090	10094	10095	10097
10098	10102	10104	10233	10237	10247	10251	10885
10888	10893	10894	10895	10898	10899	10904	10905
10908	10909	10914	10915	10918	10919	10924	10925

10928	10929	10934	10935	10938	10939	10944	10945
10948	10949	10954	10955	10958	10959	10964	10965
10968	10969	10974	10975	10978	10981	10984	10987
10990	10993	10994	10997	10998	11001	11004	11007
11008	11011	11014	11017	11018	11021	11024	11027
11028	11031	11034	11037	11038	11041	11044	11047
11048	11051	11054	11057	11058	11061	11064	11067
11068	11071	11074	11077	11078	11083	11084	11775
11777	11778	11780	11783	11784	11785	11787	11788
11794	11795	11798	11799	11801	11804	11805	11807
11808	11812	11815	11816	11818	11819	11821	11824
11825	11826	11828	11829	11832	11833	11835	11836
11838	11841	11842	11844	11845	11847	11849	11850
11852	11853	11855	11858	11859	11860	11862	11863
11866	11867	11869	11870	11872	11875	11876	11878
11879	11881	11883	11886	11889	11892	11893	11896
11897	11900	11901	11903	11906	11909	11912	11913
11915	11917	11918	11920	11923	11924	11926	11927
11931	11934	11935	11937	11940	11941	11943	11944
11948	11951	11952	11954	11957	11958	11960	11961
11963	11965	11966	11968	11971	11972	11974	11975
11977	11979	11980	11982	11985	11986	11988	11989
11991	11993	11994	11996	11999	12000	12002	12003
12005	12007	12010	12013	12016	12017	12019	12021
12024	12027	12030	12031	12033	12035	12036	12038
12041	12042	12044	12045	12049	12052	12053	12055
12058	12059	12061	12062	12066	12069	12070	12072
12075	12076	12078	12079	12081	12083	12084	12086
12089	12090	12092	12093	12095	12097	12098	12100
12103	12104	12106	12107	12109	12111	12112	12114
12117	12118	12120	12121	12123	12125	12128	12131
12134	12135	12137	12139	12142	12145	12148	12149
12151	12153	12154	12156	12159	12160	12162	12163
12167	12170	12171	12173	12176	12177	12179	12180
12184	12187	12188	12190	12193	12194	12196	12197
12199	12201	12202	12204	12207	12208	12210	12211
12213	12215	12216	12218	12221	12222	12224	12225
12227	12229	12230	12232	12235	12236	12238	12239
12241	12243	12246	12249	12252	12253	12255	12257
12260	12263	12266	12267	12269	12271	12272	12274
12277	12278	12280	12281	12285	12288	12291	12293
12294	12298	12299	12301	12304	12305	12307	12308
12310	12312	12315	12317	12318	12320	12321	12323
12326	12327	12329	12330	12332	12334	12337	12339
12340	12342	12345	12348	12351	12352	12354	12356

12361	12362	12366	12948	12949	12952	12953	12992
12993	12994	12995	13000	13001	13002	13003	13008
13009	13010	13011	13015	13016	13017	13366	13367
13370	13371	13410	13411	13412	13413	13418	13419
13420	13421	13426	13427	13428	13429	13433	13434
13435	13784	13785	13788	13789	13828	13829	13830
13831	13836	13837	13838	13839	13844	13845	13846
13847	13851	13852	13853	14202	14203	14206	14207
14246	14247	14248	14249	14254	14255	14256	14257
14262	14263	14264	14265	14269	14270	14271	14620
14621	14624	14625	14664	14665	14666	14667	14672
14673	14674	14675	14680	14681	14682	14683	14687
14688	14689	15091	15093	15137	15138	15139	15142
15143	15146	15147	15150	15151	15154	15155	15158
15159	15162	15163	15166	15167	15170	15171	15173
15195	15217	15239	15261	15283	15685	15687	15731
15732	15733	15736	15737	15740	15741	15744	15745
15748	15749	15752	15753	15756	15757	15760	15761
15764	15765	15767	15789	15811	15833	15855	15877
16279	16281	16325	16326	16327	16330	16331	16334
16335	16338	16339	16342	16343	16346	16347	16350
16351	16354	16355	16358	16359	16361	16383	16405
16427	16449	16471	16873	16875	16919	16920	16921
16924	16925	16928	16929	16932	16933	16936	16937
16940	16941	16944	16945	16948	16949	16952	16953
16955	16977	16999	17021	17043	17065	17320	17321
17322	17323	17341	17342	17343	17344	17345	17346
17347	17348	17349	17350	17351	17352	17353	17354
17355	17529	17530	17531	17532	17550	17551	17552
17553	17554	17555	17556	17557	17558	17559	17560
17561	17562	17563	17564	17738	17739	17740	17741
17759	17760	17761	17762	17763	17764	17765	17766
17767	17768	17769	17770	17771	17772	17773	17947
17948	17949	17950	17968	17969	17970	17971	17972
17973	17974	17975	17976	17977	17978	17979	17980
17981	17982	18156	18157	18158	18159	18177	18178
18179	18180	18181	18182	18183	18184	18185	18186
18187	18188	18189	18190	18191	18411	18422	18433
18444	18455	18477	18488	18499	18510	18521	18543
18554	18565	18576	18587	18609	18620	18631	18642
18653	19151	19152	19173	19174	19175	19176	19177
19178	19179	19180	19181	19182	19183	19184	19185
19186	19187	19188	19189	19190	19191	19192	19203
19214	19225	19236	19247	19313	19324	19335	19346
19357	19855	19856	19877	19878	19879	19880	19881

19882	19883	19884	19885	19886	19887	19888	19889
19890	19891	19892	19893	19894	19895	19896	19907
19918	19929	19940	19951	20017	20028	20039	20050
20061	20559	20560	20581	20582	20583	20584	20585
20586	20587	20588	20589	20590	20591	20592	20593
20594	20595	20596	20597	20598	20599	20600	20611
20622	20633	20644	20655	20721	20732	20743	20754
20765	21263	21264	21285	21286	21287	21288	21289
21290	21291	21292	21293	21294	21295	21296	21297
21298	21299	21300	21301	21302	21303	21304	21315
21326	21337	21348	21359	21425	21436	21447	21458
21469	21967	21968	21989	21990	21991	21992	21993
21994	21995	21996	21997	21998	21999	22000	22001
22002	22003	22004	22005	22006	22007	22008	22019
22030	22041	22052	22063	22129	22140	22151	22162
22173	22671	22672	22693	22694	22695	22696	22697
22698	22699	22700	22701	22702	22703	22704	22705
22706	22707	22708	22709	22710	22711	22712	22723
22734	22745	22756	22767	22833	22844	22855	22866
22877	23375	23376	23397	23398	23399	23400	23401
23402	23403	23404	23405	23406	23407	23408	23409
23410	23411	23412	23413	23414	23415	23416	23427
23438	23449	23460	23471	23537	23548	23559	23570
23581	24079	24080	24101	24102	24103	24104	24105
24106	24107	24108	24109	24110	24111	24112	24113
24114	24115	24116	24117	24118	24119	24120	24131
24142	24153	24164	24175	24241	24252	24263	24274
24285	9681	9682	9683	9684	9686	9687	9688
9689	9690	9694	9695	9697	9698	9699	9700
9704	9705	9707	9708	9709	9710	9713	9715
9716	9717	9721	9722	9724	9725	9726	9727
9731	9732	9734	9735	9736	9737	9741	9742
9744	9745	9746	9747	9750	9751	9755	9756
9758	9759	9760	9761	9767	9768	9769	9771
9772	9773	9774	9775	9778	9779	9784	9785
9786	9788	9789	9790	9791	9792	9796	9797
9799	9800	9801	9802	9806	9807	9809	9810
9811	9812	9815	9816	9820	9821	9823	9824
9825	9826	9829	9831	9832	9833	9837	9838
9840	9841	9842	9843	9846	9848	9849	9850
9853	9855	9856	9857	9860	9862	9863	9864
9868	9869	9871	9872	9873	9874	9877	9878
9881	9883	9884	9885	9888	9890	9891	9892
9896	9897	9899	9900	9901	9902	9905	9906
9909	9911	9912	9913	9916	9918	9919	9920

9924	9925	9927	9928	9929	9930	9933	9934
10074	10115	10117	10118	10125	10128	10136	10138
10145	10148	10163	10165	10167	10180	10181	10193
10195	10208	10209	12364	15071	15072	15073	15075
15077	15080	15081	15083	15085	15665	15666	15667
15669	15671	15674	15675	15677	15679	16259	16260
16261	16263	16265	16268	16269	16271	16273	16853
16854	16855	16857	16859	16862	16863	16865	16867
19140	19141	19142	19143	19144	19145	19146	19147
19148	19844	19845	19846	19847	19848	19849	19850
19851	19852	20548	20549	20550	20551	20552	20553
20554	20555	20556	21252	21253	21254	21255	21256
21257	21258	21259	21260	21956	21957	21958	21959
21960	21961	21962	21963	21964	22660	22661	22662
22663	22664	22665	22666	22667	22668	23364	23365
23366	23367	23368	23369	23370	23371	23372	24068
24069	24070	24071	24072	24073	24074	24075	24076
9221	9223	9225	9227	9232	9233	9235	9237
9238	9239	9242	9247	9248	9249	9252	9254
9256	9261	9263	9265	9266	9267	9272	9273
9276	9278	9281	9285	9286	9288	9290	9291
9294	9299	9300	9301	9304	9306	9310	9312
9314	9315	9320	9321	9324	9326	9328	9333
9335	9337	9338	9339	9344	9345	9348	9350
9352	9357	9359	9361	9362	9363	9368	9369
9372	9374	9378	9380	9382	9383	9388	9389
9392	9394	9398	9400	9402	9403	9408	9409
9412	9414	9416	9421	9423	9425	9426	9427
9432	9433	9436	9438	9440	9445	9447	9449
9450	9451	9456	9457	9460	9462	9466	9468
9470	9471	9476	9477	9480	9482	9486	9488
9490	9491	9496	9497	9500	9502	9504	9509
9511	9513	9514	9515	9520	9521	9524	9526
9528	9533	9535	9537	9538	9539	9544	9545
9548	9550	9554	9556	9558	9559	9564	9565
9568	9570	9574	9576	9578	9579	9584	9585
9588	9590	9592	9597	9599	9601	9602	9603
9608	9609	9612	9614	9616	9621	9623	9625
9626	9627	9632	9633	9636	9638	9642	9644
9646	9647	9652	9653	9656	9658	9662	9664
9666	9667	9672	9673	9676	11094	12909	12910
12911	12914	12915	12918	12919	12922	12923	13327
13328	13329	13332	13333	13336	13337	13340	13341
13745	13746	13747	13750	13751	13754	13755	13758
13759	14163	14164	14165	14168	14169	14172	14173

14176	14177	14581	14582	14583	14586	14587	14590
14591	14594	14595	17300	17301	17302	17303	17304
17305	17306	17307	17308	17509	17510	17511	17512
17513	17514	17515	17516	17517	17718	17719	17720
17721	17722	17723	17724	17725	17726	17927	17928
17929	17930	17931	17932	17933	17934	17935	18136
18137	18138	18139	18140	18141	18142	18143	18144
10153	10155	10162	10173	10177	10186	10191	10201
10205	10346	10348	10350	10352	10357	10358	10360
10362	10363	10364	10367	10372	10373	10374	10377
10379	10381	10386	10388	10390	10391	10392	10397
10398	10401	10403	10406	10410	10411	10413	10415
10416	10419	10424	10425	10426	10429	10431	10435
10437	10439	10440	10445	10446	10449	10451	10453
10458	10460	10462	10463	10464	10469	10470	10473
10475	10477	10482	10484	10486	10487	10488	10493
10494	10497	10499	10503	10505	10507	10508	10513
10514	10517	10519	10523	10525	10527	10528	10533
10534	10537	10539	10541	10546	10548	10550	10551
10552	10557	10558	10561	10563	10565	10570	10572
10574	10575	10576	10581	10582	10585	10587	10591
10593	10595	10596	10601	10602	10605	10607	10611
10613	10615	10616	10621	10622	10625	10627	10629
10634	10636	10638	10639	10640	10645	10646	10649
10651	10653	10658	10660	10662	10663	10664	10669
10670	10673	10675	10679	10681	10683	10684	10689
10690	10693	10695	10699	10701	10703	10704	10709
10710	10713	10715	10717	10722	10724	10726	10727
10728	10733	10734	10737	10743	10745	10746	10749
10752	10754	10758	10760	10762	10763	10768	10769
10772	10776	10778	10781	10784	10794	12929	12930
12931	12932	12933	12938	12939	12940	12941	13347
13348	13349	13350	13351	13356	13357	13358	13359
13765	13766	13767	13768	13769	13774	13775	13776
13777	14183	14184	14185	14186	14187	14192	14193
14194	14195	14601	14602	14603	14604	14605	14610
14611	14612	14613	17309	17310	17311	17312	17313
17314	17315	17316	17317	17518	17519	17520	17521
17522	17523	17524	17525	17526	17727	17728	17729
17730	17731	17732	17733	17734	17735	17936	17937
17938	17939	17940	17941	17942	17943	17944	18145
18146	18147	18148	18149	18150	18151	18152	18153
10790	11088	11190	11194	11202	11205	11229	11232
11239	11242	11263	11266	11273	11276	11297	11300
11310	15097	15691	16285	16879	19154	19858	20562

```
   21266     21970     22674     23378     24082         0         0         0
*BOUNDARY_SPC_SET_BIRTH_DEATH_ID
$#      id                                                     heading
        11
$#    nsid       cid      dofx      dofy      dofz     dofrx     dofry     dofrz
         1         0         1         1         0         1         1         1
$#   birth     death
     0.000 300.00000
*SET_NODE_LIST_TITLE
1st
$#     sid       da1       da2       da3       da4    solver
         1     0.000     0.000     0.000     0.000MECH
$#    nid1      nid2      nid3      nid4      nid5      nid6      nid7      nid8
        64        65       126       127       192       193       251       252
       310       311       370       371       429       430       488       489
       547       548         0         0         0         0         0         0
*BOUNDARY_SPC_SET_BIRTH_DEATH_ID
$#      id                                                     heading
        02
$#    nsid       cid      dofx      dofy      dofz     dofrx     dofry     dofrz
         2         0         1         1         0         1         1         1
$#   birth     death
     0.000 630.00000
*SET_NODE_LIST_TITLE
2nd
$#     sid       da1       da2       da3       da4    solver
         2     0.000     0.000     0.000     0.000MECH
$#    nid1      nid2      nid3      nid4      nid5      nid6      nid7      nid8
        62        63       124       125       190       191       249       250
       308       309       368       369       427       428       486       487
       545       546         0         0         0         0         0         0
*BOUNDARY_SPC_SET_BIRTH_DEATH_ID
$#      id                                                     heading
        03
$#    nsid       cid      dofx      dofy      dofz     dofrx     dofry     dofrz
         3         0         1         1         0         1         1         1
$#   birth     death
     0.000 960.00000
*SET_NODE_LIST_TITLE
3rd
$#     sid       da1       da2       da3       da4    solver
         3     0.000     0.000     0.000     0.000MECH
$#    nid1      nid2      nid3      nid4      nid5      nid6      nid7      nid8
        60        61       122       123       188       189       247       248
       306       307       366       367       425       426       484       485
```

```
     543       544        0         0         0         0         0         0
*BOUNDARY_SPC_SET_BIRTH_DEATH_ID
$#      id                                                    heading
        04
$#    nsid       cid      dofx      dofy      dofz     dofrx     dofry     dofrz
         4         0         1         1         0         1         1         1
$#   birth     death
     0.000 1290.0000
*SET_NODE_LIST_TITLE
4th
$#     sid       da1       da2       da3       da4    solver
         4     0.000     0.000     0.000     0.000MECH
$#    nid1      nid2      nid3      nid4      nid5      nid6      nid7      nid8
        58        59       120       121       186       187       245       246
       304       305       364       365       423       424       482       483
       541       542         0         0         0         0         0         0
*BOUNDARY_SPC_SET_BIRTH_DEATH_ID
$#      id                                                    heading
        05
$#    nsid       cid      dofx      dofy      dofz     dofrx     dofry     dofrz
         5         0         1         1         0         1         1         1
$#   birth     death
     0.000 1620.0000
*SET_NODE_LIST_TITLE
5th
$#     sid       da1       da2       da3       da4    solver
         5     0.000     0.000     0.000     0.000MECH
$#    nid1      nid2      nid3      nid4      nid5      nid6      nid7      nid8
        56        57       118       119       184       185       243       244
       302       303       362       363       421       422       480       481
       539       540         0         0         0         0         0         0
*BOUNDARY_SPC_SET_BIRTH_DEATH_ID
$#      id                                                    heading
        06
$#    nsid       cid      dofx      dofy      dofz     dofrx     dofry     dofrz
         6         0         1         1         0         1         1         1
$#   birth     death
     0.000 1950.0000
*SET_NODE_LIST_TITLE
6th
$#     sid       da1       da2       da3       da4    solver
         6     0.000     0.000     0.000     0.000MECH
$#    nid1      nid2      nid3      nid4      nid5      nid6      nid7      nid8
     12375     12376     12386     12387     12397     12398     12408     12409
     12419     12420     12430     12431     12441     12442     12452     12453
```

```
   12463    12464        0        0        0        0        0        0
*BOUNDARY_SPC_SET_BIRTH_DEATH_ID
$#      id                                          heading
        07
$#    nsid       cid      dofx      dofy      dofz     dofrx     dofry     dofrz
         7         0         1         1         0         1         1         1
$#   birth     death
     0.000 2280.0000
*SET_NODE_LIST_TITLE
7th
$#     sid       da1       da2       da3       da4    solver
         7     0.000     0.000     0.000     0.000MECH
$#    nid1      nid2      nid3      nid4      nid5      nid6      nid7      nid8
     12373     12374     12384     12385     12395     12396     12406     12407
     12417     12418     12428     12429     12439     12440     12450     12451
     12461     12462         0         0         0         0         0         0
*BOUNDARY_SPC_SET_BIRTH_DEATH_ID
$#      id                                          heading
        08
$#    nsid       cid      dofx      dofy      dofz     dofrx     dofry     dofrz
         8         0         1         1         0         1         1         1
$#   birth     death
     0.000 2610.0000
*SET_NODE_LIST_TITLE
8th
$#     sid       da1       da2       da3       da4    solver
         8     0.000     0.000     0.000     0.000MECH
$#    nid1      nid2      nid3      nid4      nid5      nid6      nid7      nid8
     12371     12372     12382     12383     12393     12394     12404     12405
     12415     12416     12426     12427     12437     12438     12448     12449
     12459     12460         0         0         0         0         0         0
*BOUNDARY_SPC_SET_BIRTH_DEATH_ID
$#      id                                          heading
        09
$#    nsid       cid      dofx      dofy      dofz     dofrx     dofry     dofrz
         9         0         1         1         0         1         1         1
$#   birth     death
     0.000 2940.0000
*SET_NODE_LIST_TITLE
9th
$#     sid       da1       da2       da3       da4    solver
         9     0.000     0.000     0.000     0.000MECH
$#    nid1      nid2      nid3      nid4      nid5      nid6      nid7      nid8
     12369     12370     12380     12381     12391     12392     12402     12403
     12413     12414     12424     12425     12435     12436     12446     12447
```

```
    12457     12458         0         0         0         0         0         0
*BOUNDARY_SPC_SET_BIRTH_DEATH_ID
$#      id                                        heading
       010
$#    nsid       cid      dofx      dofy      dofz     dofrx     dofry     dofrz
        10         0         1         1         0         1         1         1
$#   birth     death
     0.000 3270.0000
*SET_NODE_LIST_TITLE
10th
$#     sid       da1       da2       da3       da4    solver
        10     0.000     0.000     0.000     0.000MECH
$#    nid1      nid2      nid3      nid4      nid5      nid6      nid7      nid8
     12367     12368     12378     12379     12389     12390     12400     12401
     12411     12412     12422     12423     12433     12434     12444     12445
     12455     12456         0         0         0         0         0         0
*BOUNDARY_SPC_SET_BIRTH_DEATH_ID
$#      id                                        heading
       011
$#    nsid       cid      dofx      dofy      dofz     dofrx     dofry     dofrz
        11         0         1         1         0         1         1         1
$#   birth     death
     0.000 3600.0000
*SET_NODE_LIST_TITLE
11th
$#     sid       da1       da2       da3       da4    solver
        11     0.000     0.000     0.000     0.000MECH
$#    nid1      nid2      nid3      nid4      nid5      nid6      nid7      nid8
     12482     12483     12492     12493     12502     12503     12512     12513
     12522     12523     12532     12533     12542     12543     12552     12553
     12562     12563         0         0         0         0         0         0
*BOUNDARY_SPC_SET_BIRTH_DEATH_ID
$#      id                                        heading
       012
$#    nsid       cid      dofx      dofy      dofz     dofrx     dofry     dofrz
        12         0         1         1         0         1         1         1
$#   birth     death
     0.000 3930.0000
*SET_NODE_LIST_TITLE
12th
$#     sid       da1       da2       da3       da4    solver
        12     0.000     0.000     0.000     0.000MECH
$#    nid1      nid2      nid3      nid4      nid5      nid6      nid7      nid8
     12480     12481     12490     12491     12500     12501     12510     12511
     12520     12521     12530     12531     12540     12541     12550     12551
```

```
   12560     12561         0         0         0         0         0         0
*BOUNDARY_SPC_SET_BIRTH_DEATH_ID
$#      id                                          heading
       013
$#    nsid       cid       dofx      dofy      dofz     dofrx     dofry     dofrz
      13         0         1         1         0         1         1         1
$#   birth     death
   0.000 4260.0000
*SET_NODE_LIST_TITLE
13th
$#     sid       da1       da2       da3       da4    solver
      13     0.000     0.000     0.000     0.000MECH
$#    nid1      nid2      nid3      nid4      nid5      nid6      nid7      nid8
   12478     12479     12488     12489     12498     12499     12508     12509
   12518     12519     12528     12529     12538     12539     12548     12549
   12558     12559         0         0         0         0         0         0
*BOUNDARY_SPC_SET_BIRTH_DEATH_ID
$#      id                                          heading
       014
$#    nsid       cid       dofx      dofy      dofz     dofrx     dofry     dofrz
      14         0         1         1         0         1         1         1
$#   birth     death
   0.000 4590.0000
*SET_NODE_LIST_TITLE
14th
$#     sid       da1       da2       da3       da4    solver
      14     0.000     0.000     0.000     0.000MECH
$#    nid1      nid2      nid3      nid4      nid5      nid6      nid7      nid8
   12476     12477     12486     12487     12496     12497     12506     12507
   12516     12517     12526     12527     12536     12537     12546     12547
   12556     12557         0         0         0         0         0         0
*BOUNDARY_SPC_SET_BIRTH_DEATH_ID
$#      id                                          heading
       015
$#    nsid       cid       dofx      dofy      dofz     dofrx     dofry     dofrz
      15         0         1         1         0         1         1         1
$#   birth     death
   0.000 4920.0000
*SET_NODE_LIST_TITLE
15th
$#     sid       da1       da2       da3       da4    solver
      15     0.000     0.000     0.000     0.000MECH
$#    nid1      nid2      nid3      nid4      nid5      nid6      nid7      nid8
   12474     12475     12484     12485     12494     12495     12504     12505
   12514     12515     12524     12525     12534     12535     12544     12545
```

```
   12554     12555         0         0         0         0         0         0
*BOUNDARY_SPC_SET_BIRTH_DEATH_ID
$#       id                                                heading
      1716
$#    nsid       cid       dofx       dofy       dofz      dofrx      dofry      dofrz
        18         0          1          1          0          1          1          1
$#    birth     death
   0.000 5250.0000
*SET_NODE_LIST_TITLE
16th
$#      sid       da1       da2       da3       da4    solver
        18     0.000     0.000     0.000     0.000MECH
$#     nid1      nid2      nid3      nid4      nid5      nid6      nid7      nid8
     12564     12565     12567     12568     12570     12571     12573     12574
     12576     12577     12579     12580     12582     12583     12585     12586
     12588     12589         0         0         0         0         0         0
*BOUNDARY_SPC_SET_BIRTH_DEATH_ID
$#       id                                                heading
      1817
$#    nsid       cid       dofx       dofy       dofz      dofrx      dofry      dofrz
        19         0          1          1          0          1          1          1
$#    birth     death
   0.000 5580.0000
*SET_NODE_LIST_TITLE
17th
$#      sid       da1       da2       da3       da4    solver
        19     0.000     0.000     0.000     0.000MECH
$#     nid1      nid2      nid3      nid4      nid5      nid6      nid7      nid8
     17070     17071     17077     17078     17084     17085     17091     17092
     17098     17099     17105     17106     17112     17113     17119     17120
     17126     17127         0         0         0         0         0         0
*BOUNDARY_SPC_SET_BIRTH_DEATH_ID
$#       id                                                heading
      1918
$#    nsid       cid       dofx       dofy       dofz      dofrx      dofry      dofrz
        20         0          1          1          0          1          1          1
$#    birth     death
   0.000 5910.0000
*SET_NODE_LIST_TITLE
18th
$#      sid       da1       da2       da3       da4    solver
        20     0.000     0.000     0.000     0.000MECH
$#     nid1      nid2      nid3      nid4      nid5      nid6      nid7      nid8
     17068     17069     17075     17076     17082     17083     17089     17090
     17096     17097     17103     17104     17110     17111     17117     17118
```

```
   17124     17125         0         0         0         0         0         0
*BOUNDARY_SPC_SET_BIRTH_DEATH_ID
$#      id                                         heading
      2019
$#    nsid       cid      dofx      dofy      dofz     dofrx     dofry     dofrz
        21         0         1         1         0         1         1         1
$#   birth     death
     0.000 6240.0000
*SET_NODE_LIST_TITLE
19th
$#     sid       da1       da2       da3       da4    solver
        21     0.000     0.000     0.000     0.000MECH
$#    nid1      nid2      nid3      nid4      nid5      nid6      nid7      nid8
     17066     17067     17073     17074     17080     17081     17087     17088
     17094     17095     17101     17102     17108     17109     17115     17116
     17122     17123         0         0         0         0         0         0
*BOUNDARY_SPC_SET_BIRTH_DEATH_ID
$#      id                                         heading
       020
$#    nsid       cid      dofx      dofy      dofz     dofrx     dofry     dofrz
        22         0         1         1         0         1         1         1
$#   birth     death
     0.000 6570.0000
*SET_NODE_LIST_TITLE
20th
$#     sid       da1       da2       da3       da4    solver
        22     0.000     0.000     0.000     0.000MECH
$#    nid1      nid2      nid3      nid4      nid5      nid6      nid7      nid8
     17129     17130     17131     17132     17133     17134     17135     17136
     17137     17138     17139     17140     17141     17142     17143     17144
     17145     17146         0         0         0         0         0         0
*BOUNDARY_SPC_SET_BIRTH_DEATH_ID
$#      id                                         heading
       021
$#    nsid       cid      dofx      dofy      dofz     dofrx     dofry     dofrz
        23         0         1         1         0         1         1         1
$#   birth     death
     0.000 6900.0000
*SET_NODE_LIST_TITLE
21st
$#     sid       da1       da2       da3       da4    solver
        23     0.000     0.000     0.000     0.000MECH
$#    nid1      nid2      nid3      nid4      nid5      nid6      nid7      nid8
     24286     24287     24289     24290     24292     24293     24295     24296
     24298     24299     24301     24302     24304     24305     24307     24308
```

```
   24310     24311         0         0         0         0         0         0
*BOUNDARY_SPC_SET_BIRTH_DEATH_ID
$#      id                                        heading
       022
$#    nsid       cid      dofx      dofy      dofz     dofrx     dofry     dofrz
        24         0         1         1         0         1         1         1
$#   birth     death
     0.000 7230.0000
*SET_NODE_LIST_TITLE
22nd
$#     sid       da1       da2       da3       da4    solver
        24     0.000     0.000     0.000     0.000MECH
$#    nid1      nid2      nid3      nid4      nid5      nid6      nid7      nid8
     24313     24314     24315     24316     24317     24318     24319     24320
     24321     24322     24323     24324     24325     24326     24327     24328
     24329     24330         0         0         0         0         0         0
*BOUNDARY_SPC_SET_BIRTH_DEATH_ID
$#      id                                        heading
       023
$#    nsid       cid      dofx      dofy      dofz     dofrx     dofry     dofrz
        25         0         1         1         0         1         1         1
$#   birth     death
     0.000 7560.0000
*SET_NODE_LIST_TITLE
23rd
$#     sid       da1       da2       da3       da4    solver
        25     0.000     0.000     0.000     0.000MECH
$#    nid1      nid2      nid3      nid4      nid5      nid6      nid7      nid8
     24331     24332     24334     24335     24337     24338     24340     24341
     24343     24344     24346     24347     24349     24350     24352     24353
     24355     24356         0         0         0         0         0         0
*LOAD_SEGMENT_SET_ID
$#      id                                        heading
         1force
$#    ssid      lcid        sf        at        dt
         1         1 5.0000E-5     0.000     0.000
*PART
$# title
Needle
$#     pid     secid       mid     eosid      hgid      grav    adpopt      tmid
         1         1         1         0         0         0         0         0
*SECTION_SOLID_TITLE
Needle
$#   secid    elform       aet
         1         1         0
```

```
*MAT_ELASTIC_TITLE
needl elastic
$#     mid        ro         e        pr        da        db  not used
         1 7.8000E-6  0.050000  0.300000     0.000     0.000         0
*PART
$# title
Prostate
$#     pid     secid       mid     eosid      hgid      grav    adpopt      tmid
         2         2         2         0         1         0         0         0
*SECTION_SOLID_ALE_TITLE
Prostatevoid
$#   secid    elform       aet
         2        12         1
$#    afac      bfac      cfac      dfac     start       end     aafac
 -1.000000     0.000     0.000     0.000     0.000     0.000     0.000
*MAT_ELASTIC_TITLE
Prostate
$#     mid        ro         e        pr        da        db  not used
         2  0.002000 2.5000E-8  0.300000     0.000     0.000         0
*HOURGLASS_TITLE
HG
$#    hgid       ihq        qm       ibq        q1        q2    qb/vdc        qw
         1         1 1.0000E-6         0  1.500000  0.060000  0.100000  0.100000
*PART
$# title
Void
$#     pid     secid       mid     eosid      hgid      grav    adpopt      tmid
         3         2         2         0         1         0         0         0
*INITIAL_VOID_PART
$#     pid
         3
*DEFINE_CURVE_TITLE
velocity
$#    lcid      sidr       sfa       sfo      offa      offo    dattyp
         1         0  1.000000  1.000000     0.000     0.000         0
$#                a1                  o1
               0.000            0.015000
           10000.000            0.015000
*SET_NODE_LIST_TITLE
needle end
$#     sid       da1       da2       da3       da4    solver
        26     0.000     0.000     0.000     0.000MECH
$#    nid1      nid2      nid3      nid4      nid5      nid6      nid7      nid8
     24358     24359     24360     24361     24362     24363     24364     24365
     24366     24367     24368     24369     24370     24371     24372     24373
```

```
   24374     24375         0         0         0         0         0         0
*SET_PART_LIST_TITLE
ALE Part
$#     sid       da1       da2       da3       da4    solver
         1     0.000     0.000     0.000     0.000MECH
$#    pid1      pid2      pid3      pid4      pid5      pid6      pid7      pid8
         2         3         0         0         0         0         0         0
*SET_SEGMENT_TITLE
needle tip
$#     sid       da1       da2       da3       da4    solver
         1     0.000     0.000     0.000     0.000MECH
$#      n1        n2        n3        n4        a1        a2        a3        a4
       134       135        67         3     0.000     0.000     0.000     0.000
        69        68        67       135     0.000     0.000     0.000     0.000
       135       132         4        69     0.000     0.000     0.000     0.000
       134       133       132       135     0.000     0.000     0.000     0.000
*CONSTRAINED_LAGRANGE_IN_SOLID
$#   slave    master     sstyp     mstyp     nquad     ctype     direc     mcoup
         1         1         1         0         0         2         1         0
$#   start       end      pfac      fric    frcmin      norm   normtyp      damp
    0.0001.0000E+10  0.100000     0.000  0.500000         0         0     0.000
$#      cq      hmin      hmax     ileak     pleak   lcidpor     nvent  blockage
     0.000     0.000     0.000         0  0.100000         0         0         0
*ELEMENT_SOLID
$#   eid     pid      n1      n2      n3      n4      n5      n6      n7      n8
      50       1     118     302     539     362     119     303     540     363
      51       1     119     303     540     363     120     304     541     364
      52       1     120     304     541     364     121     305     542     365
      53       1     121     305     542     365     122     306     543     366
      54       1     122     306     543     366     123     307     544     367
      55       1     123     307     544     367     124     308     545     368
      56       1     124     308     545     368     125     309     546     369
      57       1     125     309     546     369     126     310     547     370
      58       1     126     310     547     370     127     311     548     371
      59       1     127     311     548     371     128     312     549     372
      60       1     128     312     549     372       4      69     135     132
     110       1     184     539     302     243     185     540     303     244
     111       1     185     540     303     244     186     541     304     245
     112       1     186     541     304     245     187     542     305     246
     113       1     187     542     305     246     188     543     306     247
     114       1     188     543     306     247     189     544     307     248
     115       1     189     544     307     248     190     545     308     249
     116       1     190     545     308     249     191     546     309     250
     117       1     191     546     309     250     192     547     310     251
     118       1     192     547     310     251     193     548     311     252
```

119	1	193	548	311	252	194	549	312	253
120	1	194	549	312	253	67	135	69	68
170	1	362	539	480	421	363	540	481	422
171	1	363	540	481	422	364	541	482	423
172	1	364	541	482	423	365	542	483	424
173	1	365	542	483	424	366	543	484	425
174	1	366	543	484	425	367	544	485	426
175	1	367	544	485	426	368	545	486	427
176	1	368	545	486	427	369	546	487	428
177	1	369	546	487	428	370	547	488	429
178	1	370	547	488	429	371	548	489	430
179	1	371	548	489	430	372	549	490	431
180	1	372	549	490	431	132	135	134	133
230	1	184	56	480	539	185	57	481	540
231	1	185	57	481	540	186	58	482	541
232	1	186	58	482	541	187	59	483	542
233	1	187	59	483	542	188	60	484	543
234	1	188	60	484	543	189	61	485	544
235	1	189	61	485	544	190	62	486	545
236	1	190	62	486	545	191	63	487	546
237	1	191	63	487	546	192	64	488	547
238	1	192	64	488	547	193	65	489	548
239	1	193	65	489	548	194	66	490	549
240	1	194	66	490	549	67	3	134	135

Due to the very large number of elements, the coordinates of the rest of the elements are not reproduced here.

```
*NODE
$#   nid          x            y            z      tc    rc
       3    -1.752187     0.310058     0.533012     0     0
```

Due to the very large number of nodes, the coordinates of the rest of the nodes are not reproduced here.

*END